Politecnico di Milano

School of Industrial and Information Engineering

Master of Science in Materials Engineering and Nanotechnology

Investigation of naphthalene and its hydrogenated derivatives in the formation process of polyynes by Pulsed Laser Ablation in Liquid

Supervisor: Prof. Carlo S. Casari
Co-Supervisor: Pietro Marabotti

Master thesis of:
Marco Benoliel
920412

Academic Year 2019-2020

Abstract

In this thesis work, I investigated the role of different solutions and targets in the production of carbon atomic wires, and in particular polyynes, by Pulsed Laser Ablation in Liquid (PLAL). I selected alcohols (methanol, ethanol and isopropyl-alcohol), naphthalene and two of its hydrogenated derivatives (decalin and tetralin). A Nd:YAG laser was employed to perform the PLAL synthesis, while High Performance Liquid Chromatography (HPLC) was used to separate polyynes in solution and to characterize them with a photodiode-array integrated in the system. To fulfil the thesis goal, I focused on the analysis of concentrations of H-capped polyynes in terms of the C/H ratios of the solvents, both in their pure form and as binary mixtures. I expected to promote the synthesis of longer polyynes at the expense of shorter ones by increasing the C/H ratio of the solvent. In the case of pure solvents, the increase in long polyynes production was correlated to an increase of the C/H ratio and viscosity, and to a decrease in the polarity of the solvent. In binary mixtures, these results were not confirmed, and the reason is attributed to the compatibility of the components in terms of polarity. Naphthalene was proven to be a direct source of H-polyynes when dissolved in an apolar solvent and when used as target for the ablation. These results seems to confirm a ring-opening mechanism of naphthalene structure suggested in other studies.

Sommario

Il carbonio esiste sotto forma di diverse forme allotropiche, quali il diamante, la grafite, il grafene, i nanotubi e i fullereni. In queste specie, gli atomi di carbonio presentano orbitali ibridi sp^2 o sp^3. Recentemente, è stata ipotizzata l'esistenza di un materiale composto interamente da atomi di carbonio ibridizzati sp, una catena infinita di atomi, chiamata carbyna, per cui sono predette proprietà meccaniche ed elettroniche potenzialmente rivoluzionarie. Oggi è possibile sintetizzare catene di lunghezza finita, dette Carbon Atom Wires, sotto forma di due isomeri: la poliina, più stabile, in cui si alternano legami singoli e tripli, e il cumulene, caratterizzato invece da una sequenza di legami doppi.
Lo scopo di questa tesi consiste nell' esplorare l'effetto di diverse soluzioni e target sulla produzione di poliine tramite ablazione laser pulsata in liquido. Sono stati esplorati soprattutto naftalene e due dei suoi derivati idrogenati (decalina e tetralina), sull' ipotesi che le loro strutture ad anello, in condizioni di plasma generate dal laser, possano aprirsi e favorire la sintesi di catene più lunghe. Anche alcuni alcoli (metanolo, etanolo e alcol isopropile) sono stati indagati come solventi per l'ablazione. Per la sintesi è stato utilizzato un laser Nd:YAG, mentre la caratterizzazione è stata effettuata tramite High Perfomance Liquid Chromatography (HPLC) integrata con detector UV-Vis. Per conseguire l'obiettivo, ho analizzato le concentrazioni di poliine terminate con atomi di idrogeno, al variare del rapporto C/H dei solventi, sia in forma pura che come soluzioni binarie. È stato ipotizzato che l'aumento di questo rapporto comportasse una maggiore concentrazione di catene lunghe. Nel caso di solventi puri, la maggior produzione di catene lunghe è stata correlata a un aumento del rapporto C/H e della viscosità, e ad una diminuzione della polarità. Tali risultati non sono stati confermati nel caso di soluzioni binarie, probabilmente a causa della importante differenza di polarità tra i componenti. È stato dimostrato che il naftalene rappresenta una fonte diretta di poliine se disciolto in un solvente apolare o se usato come target per l'ablazione.

Contents

List of Figures

List of Tables

Introduction

Over the last decades, carbon nanomaterials have gained huge interest in the field of nanotechnology. Graphene, fullerenes and nanotubes, which are the main representatives of this class, are constituted by carbon atoms based on sp^2 or sp^3 hybridization. While the existence of a solid material based on sp hybridized carbon atoms is still under discussion, sp carbon compounds characterized by a linear geometry have been synthesized by both physical and chemical techniques. These species are called Carbon Atomic Wires (CAWs), and their properties are predicted to outperform the ones of graphene, from both a mechanical and electronic point of view. However, these compounds are very unstable, and tend easily to undergo crosslinking and oxidation reactions. Such instability is the main obstacle towards the synthesis of the solid sp carbon crystal, that can be modeled as an infinite chain of sp carbon atoms known as carbyne. Nevertheless, the infinite chain provides the model to describe structure and properties of finite CAWs. According to this model, in fact, there are two possible isomers: cumulenes, featuring a sequence of double bonds, and polyynes, in which there is an alternation of single and triple bonds. For large chain lengths, polyynes are identified as the stable isomer by Peierls' distortion, while, moving to shorter chains, the effect of the terminal groups becomes dominant and can stabilize also cumulenic forms.
Chemical methods were the first to be employed in CAWs synthesis, but physical methods are cheaper and allow possible industrial scale-up. Pulsed Laser Ablation in Liquid is the physical technique used in this thesis work. Basically, it exploits the interaction between a laser and a carbon pellet immersed in a liquid, in order to create out-of-equilibrium plasma conditions which favour the formation of sp-carbon chains. Polyynes terminated by H atoms are the most concentrated kind of chains obtained and characterized in the ablated solutions. The synthesis of polyynes terminated by bulky groups, which are much more stable, has never been achieved up to now with this technique.
In this thesis, I investigated the effect of different materials (both solids and liquids) to deepen the knowledge of sp-chains formation mechanisms. In particular, I want to discover if increasing the amount of carbon atoms respect to the content

of hydrogen in the liquid can promote the formation of longer polyynes. Moreover, by using naphthalene and some of its derivatives, I will try to synthesize polyynes with aromatic terminations, which should largely increase their stability.
The work is organised in the following way:

- Chapter One: an overview of the properties of the most important carbon allotropes is presented, followed by a more detailed description of CAWs structure, properties, and characterization methods. It will be introduced also why Polycyclic Aromatic Hydrocarbons are believed to be effective sources of polyynes.
- Chapter Two: in the first part, the physics underlying the PLAL process are discussed, as well as the effect of ablation parameters. In the second part, the state of the art of polyynes synthesis by PLAL is described in terms of laser and materials parameters.
- Chapter Three: the materials and the experimental apparata employed in the polyynes synthesis and characterization are presented.
- Chapter Four: the experimental results are discussed in detail. The first part of the chapter involves ablations in pure solvents, while in the second one the effect of the different binary mixtures on the yield of polyynes is explored. In the last section, the ablation of a naphthalene target in different solvents is investigated and compared to the graphite counterpart.

Chapter 1

sp-Carbon atomic wires

Carbon is a fundamental element in the world as we know it. It provides not only the basis for life on Earth, but it has also a great impact in current technological applications. Its presence in the majority of any known compound is strictly related to its ability to bind almost any element of the periodic table in a large number of ways [1].
In the framework of Linear Combination of Atomic Orbitals (LCAO), hybridization theory describes the chemical behavior of carbon and the existence of some carbon compounds. In fact, carbon electronic configuration $1s^2$, $2s^2$, $2p^2$ would allow it to make only two chemical bonds. However, hybridization theory, predicts the formation of sp, sp^2 and sp^3 orbitals, which consist in a linear combination of the 2s and 2p electrons. Orbitals who are not involved in the hybridization can be used to build double and triple bonds. Geometry of carbon-based molecules is strongly linked to the hybridization state of their carbon atoms: sp carbon builds a one-dimensional geometry, sp^2 forms two-dimensional planar structures and sp^3 creates three-dimensional tetrahedral compounds. In organic chemistry, the different hybridization states lead to the family of alkanes, alkenes and alkynes, whose simplest structures are shown in Fig. 1.1, i.e. ethane, ethylene and acetylene, respectively [2]. The corresponding allotropic phases are represented: diamond is the carbon material based on sp^3 hybridization, while graphite is a stacking of sp^2 carbon planes. The existence of a material based on sp hybridization has been theorized: carbyne, an infinite chain of sp carbon atoms, which is predicted to have surprising properties which could challenge any other existing material [2]. Before describing in detail sp carbon compounds, the next sections outline an overview of the other carbon materials and nanomaterials.

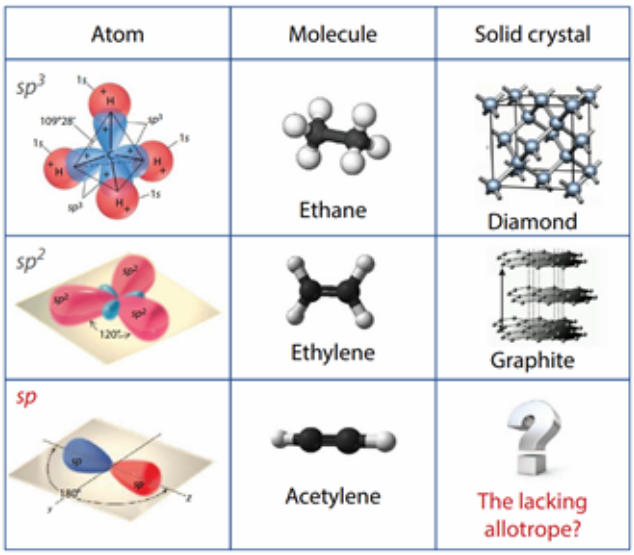

Figure 1.1: *From left to right: atoms, molecules and carbon phases of different hybridization states [2]*

1.1 Diamond and graphite

Diamond and graphite represent carbon most common phases. Diamond is thermodynamically unstable at room temperature and atmospheric pressure, unlike graphite, which is stable under such conditions. However the process of graphitization of diamond is extremely slow. Diamond shows the typical sp^3 configuration: tetrahedral geometry with a bond angle of 109°28' and a FCC unit cells, as shown in Fig.1.2a. Since every carbon orbital is involved in the hybridization, there are no free electrons available for transport, making diamond a bad electrical conductor ($\rho = 10^{18}\Omega m$ at room temperature [3]). On the other hand it is the best known thermal conductor (2200 W/mK), thanks to the combination of an high cristallinity, strong covalent bonds and low phonon scattering[4]. Diamond outperforms any other known material also in hardness (10 Mohs)[4]. Indeed, diamond is an insulator with a sizeable bandgap width (5.5 eV), which accounts for its characteristic transparent appearance[4].
Graphite properties differ extremely from those of diamond. sp^2 hybridization of graphite results in a flat network of carbon atoms arranged in a planar geometry, with bond angles of 120° and an hexagonal unit cell with four atoms per basis, as visible in Fig. 1.2b. Carbon planes are piled on top of each other and kept together by Van der Waals interactions, while strong covalent bonds are formed in-plane. This causes a strong anisotropy in most of graphite properties. Mechanical strength, for instance, is very high in the in-plane direction, due to the covalent bonds, and very low in the perpendicular direction, where the absence of

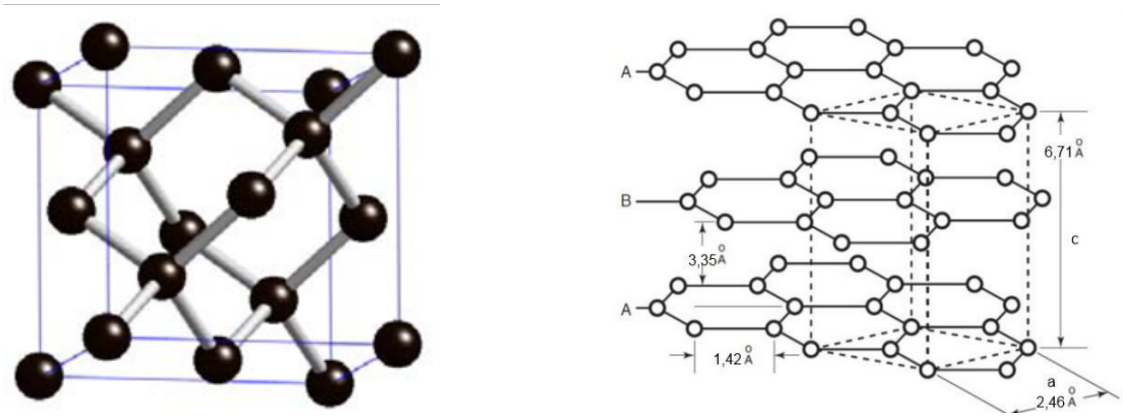

(a) *(b)*

Figure 1.2: *(a) Diamond FCC unit cell [5] (b) Graphite hexagonal planar structure [6]*

strong covalent bonds allows the sliding between adjacent planes. Also transport properties are anisotropic. In fact, one of the 2p orbitals is not involved in the hybridization and it can therefore be employed in double bonds. This produces the formation of a huge π orbital delocalization over the horizontal graphite plane. As a consequence, the in-plane electrical conductivity is extremely high (2–3 $\times$ 10^4 S cm^{-1} [4]). In the perpendicular direction, instead, Van der Waals interactions hinder the flow of electrons across planes. Thermal conductivity is also greatly reduced in the inter-layer direction respect to the in-plane one, due to different amplitudes of the vibrations in the different directions [4]. Another characteristic in contrast with diamond lies in the electronic band structure: while diamond has a wide bandgap, graphite is a zero gap semiconductor or a semimetal. Consequently, graphite has a grey-black appearance, since all photons in the visible are absorbed [7].

1.2 Carbon nanomaterials

For a long time diamond and graphite were considered the only two existing carbon allotropes. Over the last decades, a new class of carbon nanostructures has been discovered, gaining the attention of material scientists because of their potential technological applications [1]. The main common feature of these advanced materials is the confinement of at least one dimension to the nanometer level. The resulting quantum confinement, often combined with the presence of fully conjugated π orbitals, justifies their outstanding electronic properties [1].
In 1985 Kroto, Smalley and Curl discovered fullerenes, a family of carbon 0D structures, i.e structures confined in all directions [8]. In 1991 carbon nanotubes

were detected by Iijima [9] and represent an example of quasi-1D systems, while in 2004 Geim and Novoselov managed to isolate graphene, a single layer of graphite, which was for long time considered only a theoretical material [10]. In the next pages I will present a brief description of these nanomaterials and their properties.

Graphene

Although it is the last carbon allotrope to be discovered, it is useful to start describing graphene, since fullerenes and nanotubes geometries are strictly related to it, as shown in Fig. 1.3.
Graphene is a single layer of graphite, a planar sheet of sp^2 carbon atoms of monoatomic thickness. The occurrence of quantum confinement and π-electron delocalization give rise to unique electronic, optical and mechanical features. In suspended, annealed, high-crystalline quality graphene, carrier mobility has been shown to exceed 200,000 cm^2/Vs, which is the highest value ever reported for both semiconductors or semimetals [12], [13]. Moreover, it was found that the carrier

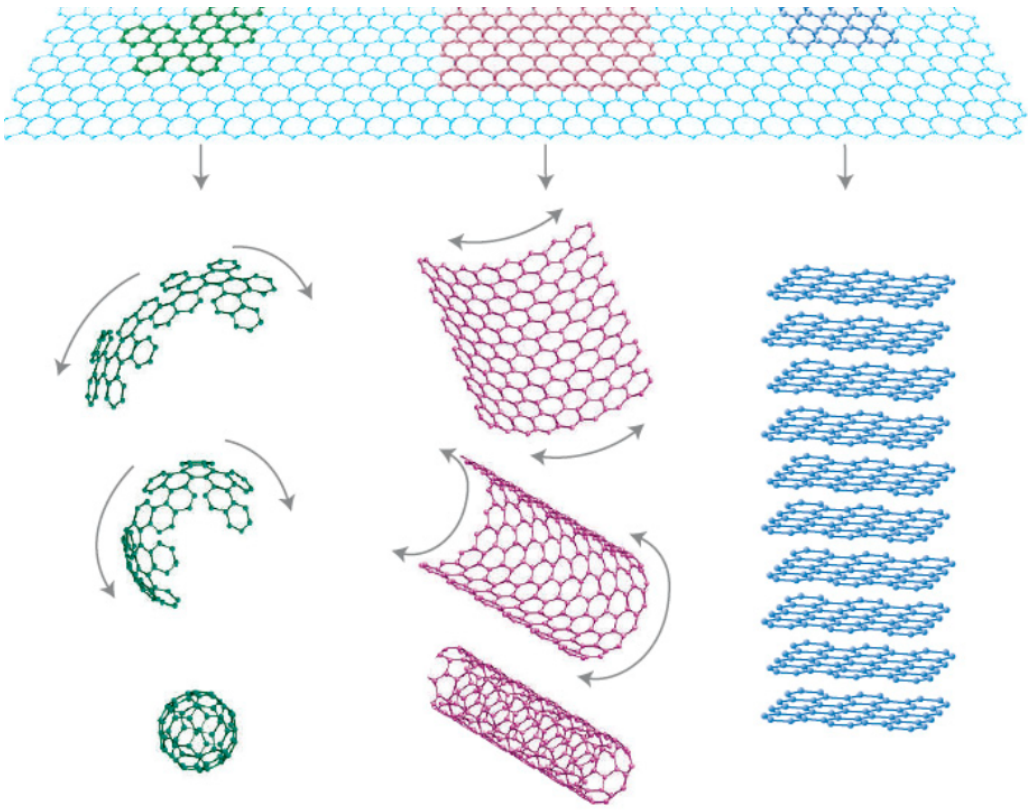

Figure 1.3: *Graphene sheet and possible structures built from it: wrapping results in fullerenes, rolling in nanotubes, stacking in graphite [11]*

.

mobility is nearly the same for both electrons and holes [14]. The possibility to achieve ballistic transport on a submicrometer scale at room temperature is surely one of graphene most appealing aspects [11]. Another electronic property, as already mentioned in Section 1.1, lies in its band structure. Graphene is in fact a gapless semiconductor: its Fermi surface is characterized by the presence of Dirac cones, where the valence and the conduction band approach linearly a contact point, where the density of states vanishes. As a result, carriers can be approximated as massless relativistic particles traveling at a Fermi velocity of $v_F = c/300$ and obeying Dirac equation[15]. The gapless electronic structure of graphene has implications also in its optical behaviour: unlike graphite, graphene is transparent, but its transmittance decreases linearly with its thickness. Such linearity is demonstrated up to a stack of five layers [13]. There are several studies in which the basic idea is to transform graphene in a nanoscopic bandgap semiconductor in order to employ it in FET applications [13], [16]. The high-crystalline quality of graphene provides not only outstanding electronic properties, but also a thermal conductance higher even than diamond one [4]. Finally, graphene, thanks to the strength of the sp^2 covalent bonds, has a Young modulus of 1 TPa, the highest reported value [17]. Considering also its incredibly large specific surface, graphene is an ideal reinforcement in composite materials and a strong candidate as pressure sensor/resonator in NEMS applications [18].
Graphene can be synthesized nowadays in various related forms: nanoribbons are strips of graphene, resulting in quasi-0D structures; it can be functionalized with oxigen or other chemical species to improve its solubility; graphene platelets consist in a stacking of few layers of graphene.

Nanotubes

Nanotubes are quasi-1D systems which can be visualized as rolled graphene sheets. More sheets can be rolled co-axially within eachother to obtain multiwall nanotubes. The most intriguing aspect of carbon nanotubes (CNTs) is the possibility to tune their properties by varying their structure. In this way, three types of nanotubes can be identified, as represented in Fig. 1.4: armchair, zigzag and chiral. The three classes of nanotubes can be understood in terms of the chiral vector $C = na_1 + ma_2$, shown in Fig. 1.4, where n and m are two integers and a_1 and a_2 are the basis vectors of graphite. When $m = 0$ a zig-zag nanotube is obtained, while for $n = m$ nanotubes are defined by armchair geometries. Any other combination of n and m generates a chiral nanotube. It was demonstrated that any nanotube for which $n - m$ is a multiple of 3 is characterized by a metallic behaviour. Therefore an armchair nanotube is always metallic, while chiral and zig-zag nanotubes can be either semimetallic or semiconducting. Moreover n and

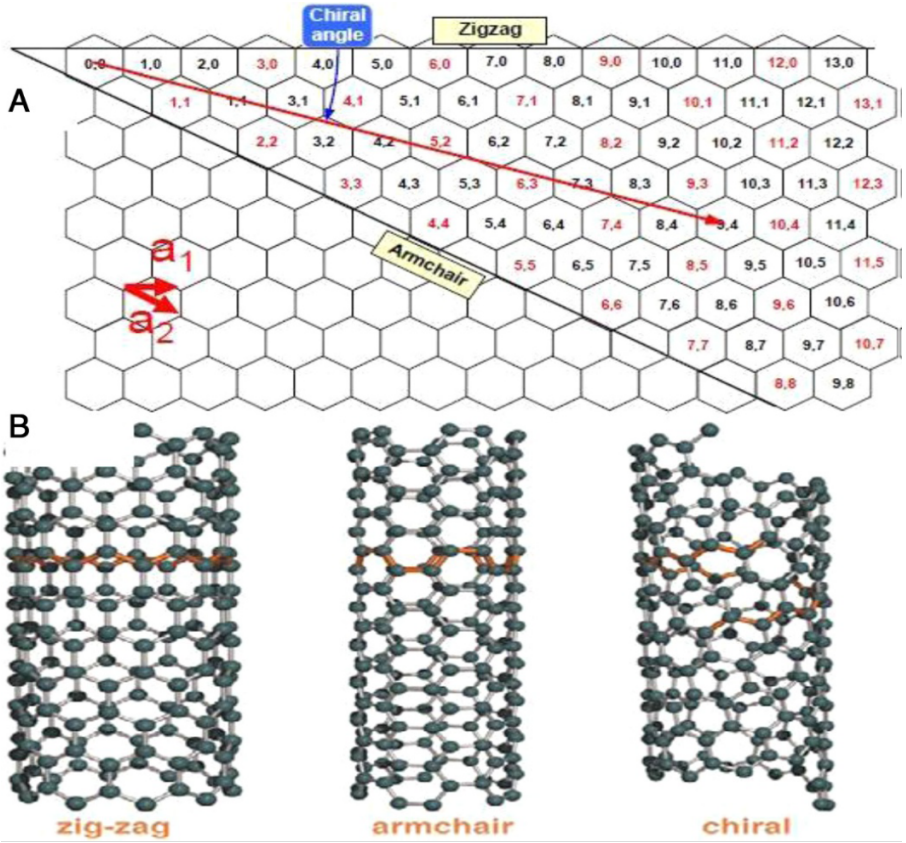

Figure 1.4: *A) Chiral vector defines both architecture and diameter of carbon nanotubes; B) The three different structures of nanotubes [19]*

m define also the tube diameter.
Similarly to graphene, nanotubes show amazing mechanical properties: a tensile strength higher than steel and an exceptional elasticity for many different stress states make CNTs an interesting option as a reinforcement in composite materials [19]. Thermal conductivity higher than diamond, but lower than graphene, has also been observed [4]. Another common feature with graphene is the possibility to functionalize CNTs with chemical groups, which opens the route to different applications. Indeed, nanotubes have been recently employed in many biomedical applications, including artificial implants, tissue engineering and drug delivery [19].

Fullerenes

Fullerenes are a class of molecular carbon allotropes whose structure can be visualized as the wrapping of a graphene sheet in order to obtain quasi-spherical networks of sp^2 carbon atoms, as shown in Fig. 1.3. By doing so, some hexago-

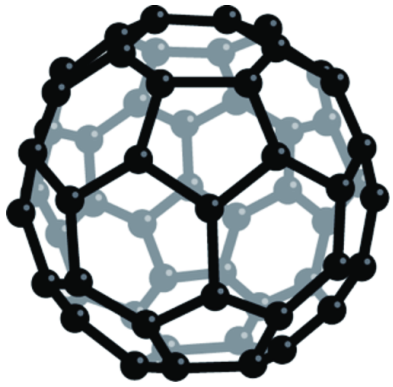

Figure 1.5: *Structure of C_{60}[21]*

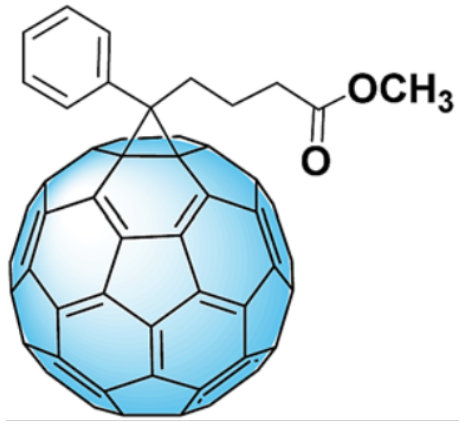

Figure 1.6: *Structure of PCBM [22]*

nal cells are replaced by pentagons to accommodate distortions and gain stability. C_{60}, the most stable fullerene, is composed by 20 hexagons and 12 pentagons arranged to form a "football-like" shape , as reported in Fig. 1.5. Direct formation of fullerene molecules from a graphene flake has actually been visualized by means of TEM microscopy [20].
In the past years, scientists have identified a high number of larger fullerenes, including C_{70}, C_{84}, C_{90}, as well as smaller ones, which have been found to be less stable. Furthermore, a countless variety of fullerenes derivatives has been obtained by chemical methods: fullerenes salts, open-cage fullerenes, exohedral and endohedral fullerenes are some of the main classes of functionalized fullerenes [1]. As in the case of nanotubes, proper chemical functionalization is the key to exploit fullerenes full potential: for example, it enables a dramatic increase in solubility in any solvent, allowing an easier processability and compatibility with other materials [1]. Fullerenes are under investigation in a large number of biological applications [23]. In photovoltaics PCBM (phenyl-C_{61}-butyric acid-methyl ester), whose structure is shown in Fig. 1.6, has already entered the market as one of the best n-type conductors [1]. Their electronic transport qualities widely overtake the other materials for photovoltaic application and they have been referred as the best on their market field [22]. Nearly-high temperature superconductivity ($T_c = 33K$) was detected in fullerene salts like K_3C_{60} [1], [24].

1.3 Carbon atom wires

In the previous sections of this chapter carbon main allotropic forms, both at the macro and at the nanoscale, have been discussed. They are fundamentally all based on sp^2 or sp^3 hybridization, or a mixed state of the two. This section, like

the rest of this work, focuses on the sp-hybridized carbon compounds.

1.3.1 Carbyne: the infinite chain model

Carbyne, the hypothetical lacking carbon allotrope based on sp hybridization, is an ideal infinite linear chain of carbon atoms, whose existence is still under debate. The efforts spent by scientists in the last years to stabilize this material are motivated by its incredible mechanical and electronic properties that have been predicted by theoretical calculations [25]–[28]. According to these, no other material can be compared to carbyne in terms of Young modulus (32 TPa [29]). Besides, highly tunable and strongly structure-dependent electronic properties make sp-chains extremely appealing systems for the implementation of nanoscale devices [2], [26], [28]. Even if real systems consist in finite chains (which will be referred to as Carbon Atom Wires, or just CAWs), it is useful to start the description from the ideal infinite model, not only for its simplicity, but also because it provides a basis to describe finite real systems.

1.3.2 Structural, electronic and vibrational properties of carbyne

Carbyne ideally exists in two possible configurations, shown in Fig.1.7: polyyne and cumulene. Polyyne is characterized by an alternation of single and triple bonds, while cumulene features a series of equalized double bonds [2], [30], [31]. The parameter used to quantitatively describe their structural properties is the Bond Length Alternation (BLA), which defines the mean difference between two adjacent bonds [2], [30]. For ideal cumulene this value is equal to zero, while it differs from zero in the case of polyyne. The presence of π orbitals delocalized over the whole chain gives rise to conjugation effects, and therefore electron transport along the chain axis. In cumulene, double bonds results in one global π orbital completely delocalized over the whole chain, allowing maximum conjugation. Conversely, lower conjugation is expected in the ideal polyyne, since the overlap of π orbitals is interrupted by the single bonds. The link between structure and electronic properties is now evident: cumulene-like systems show a metallic behaviour, while polyynes are semiconductors [2], [30]. The same conclusion can be obtained also by following a solid-state approach. As shown in Fig. 1.7, cumulene unit cell is made by one carbon atom. Every carbon atom contributes with one electron for each of its two 2p orbitals, leading to a half filled conduction band, and thus a conductive behaviour [30]. Polyyne, instead, has two atoms per basis, and therefore a doubled unit cell respect to cumulene. The valence band is thus completely filled, and a band gap is opened at the edges of the Brillouin zone [30]. This strong relationship between chain structure and electronic properties is reflected also on

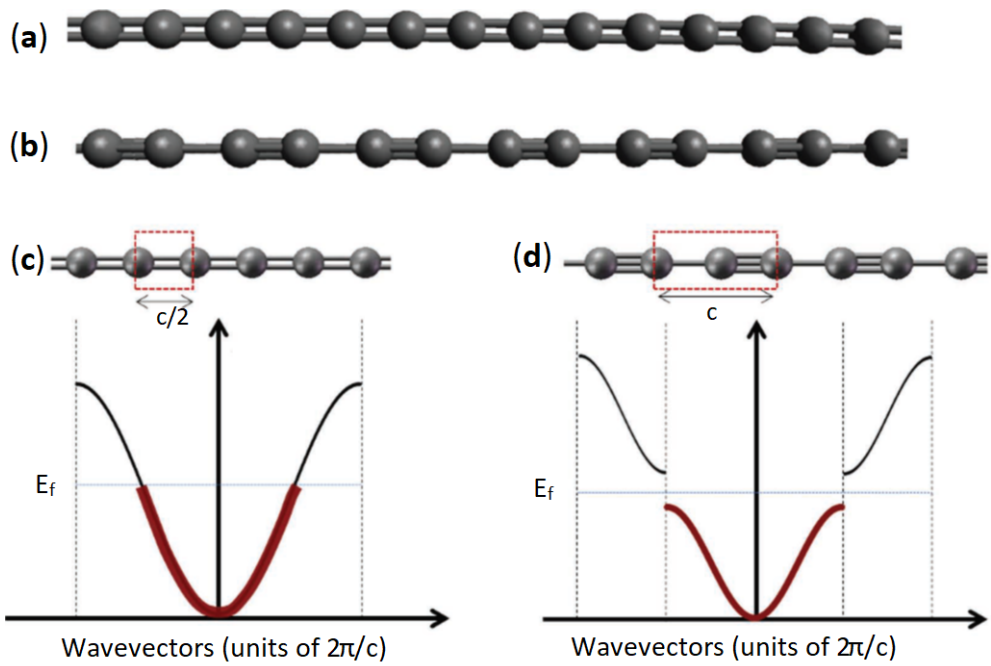

Figure 1.7: *Structures of a) cumulene ; b) polyyne. The electronic band structure of c) cumulene and d) polyyne. The red dashed areas in panels c) and d) represent the unit cell of each isomer [30].*

the BLA, which returns a measure of the degree of π conjugation [30].
The difference in the number of atoms forming the basis set of the unit cell has significant effects also in the vibrational properties of carbyne. It is well known that moving from one to two atoms per basis (i.e. from cumulene to polyyne) produces the appearance of an optical phonon branch in the dispersion relation. This implicates that cumulene, in principle, does not possess any optical activity, and therefore cannot be detected by coventional vibrational spectroscopy, i.e. Raman or infrared. Lastly, BLA affects also the optical behaviour of carbyne, since a change in the BLA leads to a change in the filling of the valence band that reflects in a variation of the optical bandgap, and thus in light absorption and emission [30]. In strong analogy with other common conjugated systems, as polyacetylene, Peierls' distortion describes the stability of carbyne isomers in terms of a change in the BLA [2]. Polyyne is identified as the stable configuration, to which also cumulene will tend if the BLA is varied. This situation is depicted in Fig. 1.8.
The ideal model of an infinite sp chain with all its implications can be adapted to explain the properties of finite CAWs: in fact real systems can be correlated to the relative infinite chain possessing the same BLA [30], provided that the effects of their finite size, such as the presence of terminations and the lack of infinite periodicity, are taken into account. The next section is dedicated to integrate these

effects in the infinite chain model.

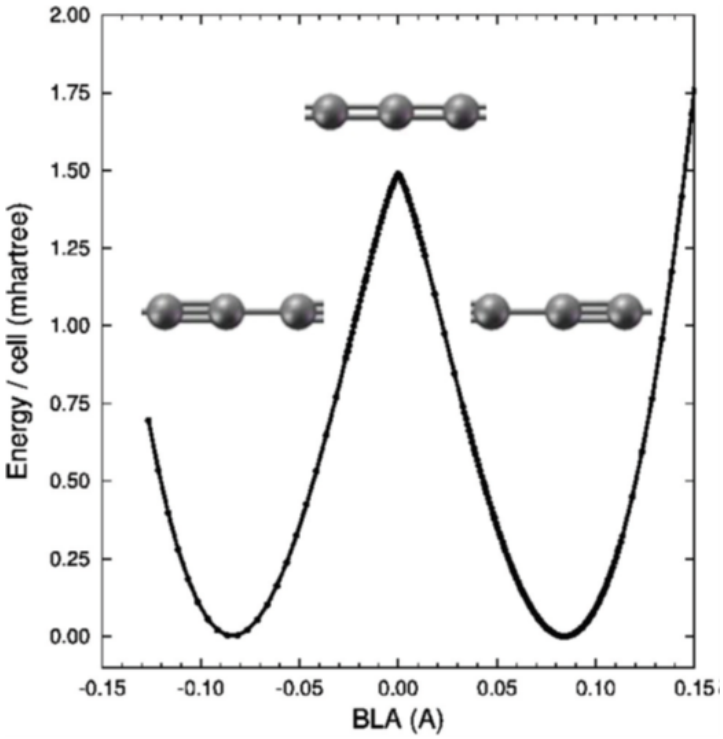

Figure 1.8: *Peierls' distortion: stability of carbyne isomers [30]*

1.3.3 Finite sp chains: endgroup effects and stability

Real sp linear carbon systems consist in finite sp chains. Last section ended with the introduction of Peierls' distortion, which is dominant in an ideal infinite wire and identifies polyyne as the stable isomer. Actually, Peierls' distortion rules structure properties of CAWs for a number of carbon atoms > 52 [30]. As we move to shorter chains CAWs are neither perfectly cumulenic nor polyynic. Indeed, the structural, vibrational and electronic properties of short wires are determined by the so-called endgroup effects. Real sp chains, in fact, never terminate with a carbon atom, they rather prefer a different chemical group, be it an atom or a molecule. In the case of polyynes, the most common termination is hydrogen, but many cases of nitrogen and methyl-group are reported in the literature of polyynes produced by physical methods [32]–[34]. Chemical synthesis, on the other hand, recently reached a much larger control, and many different "bulkier" terminations have been obtained [35], [36]. The endgroups play an important role in the stability of CAWs: the bigger they are, in fact, the higher is the steric hindrance they provide, which leads to a reduced tendency to crosslink and therefore to an increased stability. A second significant effect is the ability to modulate the BLA and to

induce a cumulenic or a polyynic structure, as shown in Fig. 1.9 [30]. Indeed, if the connection between the endgroup and the chain occur through a single bond, a polyyne structure is favored. On the other hand, cumulenic configurations are stabilized when two bonds are involved (either a double bond with one terminal group or a single bond with two groups) [31], [37]. In finite CAWs, therefore, the stable configuration, as well as the value of BLA, is the result of the interplay between Peierls' distortion and endgroup effects, with the former dominating in longer chains, and the latter in shorter. Actually there are other sources of BLA modulation [30]. Charge transfer, for example, can occur as a consequence of the interaction between wires and the surrounding environment. In particular, DFT calculations have shown that silver nanoparticles (which are contained in colloids employed to perform Surface Enhanced Raman Spectroscopy), as will be shown in the following section, can donate electrons to sp chains, with an increased tendency for longer chains [38]. As a result the excess charge is redistributed over the whole wire, equalizing bonds and leading thus to a cumulenic configuration. Photo-excitation processes can also cause a change in the BLA [30].
Stability is a key issue in the synthesis of CAWs [30]. An increase in chain length is accompanied by an increase in reactivity and instability, which are mainly caused by oxidation and crosslinking. Oxidation is related to the presence of oxidizing agents such as O_2, making CAWs unstable in air. Liquids are instead much safer environments for sp-chains, as reported in many studies [32], [39]–[41]. Crosslinking reactions, instead, happen when CAWs chemically interact among themselves, both in solutions or gas phase, bringing them to reach more stable hybridization states, i.e. sp^2 or sp^3 [30]. A wire of 6000 carbon atoms chemically grown inside a CNT by Shi *et al.* represents the longest chain ever obtained up today [42].

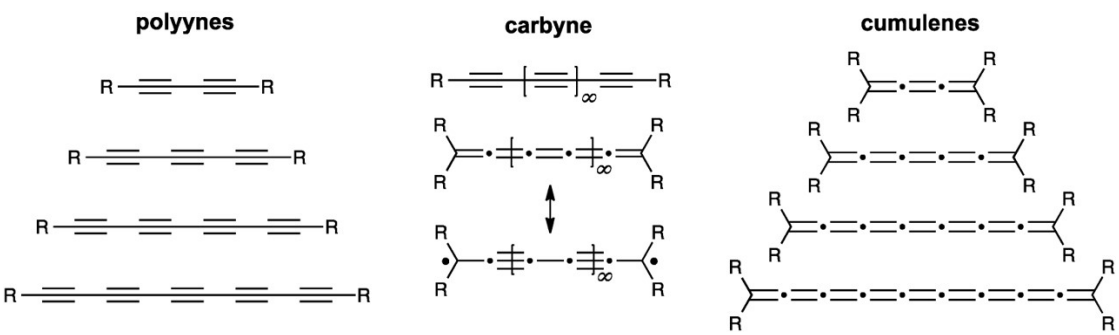

Figure 1.9: *End group effect on isomers stabilization [37]*

1.4 Characterization Methods

The last section of this chapter is dedicated to the description of the main characterization methods of linear carbon chains, particularly polyynes, which are the case of this study work. The typical techniques are UV-Vis Spectroscopy, High Performance Liquid Chromatography (HPLC), Raman Spectroscopy and Surface Enhanced Raman Spectroscopy (SERS). The last part is dedicated to mass spectroscopic methods exploited in literature to analyze fragmentation products of Polycylic Aromatic Hydrocarbons (PAHs) in plasma conditions. Though mass spectroscopy will not be used to analyze polyynes in this work, it is useful to get a better understanding of the purposes of this thesis.

UV-Vis Absorption Spectroscopy

UV-Vis absorption spectroscopy can be used as a probe of electronic transitions of compounds. The sample is illuminated by a wide spectrum of photon energies, ranging from the UV to the near infrared. In principle, species inside the sample will absorbs photons only at those wavelengths which satisfy the relation $E_{gap} = hc/\lambda_{photon}$, where E_{gap} is the energy of an electronic transition and λ_{photon} is the wavelength of the incoming photon. As a result, we obtain a series of absorption peaks centered at a wavelength (λ) related to the electronic transitions of the analytes contained in the sample. Different compounds are characterized by different spectra, and can therefore be recognized by comparison with reference spectra. However the absorption patterns do not represent unique fingerprints of a substance, since transitions at the same wavelength can occur in different species. It does though provide very useful indications. For example, it allows a quantitative analysis of the sample: the absorbance, in fact, is linearly related to the concentration of the sample, as stated by the Lambert-Beer law reported below:

$$A = \epsilon c d \tag{1.1}$$

where A is the absorbance; ϵ is the molar coefficient of extinction of the attenuating species, which by definition accounts for both scattering and absorption and is expressed in m^2/mol; c is the molar concentration of the attenuating species and d the optical path of light within the sample. Hydrogen-capped polyynes spectra are typically characterized by comb-like absorption species, whose intensity increases with wavelength. This peculiar shape makes this technique very useful in polyynes first detection and characterization. Fig. 1.10 shows typical UV-Vis spectra of polyynes of different length and termination obtained by pulsed laser ablation in liquid [32]. A first consideration can be done on how the spectra vary with chain length. It is quite immediate to see a shift towards higher wavelengths as the

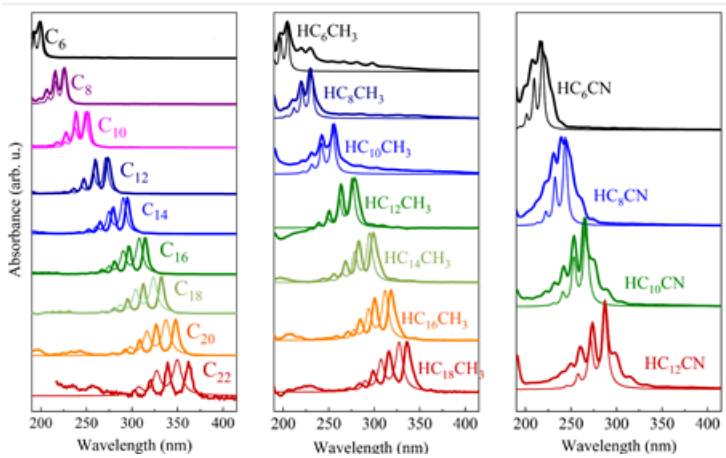

Figure 1.10: *Normalized spectra of polyynes of different length and termination. Moving from left to right: H-capped polyynes, methyl-capped polyynes, ciano-polyynes [32]*

length increases. This can be justified in terms of π conjugation: in fact, longer polyynes show higher conjugation respect to the shorter ones, because a higher number of 2p orbitals contributes to the π molecular orbital. Higher conjugation leads in turn to a smaller HOMO-LUMO gap, and thus to a longer excitation

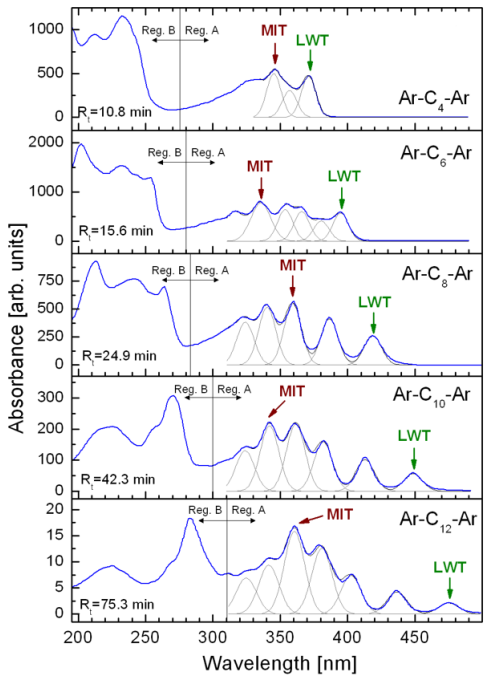

Figure 1.11: *UV-Vis spectra of dinaphthyl-polyynes of different length. Ar stands for aryl, while MIT and LWT are respectively Most Intense Transition and Longest Wavelength Transition. Notice the strong redshift with respect to the H-capped polyynes of the same length of Fig. 1.10 [43].*

wavelength [44]. Different endgroups can also cause a change in the conjugation of the chains and differences in the electronic levels, allowing to distinguish polyynes of the same length but with different termination. Indeed, the absorption maxima of methyl-capped polyynes spectra are slightly redshifted respect to those of H-capped polyynes of the same length. Ciano-polyynes spectra, instead, present differences in both shape and positions of the peaks. Spectra of polyynes with bulkier end-groups show a complicate absorption pattern compared to H-capped polyynes: the spectra of dinaphthyl-polyynes (i.e. polyynes terminated with a naphthalene molecule on both ends) obtained by chemical synthesis are reported as an example in Fig. 1.11 [43].

High Performance Liquid Chromatography

High Performance Liquid Chromatography (HPLC) is a widely used method in chemistry to evaluate a product purity or, more in general, to separate species inside a solution [45].
The core of the HPLC is a porous cylindrical column, in which the sample solution is injected. A compact network of chemical groups is attached to the inner walls of the column and constitutes the stationary phase, with which species of the sample solution interact both physically and chemically. In contrast with the stationary phase, a mobile phase, which is a liquid mixture of solvents, literally pushes the sample solution through the column and elutes the analytes out of it. The retention depends on the different interaction of the analytes with both the stationary and the mobile phases [45]: from the physical point of view, larger ones will struggle more than smaller ones in travelling through the densely packed stationary phase; on the other side, the higher the chemical affinity between the species and the column, the stronger is the retention. As a result, the different molecules contained in the sample solution are eluted at different times. The time at which substances exit the column is called "retention time" and it is the characteristic quantity of HPLC data. A detection system has to be integrated at the end of the column to probe a specific property of the eluted sample: typically it is a UV-Vis Spectrometer, but in other applications it can be a mass spectrometer or a fluorescence detector [46]. So, after a substance is eluted, a UV-Vis spectrum of it is recorded to characterize it.
HPLC exists in two main configurations: normal phase and Reverse phase. In the first case the stationary phase has a polar nature, whereas the mobile phase is rather apolar. Normal phase is used to separate and analyze polar compounds. Conversely, the Reverse phase configuration is used to detect apolar analytes, and thus the stationary phase is apolar and the mobile phase polar. The overall polarity of the mobile phase can be tuned by varying its composition, and affects

the retention time of molecules. If the composition of the mobile phase is kept constant during the elution, the method is called isocratic. If the composition is gradually changed, instead, the method is called gradient. A variety of methods can be created by acting on the mixture of the mobile phase and on the other dynamical parameters, like flow rate, temperature, as well as on the type and stacking of the stationary phase [46].
In the field of polyynes, HPLC coupled with a UV-Vis spectrometer can be used to detect and separate chains with different length and termination. Longer polyynes, in fact, are characterized by longer retention times, since they have stronger interactions with the column respect to shorter ones [32], [33], [43]. Also polyynes of the same length but with different endgroups are eluted at different times, because each endgroup interacts differently with the column [32], [33]. In Fig. 1.12 a typical chromatogram (at different wavelength channels) of polyynes separated by length and termination is shown. In many works Reverse-phase Chromatography is employed for polyyne analysis, given their apolar nature [32], [36], [43], [47]. The use of a C8 and C18 based column as stationary phase is often reported, i.e. columns in which molecules constituted mainly by alkyl chains of 8 and 18 carbon atoms are attached to the inner walls [32], [33], [36], [43]. In the Reverse phase technique, the mobile phase is usually a mixture of water and less polar organic solvents (typically acetonitrile or methanol), but some works report also the use of a 100% ACN mobile phase [33]. There are also a few cases in which HPLC is used in the normal phase configuration, with hexane as mobile phase [48], [49]. Separated polyynes can be collected and further analyzed with other methods.

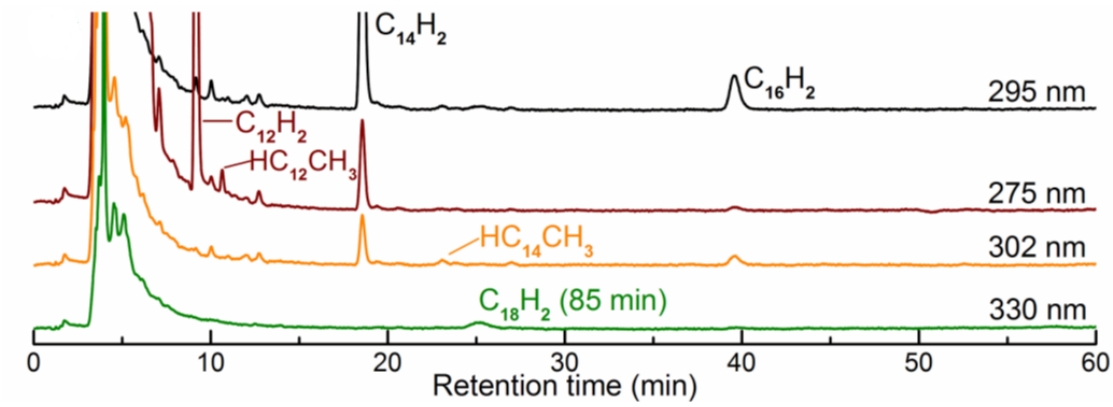

Figure 1.12: *Chromatogramm of polyynes obtained by laser irradiation of toluene. The wavelength of the channels are set on the most intense electronic transitions of polyynes [33]*

Raman Spectroscopy and SERS

Raman Spectroscopy is a powerful characterization technique based on the inelastic scattering of light. An electron, upon photon absorption, is excited from its original vibrational state, and can relax back to a vibrational state different from the original by the emission of a photon with energy different than the incident. If this energy is lower, the electron will sit in a vibrational state with a higher energy than the original, and this is known as Stokes process. If the emitted photon energy is higher, instead, the molecule will relax to a lower vibrational state than the original one, and the process will be called Anti-Stokes. Thus, Anti-Stokes processes can originate only from an excited vibrational state, while Stokes ones can arise also from the ground state. Since the ground state is more populated than the excited ones, due to Bose-Einstein distribution, Stokes processes are more probable than Anti-Stokes. The difference in photon energies is approximately equal to the energy of a specific vibrational transition. Since different molecules have different vibrational states, the corresponding Raman spectra may represent actual fingerprints of the specific molecule or material.
Raman Spectroscopy is extremely useful in the field of carbon-based materials, because of its great sensitivity to carbon hybridization state [31]. Raman spectra of the various allotropic forms of carbon are shown in Fig. 1.13(a).
Every allotrope is identified by one or more specific peaks. For CAWs, the dominant feature lies in the 1800-2200 cm^{-1} region and is due to the out-of-phase

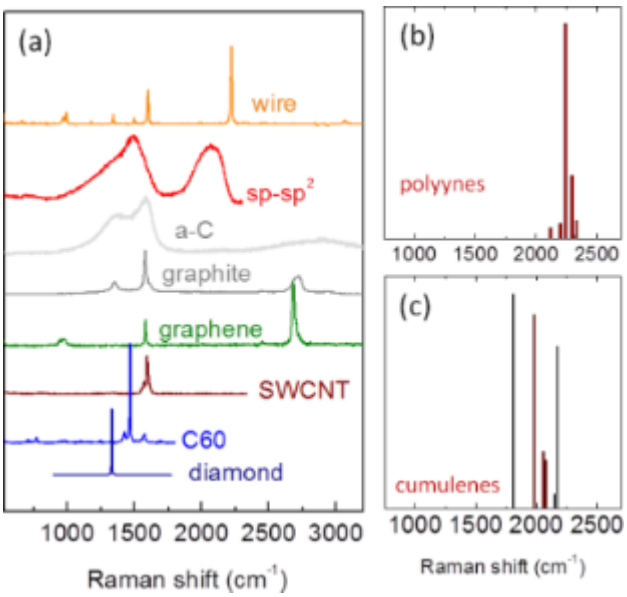

Figure 1.13: *(a)Experimental Raman signals of the different carbon allotropes; DFT computed Raman signals of (b) polyynes and (c) cumulenes [50]*

stretching of the CC triple bond. This oscillation mode is also called ECC mode (from Effective Conjugation Coordinate model). No other allotrope shows signals in the 1800-2200 cm^{-1} region, allowing an easier detection of CAWs. The signal is composed by two main bands: α, more intense and at higher wavenumbers, and β, less intense and at lower wavenumbers. Moreover, the signal shifts to lower wavenumbers as the chain length is increased. α and β can be interpreted in terms of the longitudinal optical (LO) phonon branches of the corresponding infinite chain [31]. Similarly to the electronic band gap, also the LO phonon branch is modulated by the BLA. So the vibrational stretching mode of finite polyynes with a given BLA can be correlated to the LO phonon branch of an infinte chain with the same BLA [31]. Cumulene, in principle, should not display Raman activity, due to the absence of an optical phonon branch. This is certainly true for infinite cumulene. However, Raman activity of cumulenic systems has been proven [50]. This can be explained by the fact that for finite cumulenic chains endgroups effects can cause a deviation from the perfect cumulenic structure, giving rise to optical activity.
In many synthesis techniques, the obtained concentration of polyynes is too low ($< 10^{-3}$ M) to be detected by Raman Spectroscopy. In this case Surface Enhanced Raman Spectroscopy (SERS) has to be used to achieve a good signal: this technique consists in the employement of metal nanoparticles to improve the Raman signal of the sp-chains by many orders of magnitude. The consequent generation of localized surface plasmons, upon illumination at the specific plasmonic resonance, on the metal nanoparticles, can enhance the Raman signal up to a factor of 10^6. As shown in Fig. 1.14, SERS peaks differ from Raman peaks: there is an overall shift of the peaks to lower wavenumbers, but also new features appear, which are

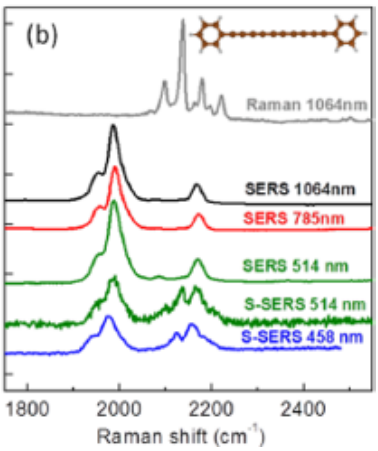

Figure 1.14: *SERS spectra at different wavelengths compared to Raman spectrum of a diphenylpolyyne [31]*

probably due to the interaction between polyynes and the nanoparticles [31].

Mass spectroscopic techniques

This last section is dedicated to two characterization techniques, which are less common than the previous ones in the field of polyynes, but, as it will be shown, can provide their characterization. The first one is standard mass spectroscopy, while the second is mass selective IR-UV spectroscopy, which combines IR absorption with Resonance Enhanced Multiphoton Ionization (REMPI) spectroscopy [51]. These two techniques have been used in two different experiments to analyze the fragmentation products of naphthalene in plasma conditions. These studies are actually an attempt to explain the possible formation mechanisms of large Polycylic Aromatic Hydrocarbons in the interstellar medium. In this sense, a plasma of naphthalene, which constitutes the fundamental PAH, represents an attempt to recreate the interstellar conditions. In both cases polyynes were detected, and seem to be an intermediate stage in the formation of PAH in space, which is reasonable given that polyynes were already found in interstellar media [52].
Mass spectroscopy is used to separate ions with different mass to charge ratio, by exploiting the Lorentz force. Once ions are created, they are accelerated by means of a potential difference towards a region where a constant magnetic field is set. Ions entering this region are isoenergetic, provided that they are all charged equally, and therefore have the same velocity. Due to Lorentz force $F_L = qv \times B$, ions are subjected to a centripetal force, resulting in circular orbits. By equating these forces the following relation is obtained:

$$r = \frac{mv}{qB} \tag{1.2}$$

where r is the curvature radius, m the mass, v velocity, q the charge and B the magnetic field. If v and B are kept constant, r only depends on the mass to charge ratio. This is the basic principle of a mass spectrometer. In the work of Alliati *et al.* [53], mass spectroscopy is used to identify ions produced by the fragmentation of naphthalene plasma. Experimentally, after vacuum is created, naphthalene powder is let in, where it sublimates. RF discharge is then applied, creating a pure naphthalene plasma, whose fragmentation products are then analyzed by the mass spectrometer. The mass spectra of both cations and anions are reported in Fig. 1.15. The anions spectrum clearly shows how ionic H-polyynes of four and six carbon atoms are the major fragmentation products. Also a small signal of C_8H^- is observed. Regarding the cations spectrum, signals of $C_2H_2^-$, $C_4H_2^-$ and $C_6H_2^-$ are detected. This suggests an opening of naphthalene's rings in favour of short linear structures, as already predicted by the work of Chen *et al.* [54].

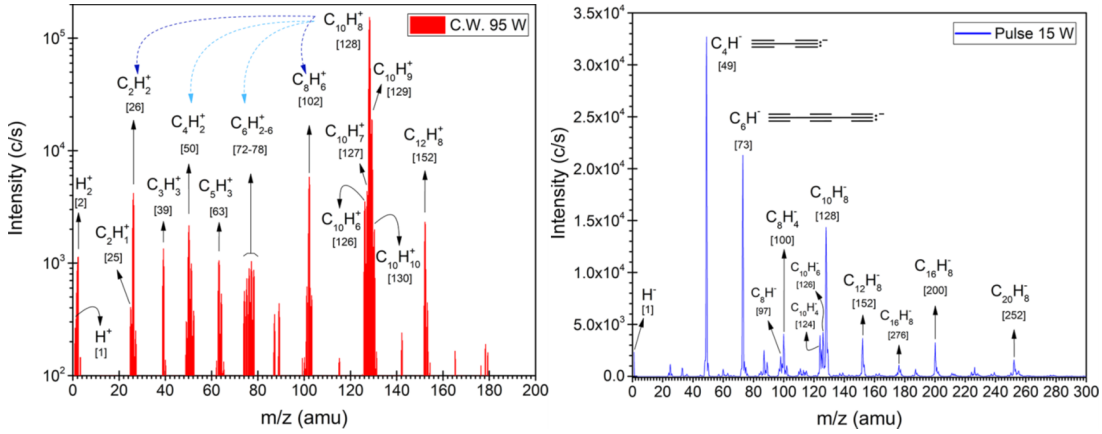

Figure 1.15: *Mass spectra of fragmentation and reaction products of a pure naphthalene plasma: cations in red, anions in blue [53]*

The second and last technique of this section is IR-UV ion-dip spectroscopy. It is a powerful but complex characterization method, which can implement traditional mass spectroscopy by detecting and identifying not only ions, but also neutral molecules. Moreover, since more isomers can refer to the same mass to charge ratio (especially at growing m/q), integrating this technique with theoretical computations can identify the correct isomer corresponding to a specific m/q. The basic principle will be briefly explained in the next lines. IR–UV ion dip spectroscopy is based on the change of the vibrational population in the electronic ground state of a molecule by IR absorption, which is probed by resonance-enhanced multiphoton ionization (REMPI) spectroscopy [51]. Basically, one laser is scanning in the UV-Vis region. When the laser energy is resonant with an electronic transition, the corresponding laser wavelength is fixed. Then, another laser wavelength in the UV-Vis region is set to ionize the excited molecule. The produced ions are then analyzed by a mass spectrometer. Once the two UV laser wavelengths are fixed, a laser scanning in the IR is introduced. This laser is set to fire just before the UV laser (in the order of nanoseconds). When the IR laser is resonant with a vibrational transition, the ground state of the molecule is depopulated and a decrease in the magnitude of the REMPI signal (an ion dip) will be observed [51]. The procedure is then repeated for all the other UV wavelengths which are found to be resonant with electronic transitions. In this way, IR spectra of specific m/z ratios are obtained, which can be assigned to the correct isomer by comparison with computed theoretical spectra. This is a simplified explanation of the method used by Lemmens *et al.* [55] to characterize the fragmentation products of a naphthalene plasma, very similarly to the experiment presented before. The mass-selective IR spectra of the main products are reported in Fig. 1.16, along with the theoretical simulations and the molecular structure of the correspond-

ing isomer. In this way molecules belonging to the different m/q are structurally identified. According to the authors, the most abundant fragment corresponds to $m/q = 126$, whose corresponding isomer is diacetylenebenzene, which can also be seen as a short polyyne of 4 carbon atoms, H-terminated on one end and with a phenyl group on the other (Fig. 1.16(a)). The formation of naphthalene with one (c) and two acetylenic units (e) is also a very interesting result.
Using naphthalene in a top-down approach as a source of phenyl-polyynes or naphthyl-polyynes, which are expected to be very stable, is one of the motivations that support this work.

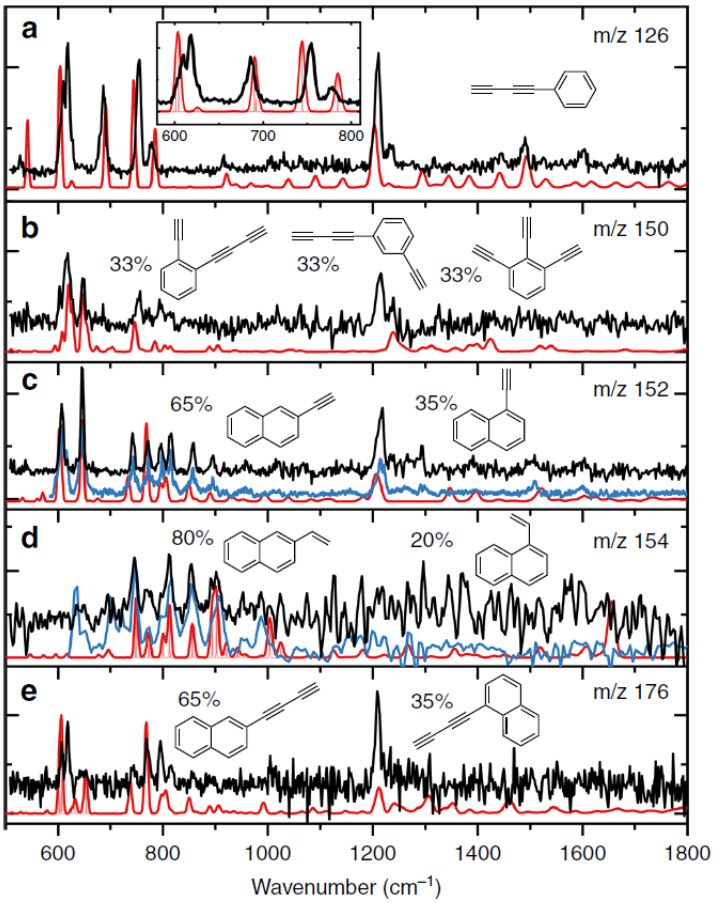

Figure 1.16: *Mass selected IR spectra (black) of discharge products with the assigned theoretical IR spectra (red). For b–e, two or more theoretical IR spectra of structural isomers are used to fit the experiment allowing for the determination of the ratio between the formed isomers. The blue trace in c and d corresponds to FT-IR reference spectra of the reported isomers combined with the reported ratio [55]*

Chapter 2

Pulsed Laser Ablation in Liquid

In the world of nanomaterials production, there are two main approaches: *top-down*, in which bulk materials are broken into nanosized particles, and *bottom-up*, in which nanostructures are built up atom by atom, molecule by molecule or cluster by cluster. Another common classification distinguishes physical methods from chemical methods.
Chemical methods were the first to be employed in the synthesis of carbon atomic wires. The first reported synthesis of a polyyne was performed in 1869 by Carl Andreas Glaser, who observed that copper phenylacetylide ($CuC_2C_6H_5$) undergoes oxidative dimerization in the presence of air to produce diphenylbutadiyne ($C_6H_5C_4C_6H_5$) [56]. During the years more elaborate methods were developed, and single-step polyyne synthesis in solution was achieved and attested by many authors [36], [43]. Today two approaches are pursued: the first follows a polymerization strategy, typically of acetylenic units, while the second is based on the dimerization reaction of ethynyl groups of targeted molecules with defined length and endgroup constitution [30]. Chemical methods offer higher control respect to physical ones: at the moment, in fact, they allow the synthesis of longer chains and the possibility to cap polyynes with bulkier endgroups [43], [57], [58]. In this sense, carbon chains with 44 atoms stabilized by bulky capping groups have been produced [57]. Moreover, the higher control on terminal groups can allow the stabilization of cumulenic structures [37]. The major drawback, however, lies in the material consumption: specific reagents are needed for the proper chemical reactions, as well as purification steps to eliminate unreacted reagents and unwanted products. As a result, chemical methods are quite expensive and not suitable for industrial production.
Physical methods, instead, are typically cheaper, simpler and more likely to fit the needs of production at an industrial level. The most relevant in the field of sp carbon chains are Submerged Arc Discharge in Liquid (SADL) and Pulsed Laser

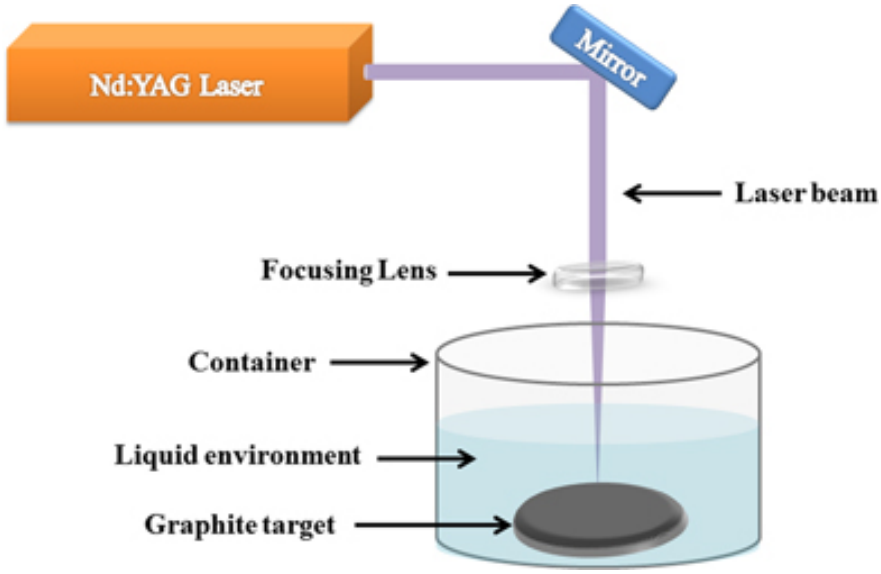

Figure 2.1: *PLAL schematic experimental set-up [61]*

Ablation in Liquid (PLAL). They both involve the formation of a plasma in a liquid solvent, creating unusual out-of-equilibrium conditions which promote the formation of sp-hybridized carbon [30]. The main difference between the two processes lies in how the plasma is created: in SADL, an electric discharge is applied between two conductive electrodes immersed in a liquid, leading to the generation of carbon nanoparticles and to the assembly of carbon nanostructures; in PLAL, instead, plasma arises by focusing laser pulses on a bulk target (typically graphite), also immersed in a solvent. In both cases the liquid has the double role of confining the plasma and providing a safe environment for polyynes. Moreover, in the case of organic solvents, it acts as an additional source of carbon atoms, leading to a higher concentration of polyynes [32], [59], [60].
In this chapter I will present a description of the physical processes occurring in PLAL, as well as the main parameters of this technique and some experimental and theoretical works about polyyne synthesis by PLAL.

2.1 PLAL physics

Pulsed Laser Ablation in Liquid consists in the ablation of a target immersed in a liquid solution by the action of a pulsed laser. As the laser hits the surface of the target, bulk portions of it are fragmented into nanoparticles, and a confined plasma region is generated. In most cases, also chemical modifications of matter occur. As a consequence, PLAL embodies aspects of both physical top-down and chemical bottom-up methods, with nanoparticles resulting both from nucleation

and growth and from ejection of target's fragments [62]. Several phenomena occur before and after a laser pulse, as displayed in Fig. 2.2, and strongly depend on the laser parameters. However, a complete understanding of the processes involved in laser ablation is not yet achieved.
Before reaching the target, the laser pulse must pass through a layer of liquid. Therefore, as a general rule, the liquid must be transparent in order to deliver the maximum amount of energy to the target. Moreover, liquid breakdown must be avoided, and this can be easily achieved by working with picosecond or longer pulses under defocused conditions [62]. For femtoseconds pulses, instead, non-linear optical effects arise at the fluences required for laser ablation, leading to multiphoton absorption by the liquid medium and to a consequent reduced energy density at the target depth [62]. Both linear and non-linear absorption processes occur when the pulse hits the target [63], and the thickness of the target in which

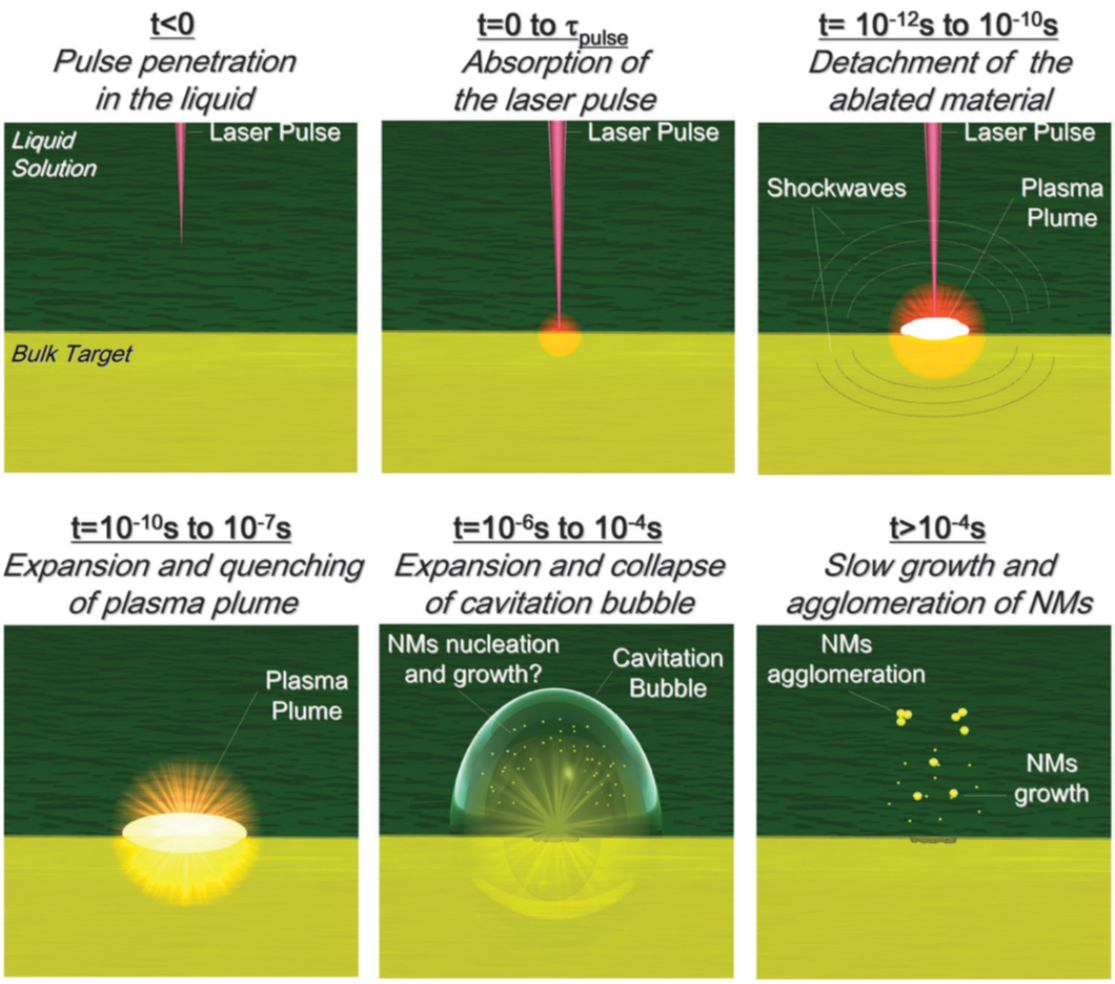

Figure 2.2: *Sketch of the timeline of all the processes occuring before and after the laser pulse hits the target [62]*

these happen is called skin depth. Since optical absorption is simultaneous to laser-matter interaction, direct photoionization lasts for a time equal to the pulse duration [64]. Direct photoionization is highly probable for pulses up to 10^{-8} s [64] and, together with multiphoton absorption, initiates the detachment of target fragments [65]. These processes induce local space charge fields and electron-ion collisions, which in turn lead to material ejection [65]. Additionally, if the pulse duration is higher than 10^{-12} s (i.e. the minimum time required for electron-lattice thermalization), electrons can transfer kinetic energy to the lattice, triggering thermal processes such as boiling, melting and thermoionic emissions [62]. In this case, material detachment is promoted also by the heating of the lattice, increasing the volume of the ablated material. A complete description of the ablation mechanism is quite complex, since many fragmentation paths are possible. According to classical thermodynamics, which can be used as a first approximation, three classes of thermal processes lead to material detachment: vaporization, normal boiling and explosive boiling [66]. Explosive boiling, also called phase explosion, is considered the primary process for pulses shorter than 10^{-7} s. It consists in solid matter superheated up to thermodynamic critical temperature, at which the spinodal decomposition in vapor and liquid in the irradiated material occurs by homogeneous nucleation [62], [66]. For fs or ps pulses, out-of-equilibrium conditions are set and do not permit a classical thermodynamic description.
During the ablation process, the recoil pressure of the ablated material induces one shockwave propagating inside the target and one specular propagating into the liquid [63]. Shockwaves represent discontinuities in density and temperature profiles, heating both the target and the liquid, and thus promoting material ejection [67]. The ablated material is considered as a "plasma plume" out of equilibrium, with temperatures reaching 10^3 K and pressures of the order of 10^9 Pa [62]. It contains highly ionized species, electrons, but also melted drops and solid fragments. The liquid spatially confines the plasma plume onto the target surface. This has the important consequence that target ablation occurs not only by energy transfer from the laser pulse, but also from the heating by plasma plume itself [68]. Energy transfer from the plasma plume can go on even after the end of the laser pulse [68]. Indeeed, after about 10^{-7} - 10^{-8} s from the pulse generation, the plasma is quenched and its energy is released to the surrounding liquid, which instantaneously evaporates leading to the formation of cavitation bubbles [62]. These bubbles travel at supersonic speed (10^3 m/s), expand and collapse when the inner pressure drops below the pressure in the liquid. The collapse causes the emission of another shockwave. Moreover, temperatures and pressures can reach levels similar to the ones of the plasma plume, and this can lead to aggregation, phase transitions and precipitation of the atomic species contained in the bubble.

An important and still unclear point of the physics of the laser ablation in liquid, is connected to the time window in which the formation of nanoparticles takes place [62]. Some suggest that nanomaterials travel in front of the cavitation bubbles [69], others that they are formed inside the bubbles [68]. Another hypothesis is that, being thermal conductivity higher in liquid than in gases, a temperature gradient establishes at the bubble-liquid interface, inducing condensation of nanostructures [70].

2.2 PLAL parameters

In the last section the complexity of the PLAL physics has been outlined. The incomplete understanding of the whole process is also due to its strong dependence on the operating conditions. In the next paragraphs, I will discuss the main PLAL parameters (i.e. laser and material parameters) and their effect on the ablation process in the case of nanoparticles.

2.2.1 Laser parameters

The laser wavelength is a primary parameter. Typically employed wavelengths range from the UV to the near IR. It is common practice to use a wavelength that is not absorbed neither by the solvent nor by the nanoparticles. Excitations of the nanomaterials just synthesized, in fact, may lead to further modification and reactions [71]. The target skin depth depends on the wavelength: UV radiation is more uniformly absorbed, while IR photon are preferentially absorbed by defects and impurities [72]. Moreover, wavelengths in the UV favour processes like multiphoton absorption and photoionization, with direct effects on the plume temperature and pressure [73].
Pulse energy is another major parameter. The amount of nanoparticles increases linearly with the pulse energy, as far as the dominating ablation process remains the same [62]. Higher energies activate multiple ablation mechanisms, and can promote the detachment of solid and melted fragments [73] A broader size distribution of nanoparticles is observed when the pulse energy is increased [74].
The spot area is the portion of target hit by the laser pulses. The ratio between pulse energy and spot area is called "fluence", and is expressed in J/cm^2. Increasing the spot area at constant fluence results in a larger amount of ablated material, and therefeore a higher production of nanoparticles. Larger size distribution and larger mean size of NPs have also been reported when the spot was increased at constant fluence [62].
Pulse duration (τ_{pulse}) has already been shown to determine the hierarchy of pro-

cesses in the ablation mechanism. Pulses longer than the thermalization time of electrons activate thermal detachment processes, and are favoured at the expense of photoionization mechanisms when τ_{pulse} is increased at constant fluence [73]. In this case, craters on targets surface have more blurred edges respect to shorter pulse durations [73]. For microsecond and millisecond pulses thermal ablation phenomena largely prevail, and a plasma plume is no longer required to generate fragments and nanoparticles [62]. When τ_{pulse} is longer than 10 ps, there is a temporal and spatial overlap of the laser pulse with the plasma plume, meaning that the plume itself absorbs energy from the laser pulse [62]. This effect is called "plasma shielding", because it reduces the amount of laser energy directly delivered to the target, while increasing the temperature and the lifetime of the plasma plume [65]. Size distribution of NPs was found to be sharper with ns pulses respect to ps and fs pulses [71].
Repetition rate is inversely proportional to the interval of time between two consecutive laser pulses. Productivity per unit time increases with repetition rate, but only for time intervals longer than the lifetime of the cavitation bubble, which is in the order of 10^{-4} - 10^{-3} s [75]. This corresponds to repetition rates of 10^3 - 10^4 Hz, and represents an upper limit beyond which the synthesis yield decreases [75]. Increasing the repetition rate increases also the local concentration of NPs near the crater, and this can lead to coalescence, aggregation and scattering of the incoming laser pulses [76].
The number of pulses is defined as the product between repetition rate and ablation time [62]. A higher number of pulses leads to a larger amount of ablated material, but it may induce also morphological transformations in the ablation products and in the target geometry, which can undergo modifications [62]. An irregular target surface can, in turn, lead to a decrease ablation efficiency and possibly trigger unwanted secondary mechanisms [62].

2.2.2 Material parameters

Physical processes happening during the ablation depend not only on the laser operating conditions, but also on the materials involved, i.e. the target, the solvent and, if present, the solutes.
The target provides the raw material for the synthesis of nanostructures, even if, in some cases, also the solvent can contribute. Since NPs production is the most popular use of PLAL, the most common ablated materials are metals, like gold, silver, copper, platinum, cobalt and many others [77]. Also metal alloys can be ablated, although in this cases it is more difficult to control the NPs stoichiometry [62]. Other ablations can involve semiconductors, oxides, and graphite. The shape of the target has a relevant effect on NP's production. The most common geome-

tries are disks, cylinders and wires. It has been demonstrated that wire-shaped silver targets increase the productivity up to a factor of 15 respect to ablation of a planar surface [78]. The roughness also affects the ablation yield: polished planar targets possess higher reflectivity, while rough surfaces absorb more light [62].
The role of the solvent, besides the collection of nanoparticles, lies in the confinement of the plasma plume, which provides additional energy transfer to the target. The confinement of the plasma is influenced by the physical and chemical properties of the solvent. Viscosity, for example, enhances the confinement and hinders the diffusion of fragments and nanoparticles. It also prolongs the lifetime of cavitation bubbles [62]. The solvent chemistry has a deep effect on the ablation products: the use of water in the ablation of metal targets like Cr, Co, Cu or Mn, for instance, favours the formation of oxide NPs rather than metallic ones, which are more likely to be obtained in organic solvents [62]. Moreover, different organic solvents yield differences both in the shape and in the composition of NPs. A visual example of the diversity of species obtained ablating different targets in different liquids at the same laser parameters is shown in Fig. 2.3 [62]. Another

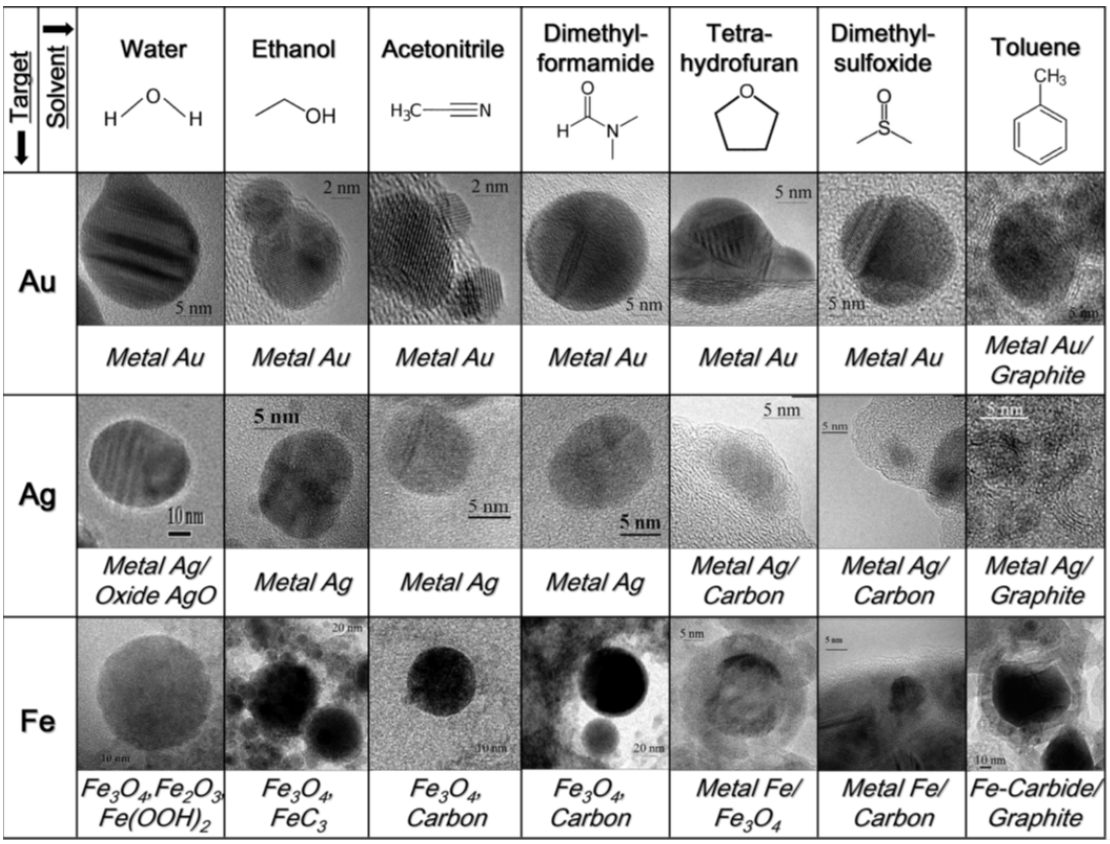

Figure 2.3: *Comparison between the NMs obtained by laser ablation of Au, Ag and Fe bulk targets in different solvents with 9 ns pulses at 1064 nm and 10 J/cm^2 [62]*

important aspect is the solubility of gases in the solvent. Oxygen, for example, is detrimental for metallic NPs, because it causes oxidation reactions and therefore degradation. Also solvents can degrade during ablation or over time, leading to products different from the expected ones. The volume of the liquid is also an important aspect, because it defines the liquid layer thickness that the laser beam has to go through before reaching the target. An optimal value of thickness has been reported in the ablation of bulk silicon in water, for which the ablation rate is maximized [79].
Solutes modify the physico-chemical properties of the liquid solution, acting on viscosity, density and surface tension. However a complete understanding of the the effect of solutes on the liquid during ablation is impeded by the interaction of solutes with the ablated material, which can have different degrees of intensity [62]. At the lowest level of interaction, solutes and NPs interact only physically. Many works show how the average mean size of NPs is reduced when solutes are added: it is believed that solutes are physically adsorbed on NPs surfaces, limiting growth and coalescence [62]. When the interaction is stronger, chemical bonding can occur between solutes and NPs, resulting in irreversible capping and effective growth limitation [62]. At the highest level of interaction chemical reactions modify the composition of NPs. This can happen even at lower level of interaction due to temperature activated chemical reactions [62].

2.3 PLAL for polyyne synthesis

The use of PLAL to synthesize carbon nanostructures is quite recent and not fully consolidated, therefore many studies were performed using different apparata. In the field of polyynes, the first laser ablations were carried out in a gaseous environment, then liquids proved to be much more efficient in nanomaterials collection and stabilization [29].

2.3.1 Formation mechanisms of hydrogen-capped polyynes

As for the case of nanoparticles, the formation mechanism of polyynes during laser ablation is not fully understood. In 1993, Wakisaka *et al.* experimentally confirmed the simplest growth process of carbon clusters, namely $2C \rightarrow C_2$, by ablating a graphite target in benzene[80]. In their work H-capped polyynes were not observed. However, due to the interaction of carbon clusters with benzene, phenyl rings attached to one and two acetylenic units were detected, which may be seen as a very first step towards stable phenyl-capped polyynes. In 1996, Gaumet and his team extended this study by exploring different wavelengths and different pulse energies

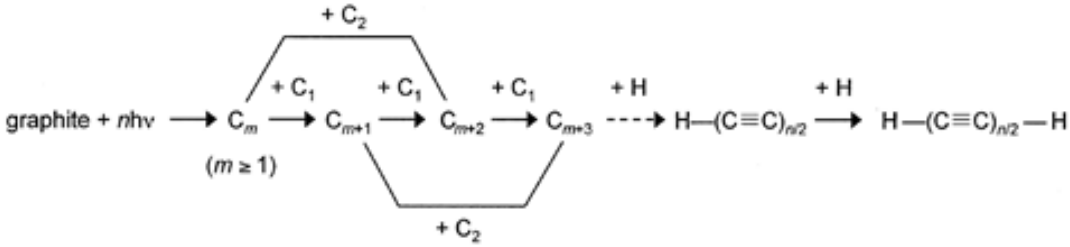

Figure 2.4: *Schematic representation of the competition between polymerization and termination of H-polyynes [82]*

[81]. The main outcome of the work was the distinction between two competing reactions: the addition of carbon clusters to a phenyl radical and the aggregation of carbon clusters resulting in H-polyynes. In 2002, Tsuji, while exploring the effect of different solvents in the ablation of suspended graphite particles, proposed a scheme, depicted in Fig. 2.4, for the formation mechanism of H-polyynes [82]. It explains the formation of polyynes on the basis of the competition between polymerization (addition of C atoms) and termination (C-H reaction). The degree of polymerization (i.e. amount of long chains) is found to be solvent-dependent [82]. Also Compagnini *et al.*, who reported the formation of polyynes by pulsed laser ablation of a carbon rod in water, claimed that hydrogen-capped polyynes are formed by polymerization and hydrogenation of C_2 and C_2H radicals through a chain reaction [83]. Therefore, it is considered that the concentration of hydrogen and C_2 radicals in the plume plays an importance role in the formation of hydrogen-capped molecules [60].

This work aims to a better comprehension of this competition by analyzing how the yield of polyynes varies as the the C/H ratio of the solvent changes, in order to achieve a deeper understanding of the nature of polyynes formation in laser ablation in liquid. The C/H ratio of a solvent constituted by m components is defined in the following way:

$$\frac{C}{H} = \frac{\sum_{m=1}^{\infty} N_A n_m N_{C,m}}{\sum_{m=1}^{\infty} N_A n_m N_{H,m}} \tag{2.1}$$

where N_A is the Avogadro number, n_m the number of moles of the m component, $N_{C,m}$ and $N_{H,m}$ the number of carbon and hydrogen atoms contained in the m component, respectively. Only H atoms bound to C atoms are taken in account in this calculation.

Furthermore, I will try to explore the conditions which favour the formation of longer polyynes. In the next paragraphs, following the scheme of the previous section, the effects of PLAL parameters on polyynes formation are discussed. Since this thesis focuses on the material parameters, higher attention will be dedicated

to this part. The motivations under this work will be justified in the framework of the results reported in literature.

2.3.2 Laser parameters

Laser wavelength

In the majority of the works in literature, the most employed wavelengths are 1064 nm, 532 nm and 355 nm, which respectively correspond to photons in the near infrared, in the visible (green), and in the UV region [82], [84]–[86]. The effect of the wavelength on polyynes' yield is not completely clear, due to contradictory results in literature. In the already mentioned work of Tsuji, the effect of different wavelengths (355, 532 and 1064 nm) in ablations of suspended graphite particles (75 μm average diameter) in solution was explored [82]. The result showed a decrease in polyyne signal as the wavelength was increased, concluding that photochemical processes provoked using 355 nm are more relevant in the formation of polyynes respect to the thermal processes induced by the other two wavelengths [82]. Matsutani and coworkers, instead, found an opposite trend, confirmed also by others: the production of polyynes increased at longer wavelengths, when ablating a graphite and a fullerene pellet in the same solvents empolyed by Tsuji [84]. This outcome was explained in terms of scattering of photons and absorption by the solvent: shorter wavelenghts, in fact, are more easily scattered by impurities present in solution, as well as more easily absorbed by the solvent. Longer wavelengths, therefore, can deliver more energy to the target. The contrast with the previous results was reasonably justified in terms of the difference in target geometry: Tsuji *et al.* used a graphite powder dispersed in solution (magnetically stirred, and thus uniform in the distribution of graphite particles) [82], while in the research of Matsutani *et al.* the graphite target was a pellet, deposited at the bottom of the optical cell [87]. Since the laser beam enters the cell from the top, a great amount of polyynes is produced in the upper region of the cell when graphite powder is used [87]. Therefore the laser beam irradiates graphite particles without really passing through the solvent, thus avoiding scattering by impurities and absorption by the solvent when the UV laser is used [87]. On the other hand, because the pellet lies at the bottom of the cell, the beam has to go through the solvent before reaching the target, causing scattering and absorption at the shorter wavelength [87].

Pulse energy and duration

In Section 2.2.1, it was reported that a higher amount of energy implies a higher production of ablated material, and thus a higher amount of nanoparticles. This

general rule can be applied also to polyynes. In the work of Park, for example, a doubling of the pulse energy led to a larger amount of polyynes, irrespective of the wavelength employed [86]. The improvement, however, was more relevant for the shorter polyynes respect to the longer ones.
About pulse duration, unfortunately, no systematic study was found in literature. It is fair to say that in most works a laser system pulsing in the order of ns is used, although there are examples of ablations with femtoseconds laser pulses [33], [88]–[90]. However, most of these works deploy a different setup and the laser beam is focused in the solvent [33], [91].

Repetition rate and ablation time

The most common repetition rate in the field of polyynes is 10 Hz. It was experimentally found that higher repetition rates (1 kHz) lead to the formation of nanodiamond, which is stabilized by the high pressure generated [92].
Regarding ablation time (or number of pulses), there is no agreement in the experimental results found in literature. It is accepted, however, that ablation time has a strong effect on polyynes' length distribution, though this effect is not totally clarified. Tabata *et al.* claimed that a higher fraction of long polyynes is produced at shorter ablation times, and that their formation occurs in the first stages of ablation [93]. According to Park *et al.*, instead, polyynes concentration of any length increases with ablation time [85], while for Shin *et al.* a saturation in polyynes production is observed for ablation times longer than 30 minutes [94]. Moreover $HC_{30}H$, the longest polyyne obtained by PLAL, was observed at an ablation time of 52.5 min, which has been defined as an optimized time by the authors of this study[48].

2.3.3 Material parameters

Target

Graphite is the most used target in PLAL for polyyne synthesis. Different shapes are found in literature: graphite particles can be dispersed or suspended in solution [82], or a bulk target is ablated [32], [48], [49], [60]. Bulk targets can have different geometries: ablations of graphite rods, disks and pellets are easily found in literature. It has already been explained in Section 2.3.2 how the trend of polyynes production as a function of wavelength is inverted when moving from a graphite pellet to a dispersion of graphite particles. Also the concentration of produced polyynes differs in the two cases: experimental results show that a greater amount of polyynes is obtained from powder rather than pellets [87]. On the other hand, concentration of longer polyynes is higher from pellets than powder. This can be

explained as follows: when powder is irradiated, more nucleation sites are created, and so more polyynes are produced; at the same time, graphite powder can more easily undergo termination by H-atoms, since particles are surrounded by the solvent, and therefore longer polyynes are produced in lower quantities. In a graphite pellet, instead, a higher amount of energy can be focused on their surface: if the rate of radicals production exceeds the diffusion rate of the same radicals, than longer chains are obtained [87]. Analogously, graphite cylindrical rods were found to produce less but longer polyynes respect to pellets [48]. This is explained in terms of the target hardness: the higher hardness of rods leads to a lower dispersion of graphite powder, and thus to a lower total amount of polyynes, but to a higher concentration of the longer ones. Matsutani *et al.*, in fact, were able to characterize $HC_{30}H$ when ablating the rod, while the longest polyyne produced when using a pellet was $HC_{28}H$ [48].
Besides graphite, there is also record of ablations of carbon nanostructures suspended in solution. A nanodiamond dispersion in ethanol was shown to lead to the formation of $HC_{16}H$, while $HC_{14}H$ was the longest chain obtained from a dispersion of graphite [93]. According to the authors, this is due to the direct evaporation of sp^3 carbon. In fact, the energy of the photons is absorbed by the first amorphous layers of the diamond nanoparticle and converted into thermal energy in the inner layers, causing the graphitization of diamond. Then, graphitic carbon evaporates. If the thermal energy is large enough, diamond carbon atoms can evaporate without passing through the stage of graphite, and this is believed to increase the concentration of longer polyynes. Other examples of ablated carbon nanostructures are nanotubes and fullerenes [95], [96]. In both cases only polyynes up to $HC_{12}H$ were observed. In the case of fullerenes, the yield of polyynes decreased when a higher concentration of C_{60} was irradiated.
There are also a few cases in literature in which a target different from a carbon material is used. Solid methane and hexane films have been ablated in appropriate conditions [97], [98]. Matsutani and his team compared ablations in various solvents of PTCDA (a dye molecule) and graphite: graphite led to a higher concentration and longer polyynes [87]. However, a correlation was found between the amount of polyynes produced from PTCDA and the polarity of the solvent. In the next section, the solvent influence on polyynes production will be discussed.

Solvent

The solvent properties strongly affect the production of polyynes. A variety of solvents has been employed in laser ablations: deionized water, alcohols, alkanes, acetonitrile, aromatic solvents are some of the main examples [32], [60], [82], [83], [87]. Among these, water is the only one which does not contain carbon. Therefore,

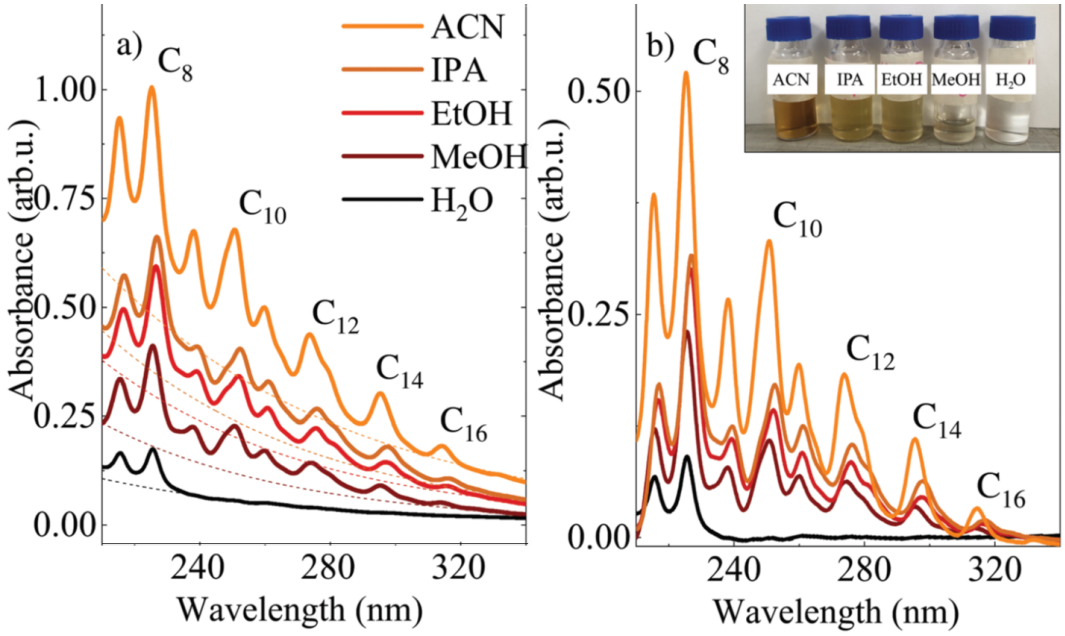

Figure 2.5: *UV-Vis spectra of filtered solutions of polyynes before HPLC separation with (a) background (dotted lines) and (b) with background subtraction. [32]*

it does not provide additional carbon atoms in the polyynes formation process, and results in being the worst solvent in terms of polyynes production [32], [60]. The importance of organic solvent contribution to polyynes formation is proved by the synthesis of polyynes up to $HC_{18}H$ by fs laser irradiation of toluene focusing the laser on the liquid meniscus, reported by Ramadhan *et al.* [33]. Laser ablations in water as solvent, instead, have never led to polyynes longer than $HC_{12}H$ [83]. Also hydrogen generation rate is believed to be lowest in water: the H-O bond (4.8 eV) is less likely to break respect respect to molecular bonds in organic liquids such as C–H (4.3 eV), C–C (3.6 eV) and C–O (3.7 eV) [32]. This could hinder the termination by hydrogen and thus the formation of H-polyynes. However, some found that the relevant factor in the production of polyynes is not the bond dissociation energy, but the relative amount of hydrogen respect to carbon [60]. In the work of Peggiani *et al.* [32], in which the effect of water, methanol, ethanol, isopropanol and acetonitrile has been systematically investigated at the same experimental conditions, a higher total concentration of polyynes for increasing C/H ratios of the solvent was observed. The UV-Vis spectra of the polyyne mixtures obtained in the different solvents are reported in Fig. 2.5, with (b) and without background subtraction (a). The background is related to the presence of hydrocarbons, which are formed as side products during the ablation. Acetonitrile is more prone to carbonization respect to alcohols, thus the higher contribution of C

	Water	**Methanol**	**Ethanol**	**Isopropyl-alcohol**	**Acetonitrile**
C/H	0	0.33	0.4	0.49	0.66
Polarity	100	76.2	65.4	54.6	46
Oswald coefficient	0.031	0.2476	0.2417	0.2463	0.00083

Table 2.1: *Relevant solvent properties considered in [32]*

atoms in the plasma plume results in a higher amount not only of polyynes, but also of hydrocarbons [32]. Since polyynes are liable to oxidation, the quantity of oxygen dissolved in the solvent is also a relevant factor. Oxygen solubility can be expressed with the Oswald coefficient "I", defined as the ratio of concentrations of the oxygen in the liquid and in the gas phases [32]. Indeed, acetonitrile has the lowest Oswald coefficient respect to alcohols and water, as reported in Table 2.1, and therefore undergoes minor degradation respect to the other solvents. This also partly explains why polyynes are more concentrated in ACN [32].
The increase in polyyne production was correlated also to a decrease in the polarity of the solvent. This trend, shown in Fig. 2.6, is found to be opposite (excluding H_2O) respect to the "index of purity" χ_p, which is defined as the ratio of the absorption related to H-polyynes to that of the fitted background of hydrocarbon by-products [32], [99], [100]. The effect of polarity on polyyne concentration is in agreement with the work of Matsutani, although the trend was observed only for the PTCDA pellets, and not for graphite [87]. Their result is shown in Fig. 2.7,

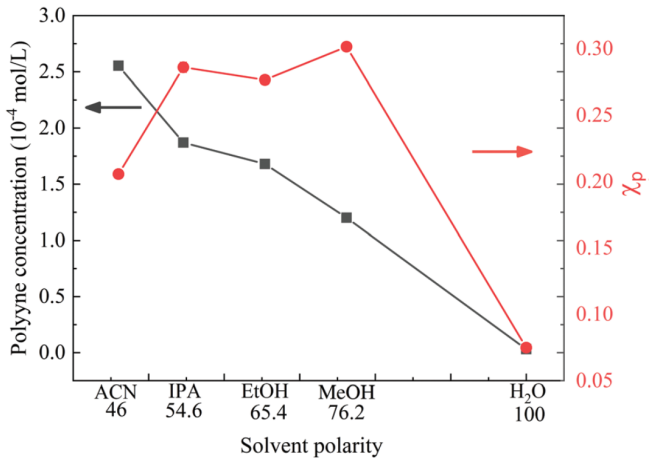

Figure 2.6: *Polyyne concentration (black) and index of purity (red) as a function of solvent polarity [32]*

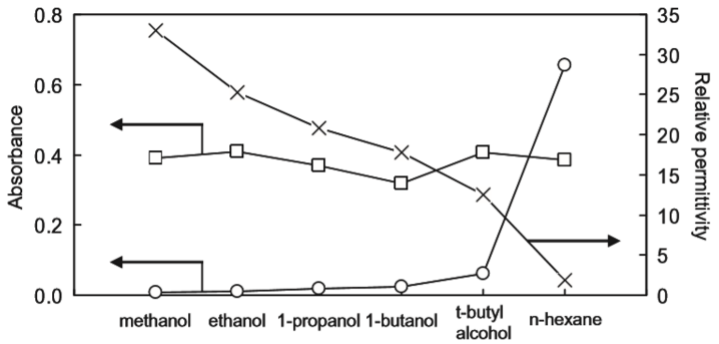

Figure 2.7: *Absorbance at peak tops of $HC_{10}H$ produced from pellets of PTCDA (circles) and graphite (squares). The irradiation times were 45 (PTCDA) and 5 min (graphite). Permittivity is also shown (crosses) [87]*

in which permittivity is reported as a measure of polarity.
Another aspect strictly related to the solvent nature is the possibility to obtain terminations different than -H. Deuterium terminated polyynes were obtained in deuterated water [60]. Cyano-polyynes (H-C$_n$-CN) have been detected only when using acetonitrile as solvent [32], [59], [101]. Methyl-polyynes (H-C$_n$-CH$_3$) were synthesized in hexane [102], in alcohols [32] and in laser irradiation of toluene [33]. Viscosity is also believed to be an important parameter: HC$_{30}$H, the longest polyyne ever produced by PLAL, was obtained ablating a graphite rod in decalin at 1064 nm [48]. The authors attributed this result to the high viscosity of decalin, which suppresses the diffusion of C_2 radicals and favours polymerization at the expense of termination. Moreover it was supposed that termination by H on both ends of a polyyne molecule may hardly occur in decalin with relatively smaller number of hydrogen atoms [48]. This is one of the reasons that motivated the investigation of tetralin and naphthalene in this thesis work. From the comparison between the molecular structures of decalin, tetralin and naphthalene, represented in Fig. 2.8, it can be seen how the major difference lies in the number of hydrogen atoms. Unluckily, naphthalene is a solid at room temperature, which

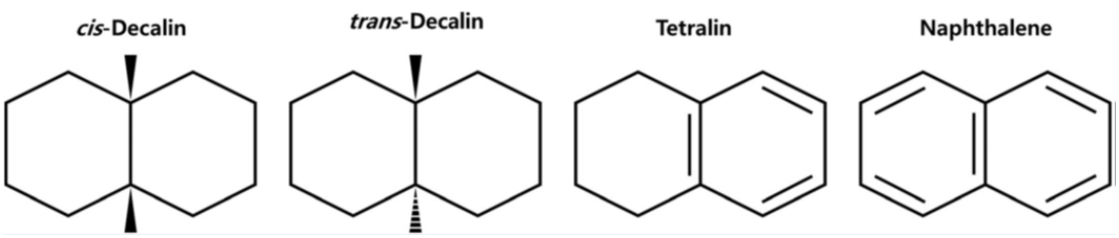

Figure 2.8: *Molecular structures of trans- and cis-decalin ($C_{10}H_{18}$), tetralin ($C_{10}H_{12}$) and naphthalene ($C_{10}H_8$) [103]*

makes it difficult to compare its effect to its hydrogenated derivatives (i.e. decalin and tetralin).
Anyway, I expect that moving from decalin to tetralin, the formation of long polyynes is promoted. Besides, it has been shown in the previous chapter how naphthalene, under plasma conditions, can lead to H-and phenyl-capped polyynes [55]. Investigation of this substances for the formation of longer and/or phenyl-capped polyynes is the main goal of this work.

Chapter 3

Materials and Experimental Methods

The first part of this chapter presents the materials used in the experiments, while in the second part, the experimental techniques used for the polyynes synthesis and characterization will be described.

3.1 Materials

3.1.1 Targets

For almost all the experiments conducted in this thesis work, the target used in PLAL synthesis of polyynes was a bulk graphite disk with a purity of 99,999 % (Testbourne Ltd), a diameter of 8 mm and a thickness of 2 mm. In the remaining ablations, a naphthalene target was employed, conceived and crafted in our laboratory during this project. Graphite was chosen as reference target, and its dimensions are related to the ones of the glass vials in which ablations are performed. The use of a naphthalene target, which has never been explored to synthesize polyynes according to present literature, was motivated by the hypothesis of producing polyynes capped by phenyl- or naphthyl-groups[43], [55]. Moreover, as it will be shown in the next chapter, ablations of naphthalene yield polyynes regardless of the solvent employed, and therefore the concentrations of the polyynes obtained by naphthalene will be compared to those synthesized from graphite at equal experimental conditions. The targets and the vial are shown in Fig. 3.1.

Graphite properties have already been introduced in Section 1.1. About naphthalene, instead, only a few features have been mentioned. Naphthalene is the simplest Polycyclic Aromatic Hydrocarbon, constituted by two fused aromatic rings, as shown in Fig. 2.8. At room temperature, it appears as a white crystalline solid. Naphthalene melts at 80 °C (at atmospheric pressure) [104], a feature that

Figure 3.1: *From left to right: the glass vial, the graphite target and the naphthalene target*

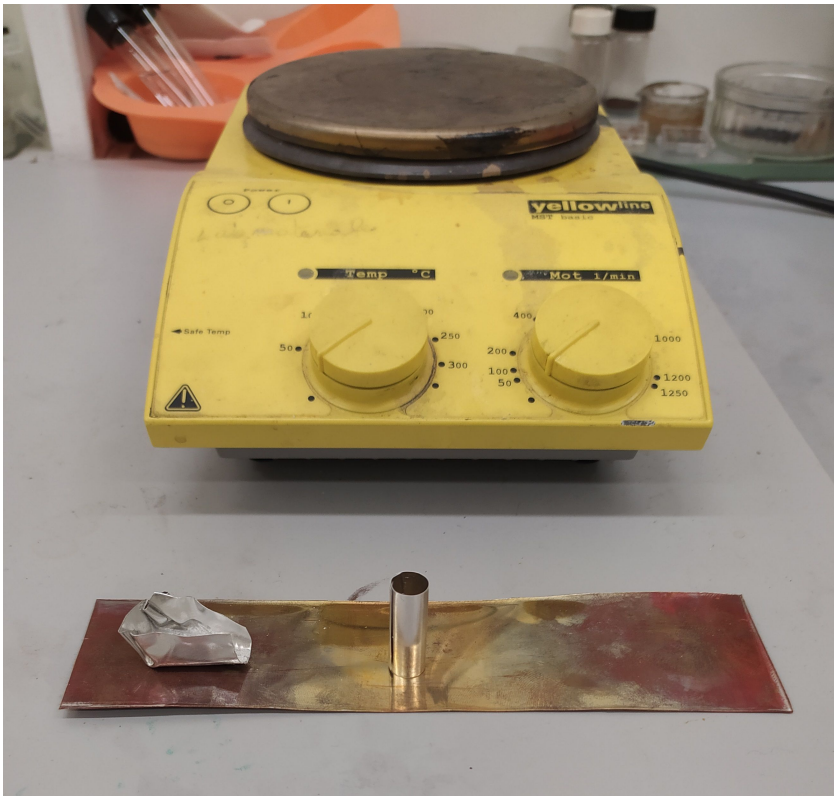

Figure 3.2: *Tools used to manufacture the naphthalene target: the substrate, the cylinder, the cup and the hot plate*

has been exploited to manufacture the target by pouring liquid naphthalene in a disk-shaped mold. The procedure is the following: first of all, a metal crucible is needed in order to melt naphthalene inside it. To do that, part of an aluminium foil was shaped in a "cup-like" geometry. Another part of the same foil, instead, was used to build the "mold", by wrapping it like a tube with the diameter of the final target. This tube is vertically placed on a metallic substrate, in order to be filled by liquid naphthalene. A picture of these tools is shown in Fig. 3.2. The handmade *Al* crucible is put on a hot-plate ($T_{max} = 350$ °C is the maximum reachable temperature) set on $T = 100$ °C. When the plate is at temperature, naphthalene crystals (approximately 150 mg) are placed inside the crucible, where they rapidly liquefy. Liquid naphthalene is quickly poured inside the Al "tube", where it solidifies. By doing this, given the fast solidification rate, a considerable fraction of naphthalene solidifies on the inner sides of the tube before reaching the substrate. Moreover, the surface tension of the liquid naphthalene generate a meniscus-like surface geometry. Thus, a second round of liquid naphthalene is needed to fill the concavity and obtain a nearly flat surface. Finally, the disk is polished on sand-paper until the desired thickness is reached. The final naphthalene target has a diameter slightly larger than the graphitic one and a comparable thickness. Unluckily the naphthalene target turned out to be strongly ruined by the laser pulses, and thus could be used only once.

3.1.2 Solvents

Different solvents have been used in order to analyze polyynes production in terms of their C/H ratio. Methanol (MeOH), ethanol (EtOH), isopropyl-alcohol (IPA), decalin (cis + trans mixture), tetralin and deionized water have been used as liquid media. The chemical structures of decalin and tetralin have already been shown in Fig. 2.8, while those of water and alcohols are shown in Fig. 3.3. Their main properties of the solvents are summarized in Table 3.1. Among these, decalin has been most extensively investigated, because it is the solvent in which the longest

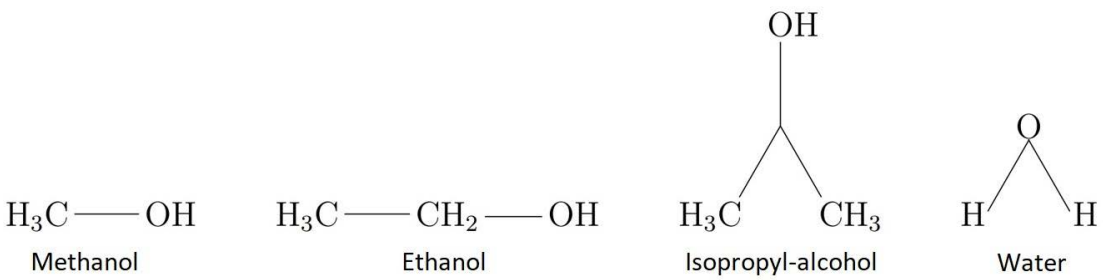

Figure 3.3: *Chemical structures of methanol, ethanol, isopropyl-alcohol and water*

polyyne has been synthesized [48]. For obvious reasons, water was not considered in the analysis of the C/H ratio of the solvent. It has been used only when ablating the naphthalene.
Apart from ablations in pure solvents, also binary liquid mixtures were investigated, in order to observe the effect of a more gradual increase of the C/H ratio: decalin and tetralin, featuring a higher value of C/H, were dissolved at increasing concentrations in ethanol, used as the low C/H reference solvent. The other properties were clearly affected: viscosity, for example, is increased, which is believed to favour the formation of longer polyynes [48]. Binary mixtures were carried out also by using naphthalene as a solute in ethanol, decalin and tetralin. Ablations at increasing concentration of dissolved naphthalene were performed with two goals:

- increase the C/H ratio of the system to favour the synthesis of long H-capped polyynes;
- promote the termination of polyynes by aromatic endgroups.

All binary mixtures were magnetically stirred for at least 10 minutes at room temperature to ensure homogeneity.
The solvents purities are HPLC grade type, i.e. $\geqslant$ 99% pure, except for tetralin, whose purity was $\geqslant$ 97%. Indeed, when performing HPLC measures, traces of naphthalene and decalin were detected in tetralin, along with other unrecognized

	Water	**Methanol**	**Ethanol**	**Isopropyl-alcohol**	**Decalin (cis+trans mixture)**	**Tetralin**
C/H	0	0.33	0.4	0.49	0.56	0.83
Dielectric constant at 20°C	80	32.6	22.4	18.3	2.2	2.77
Oswald coefficient	0.031	0.2476	0.2417	0.2463	0.1919	0.1186
Boiling Temperature [°C]	100	64	78	82	189-191	205
Viscosity at 25 °C [MPa s]	0.8949	0.6	1.08	2.0	1.948 trans, 3.042 cis	2.02
Refractive index at 25 °C	1.333	1.326	1.359	1.375	1.481	1.539

Table 3.1: *Properties of investigated solvents. Dielectric constants, boiling points, viscosities and refractive indexes are taken from [105]. Oswald coefficients of water and alcohols are taken from [32], the one of tetralin is from [106], while for decalin the value is obtained by conversion of its Henry constant [107], [108]*

peaks. The purity of the solvent is not only required by the HPLC instrument, which is very sensitive to impurities, but it is also expected to favour polyynes synthesis, since impurities might interfere in the formation process.
The solvent volume in the preliminary set of ablations was fixed at 2 mL, but then it was reduced to 1.5 mL for all the following experiments. A lower volume was chosen in order to optimize the consumption of solvents and increase the concentration of polyynes. In the ablations, the glass vial was placed inside a beaker filled with water at ambient temperature, to cool down the ablation solvent and avoid its evaporation, which can be relevant in alcohols, as can be observed by the low boiling points in Table 3.1. Moreover alcohols, especially ethanol, are quite flammable, so cooling by water was motivated also by safety reasons.

3.2 Experimental methods

3.2.1 PLAL

The experimental set-up of the PLAL apparatus is showed in Fig. 3.4. The laser is a Quantel Q-switched nanopulsed Nd:YAG laser with a repetition rate of 10 Hz. Its fundamental wavelength is 1064 nm, but also 532 nm and 355 nm can be employed by using second and third harmonic generator modules, respectively. In all the experiments performed the selected wavelength was 532 nm. I decided to work with this wavelength because the set-up is already optimized and many data are available coming both from the group experience and literature works. Using this

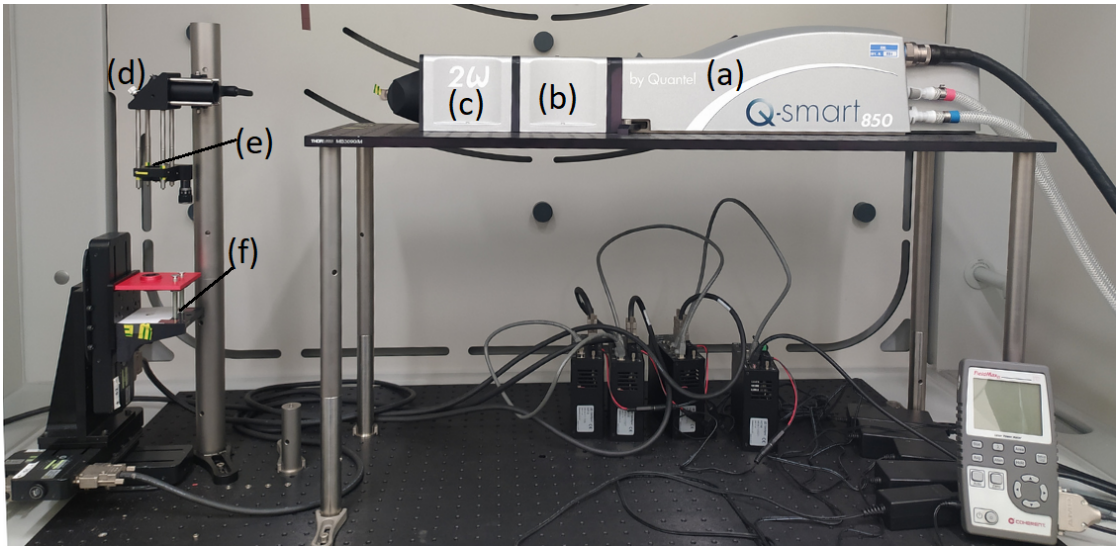

Figure 3.4: *PLAL experimental set-up: the laser head (a), the beam attenuator (b), the second harmonic generation module (c), the mirror (d), the focusing lens (e) and the stage (f)*

wavelength the pulse duration is 5 ns and the maximum energy per pulse is 380 mJ. It is possible to regulate the pulse energy from 380 down to approximately 0 mJ by means of a beam attenuator. The pulse energy is measured with the power-meter the set-up is equipped with. Once the energy is fixed, the mirror is removed and the ablation can start.
The laser beam has with a diameter of 9 mm. The optical path features a 45° degrees cut mirror that deviates the laser beam towards the focal lens, which has a focal length of 20 cm. Ablations were always carried out under defocusing conditions to avoid splashes of the solvent. As we move closer to focusing conditions, in fact, laser fluence becomes too high and results in the generation of splashes and, in the worst cases, flames. During the ablation, the target is kept in constant spiral motion to ensure a uniform irradiation of its surface. This is done thanks to a stage free to move in the three directions. The stage is composed by three translators (one per direction) connected to a controller which is connected to a computer and governed by a custom with an appropriate Python code. The code is used to calculate the fluence on the target, requiring the experimental parameters as inputs, and to control the laser flashlamp and firing activations.

3.2.2 High Performance Liquid Chromatography

High Performance Liquid Chromatography was the most widely used analysis method in this work. The system, represented in Fig. 3.5, is composed by an autosampler, a pump system, a degassing unit, an oven, a photodiode array detector and a fraction collector. It is a C8 column, whose stationary phase is constituted by silica particles (diameter of 5 μm), to which an alkyl ligand chain of 8 carbon atoms is attached. The column used is 25 cm long and has a inner diameter of 4.6 mm.
The photodiode array (UV-Vis spectrometer) is equipped with two lamps, a tungsten one and a deuterium one and allows simultaneous acquisition across a range of wavelength between 190 and 800 nm, rather than scanning one wavelength at the time. Thus, multiple spectra can be collected across the same chromatographic peak. Concentrations of polyynes have been calculated from the UV-Vis spectra extracted at specific wavelengths, i.e. the wavelengths corresponding to polyynes Most Intense Transitions, reported in Table 3.2.
A limit of this method is related to the solvents cut-off, which is the wavelength below which the spectrum is dominated by the absorption of the solvent. If the cut-off wavelength is longer than those of polyynes most intense electronic transitions, their signal is covered. From Table 3.3 and 3.2 one can see how this problem arises when tetralin and naphthalene-containing solutions are analyzed by UV-Vis spectroscopy.

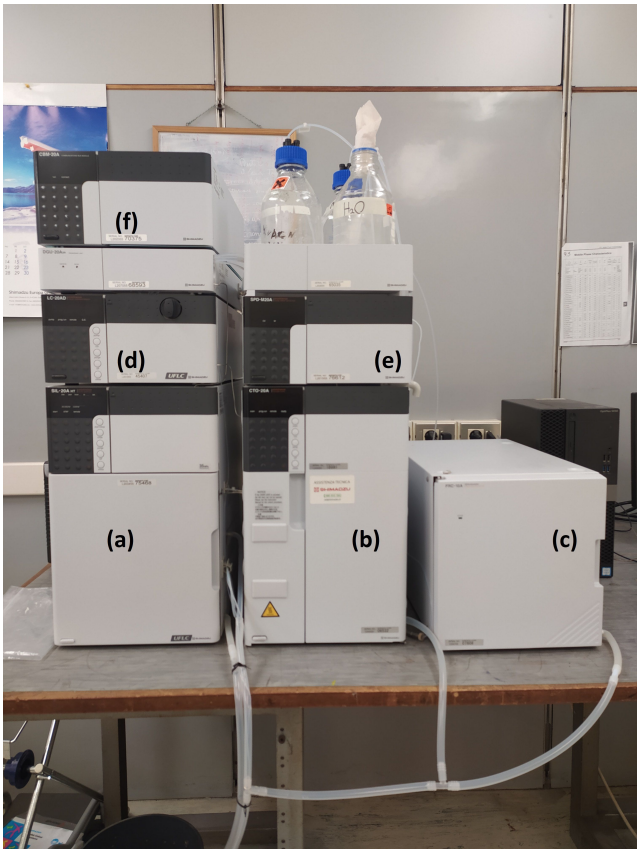

Figure 3.5: *HPLC system used in this work: the autosampler (a), the oven containing the column (b), the fraction collector (c), the pump system (d), the photodiode array detector (e) and the control system (f).*

	HC_6H	**HC_8H**	**$HC_{10}H$**	**$HC_{12}H$**	**$HC_{14}H$**	**$HC_{16}H$**	**$HC_{18}H$**	**$HC_{20}H$**
MIT wavelength [nm]	198	226	251	273	295	315	332	348

Table 3.2: *Most Intense Transition (MIT) wavelength of absorption of H-polyynes*

	Water	**MeOH**	**EtOH**	**IPA**	**Decalin**	**Tetralin**	**Naphthalene solution**
Cut-off wavelength [nm]	190	205	210	205	240	280	290

Table 3.3: *Cut-off wavelengths of investigated solvents. Values of water and alcohols are taken from [109], the remaining from laboratory measurements*

The mobile phase employed in my experiments was always a solution of water and acetonitrile (ACN), with a relative composition depending on the chromatographic method used. For almost all the experiments, a gradient method was adopted in the HPLC analysis: the flow of the mobile phase starts with a 50 % fraction of ACN for the first 3 minutes, then ACN concentration linearly increases until it reaches 90 % after 30 minutes of analysis. For the remaining 15 minutes of the analysis, the composition is kept constant. A gradient method with such as a smooth increase of ACN concentration was employed to ensure a good separation of the chromatographic peaks. Good separation was essential for two purposes, in this work: to obtain a precise value of the chromatographic area related to polyynes with specific length and termination, which allows a reliable calculation of their concentration; polyynes of the same length and different termination may have very similar retention times, thus their signal could be covered by the most intense peak related to the H-polyyne. The main defect of this well-separating method is the large amount of time requested for one analysis (45 minutes). Other major drawbacks are related to the compatibility of the some of the analyzed solvents with the HPLC column: decalin, tetralin and naphthalene, given their high apolar character, are strongly retained by the column and thus eluted as analytes. Thus, for the solutions containing these substances, only low volumes could be injected, in order to preserve the column integrity. Unluckily, these substances are eluted at the same retention time of some of the investigated polyynes. Fig. 3.6 and Fig. 3.7 show the chromatograms collected at 226 and 251 nm, respectively, of a mixture of polyynes from ablations in ethanol and in tetralin. Indeed, naphthalene was eluted at almost the exact time as HC_8H. In addition, the strong overlap between their absorption spectra did not allow to acquire data regarding HC_8H that were are totally lost in the naphthalene-containing solutions. Analogously, the peak related to tetralin overlapped with that of $HC_{10}H$ for injections of tetralin higher than 1 μL. Finally, also decalin was eluted almost together with $HC_{14}H$, but in this case decalin cut-off frequency lies below the electronic transitions of $C_{14}H_2$, allowing for a quite precise determination of the chromatographic peak of the polyyne.
An isocratic 80-20 ACN- water method of 20 minutes was used only in the ablations in water in the graphite and naphthalene targets.
Before being injected in the HPLC system, ablated solutions were all filtered through Phenomenex Phenex RC-membrane syringe filter having a pore size of 0.45 μm in order to remove particulates which could obstruct and damage the column.

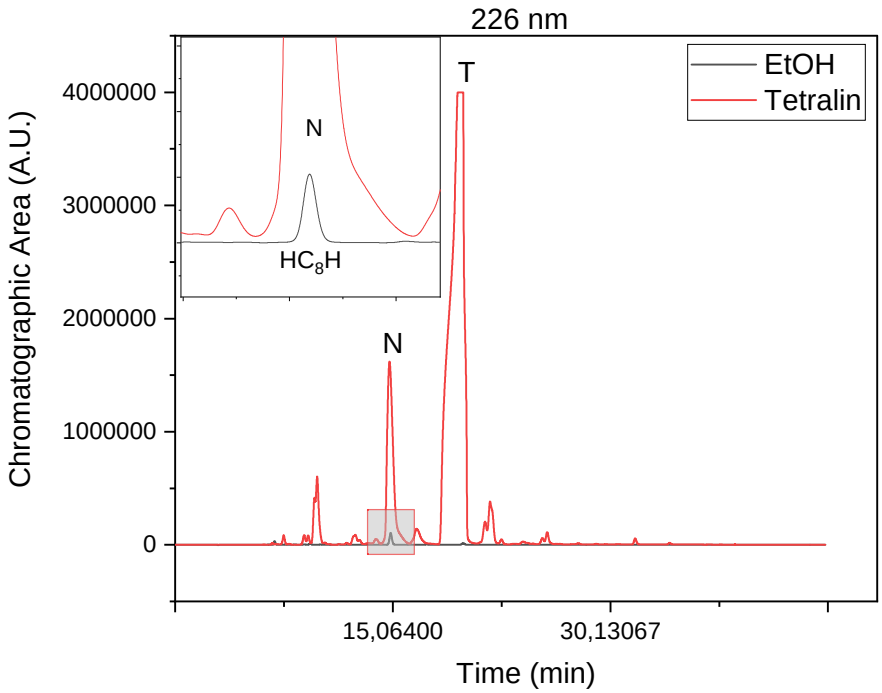

Figure 3.6: *Superposition of two chromatograms of ablations in EtOH and tetralin, both extracted at 226 nm. The peak of naphthalene (N) completely dominates* HC_8H*. Also the peak related to tetralin (T) is shown*

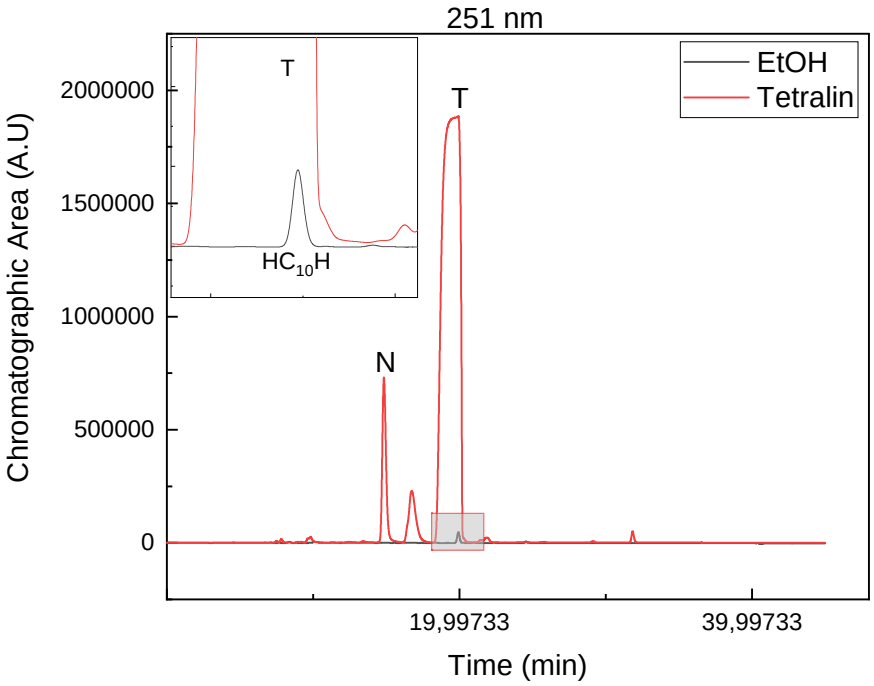

Figure 3.7: *Superposition of two chromatograms of ablations in EtOH and tetralin, both extracted at 251 nm. The peak of tetralin (T) completely dominates* $HC_{10}H$*. Also the peak related naphthalene (N) is shown*

Chapter 4

Experimental results

In the first part of this chapter, I will show the results of a preliminary analysis of the laser parameters to favour the production of longer H-polyynes at the expense of the shorter ones. The boundary that divides long and short chains was set to $HC_{14}H$. Ablation time and spot size have been more extensively investigated, while other quantities, such as the pulse energy, were kept constant throughout the work. The optimized parameters were employed in the following experiments of the second part, which focuses on the effects of the materials employed in the ablation process. Results regarding the effect of pure solvents and binary mixtures on the production of polyynes of different length will be presented.
The last part is dedicated to the ablations of a naphthalene target in different solvents, which will be compared to the case of graphite, kept as the reference case. In the results I considered the concentration of H-polyynes with 8, 10, 12, 14, 16, 18 atoms. Although the signal of $HC_{20}H$ was often detected, it was also too low to be considered in a reliable way, due to experimental error.
All the reported concentrations were converted from the relative chromatographic areas through a calibration curve obtained from a set of experimental data. The concentrations of a group of collected polyynes were calculated exploiting an external UV-Vis instrument and the molar extinction coefficients reported in the work of Eastmond *et al.* [110]. A linear regression fit was performed to evaluate the conversion from the chromatographic area of a specific chain to its corresponding concentration. So the following equation was used to analyze the data:

$$C = \frac{1.89749393825103 * 10^{-11}}{V_{inj}} A \tag{4.1}$$

where the concentration C is measured in mol/L, the injection volume V_{inj} in μL, while the chromatographic area A has arbitrary units. The fit possesses an error of 5.314 %, included in my analysis.

4.1 Optimization of parameters for the synthesis of long polyynes

In the first set of experiments, the conditions which can favour the formation of long polyynes were investigated, in terms of both laser and material parameters. Laser parameters were explored by employing decalin as solvent, since the longest polyynes obtained by PLAL reported in literature were synthesized using this solvent [48]. Regarding materials parameters, pure solvents were analyzed with the optimized laser parameters. A graphite disk was used as target in both parts.

4.1.1 Laser parameters: effect of ablation time and laser fluence

Ablation time

In Section 2.3.2 it was outlined how there is no particular agreement in the effect of the ablation time on the production of long polyynes. Therefore I performed ablations of 5, 15, 30 and 60 minutes, in order to analyze its effect on the yield of long polyynes. Pulse energy was fixed at 50 mJ/pulse, solvent volume at 1.5 mL and spot radius at 1 mm. Thus, the laser fluence, calculated exploiting geometrical optics and the setup described in Section 3.2.1, was 1.59 J/cm^2. Fig. 4.1 shows how the relative concentration of longer polyynes with respect to HC_8H decreases by increasing the ablation time. In other terms, at longer ablation times, the

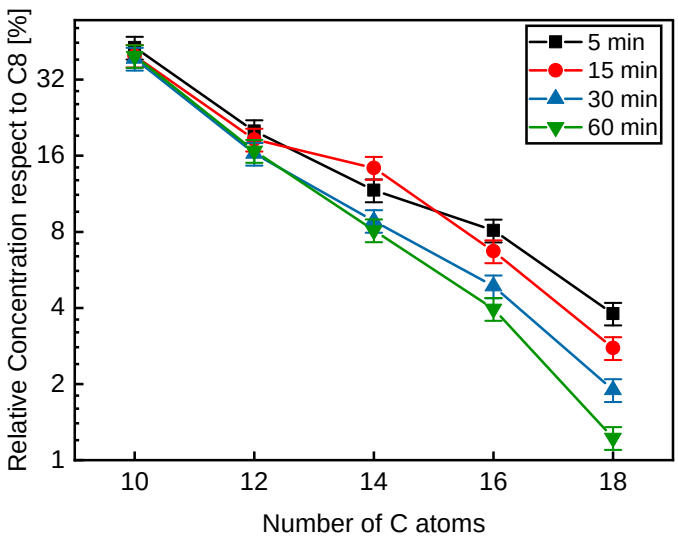

Figure 4.1: *Relative concentration of H-polyynes made by different numbers of carbon atoms respect to the concentration of HC_8H in each ablation*

increase in polyynes concentration is more relevant for short polyynes than for longer ones. Indeed, the concentration of HC_8H was more than six times higher in the 60 min ablation respect to that at 5 minutes, while the concentration of $HC_{18}H$ approximately doubled. Since the total concentration of polyynes increases at longer ablation times, we can suppose that long polyynes, which are more unstable than shorter ones, are affected by a stronger competition between production and degradation (i.e. crosslinking) as the ablation time is increased. The only two out-of-trend values are related to $HC_{14}H$ in the ablations at 5 and 15 minutes. However, as explained in the previous chapter, $HC_{14}H$ is eluted by the HPLC column with decalin, and therefore the values of its concentration are less reliable than polyynes of different length in ablations in decalin. For all the following results, the ablation time is fixed at 5 minutes.

Laser fluence

The other main laser parameter analyzed in this work is the spot area, which is strictly connected to the laser fluence. A set of experiments was performed to optimize the laser fluence by varying the spot area and keeping the pulse energy at a constant value of 50 mJ/pulse. All the ablations were carried out in 1.5 mL of decalin and for a time of 5 minutes. By definition, increasing the spot area at constant pulse energy causes a decrease in the laser fluence. Fig. 4.2 shows the concentration of H-polyynes of different length as a function of the spot area. Polyynes made by 8, 10, 12 and 14 carbon atoms are produced to a higher extent for a spot radius of 0.5 mm, corresponding to a fluence of 6.37 J/cm^2. The concentrations obtained at the smallest analyzed spot area (0.33 mm), corresponding to focusing conditions and to very high fluence (14.61 J/cm^2), lie always below the values obtained at 0.5 mm. For longer H-polyynes (i.e. $HC_{16}H$ and $HC_{18}H$), instead, an optimum was found at 0.75 mm, and thus at a fluence of 2.83 J/cm^2. Furthermore, the amount of $HC_{18}H$ was found to be higher at a spot radius of 1 mm (1.59 J/cm^2) respect to 0.5 mm (6.37 J/cm^2). Therefore it can be concluded that the formation of longer polyynes seems less favoured at higher fluences. Thus, the spot radius has been fixed at 0.75 mm for all the following ablations, since it appears to promote the formation of long polyynes, at a pulse energy of 50 mJ. The results I will present in the next pages, apart from a few exceptions, have all been obtained with the following parameters:

- ablation time: 5 minutes
- spot radius: 0.75 mm
- pulse energy: 50 mJ/pulse

- solvent volume: 1.5 mL

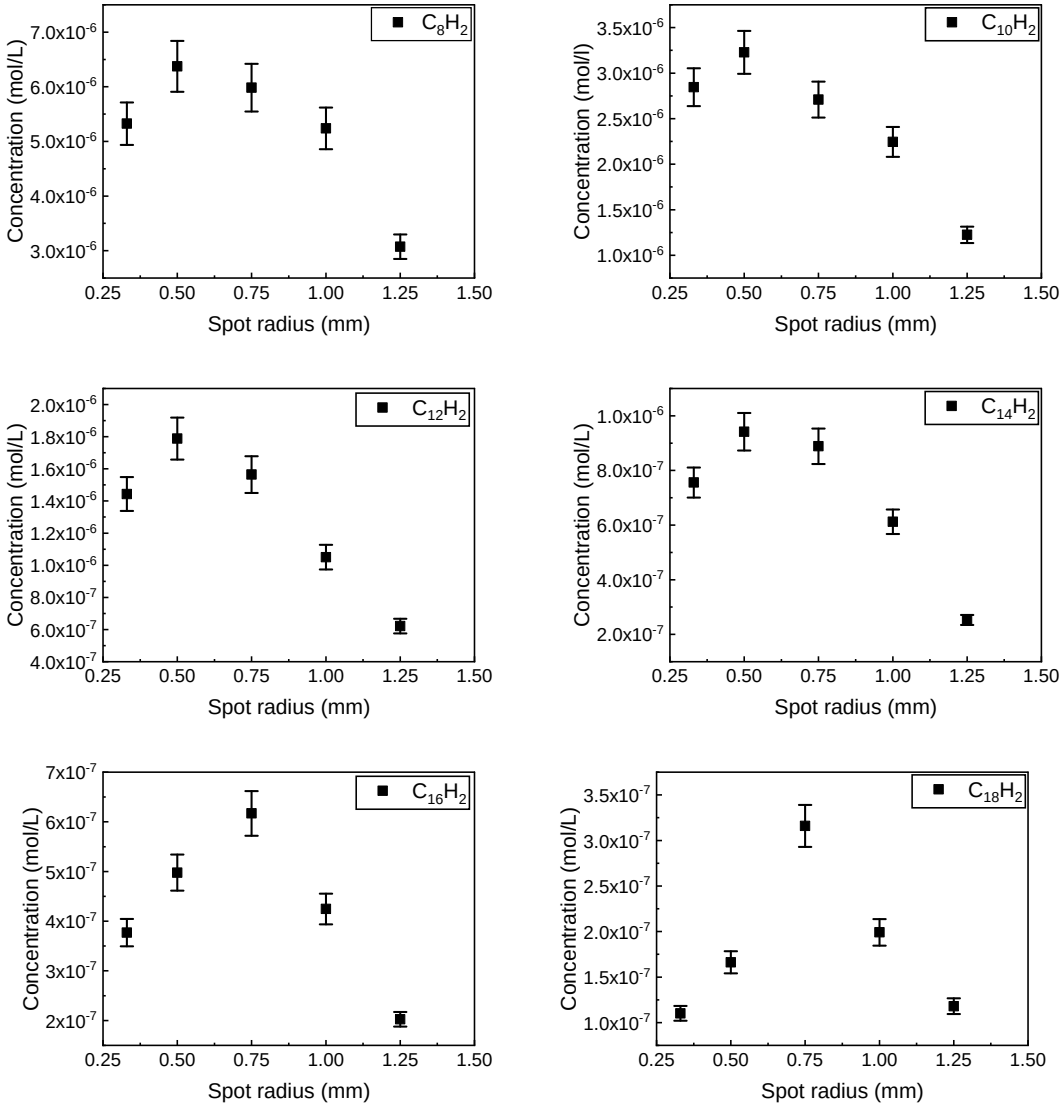

Figure 4.2: *Polyynes concentration as a function of spot radius. Ablations were performed for a time of 5 minutes in 1.5 mL of decalin, at 50 mJ/pulse.*

4.1.2 Material parameters: pure solvents effect

The second part of the optimization regards the analysis of the organic solvents considered in this thesis in terms of long polyynes production. Ablations have been performed with the optimized laser parameters, which have just been discussed. Let us start the analysis by investigating how the yield of long polyynes depends on the solvents. The data suggest an interesting correlation between the

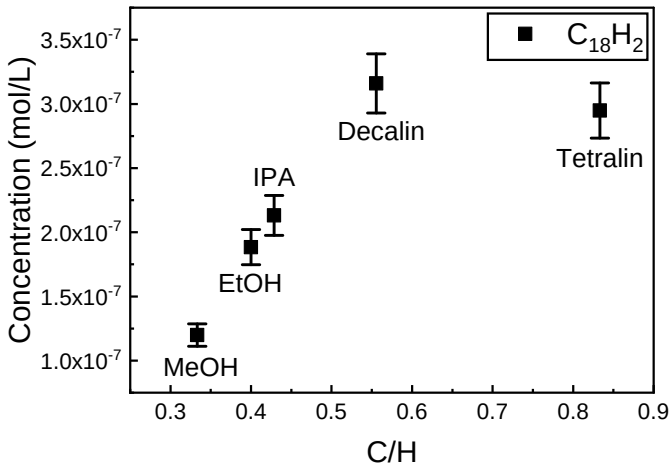

Figure 4.3: *Concentration of $HC_{18}H$ in the different pure solvents. Results are presented as a function of the C/H ratio*

C/H ratio of the tested solvents and the concentration of $HC_{18}H$, as shown in Fig. 4.3: higher amounts of long sp-chains were observed in solvents with a higher C/H ratio, apart from tetralin, which gave results slightly lower than decalin. Interestingly, a similar trend can be found looking at the viscosity, of the solvents, as reported in Fig. 4.4a. This progression seems to confirm the hypothesis of Matsutani *et al.*, according to whom high viscosity suppresses the diffusion of C radicals far from the plasma region and favours the synthesis of long polyynes [48]. The gap between IPA and tetralin, which share almost the same viscosity, might be explained by the higher C/H ratio and the lower polarity of tetralin. In fact, the trend can be also correlated to a decrease in the polarity of the solvent, as visible

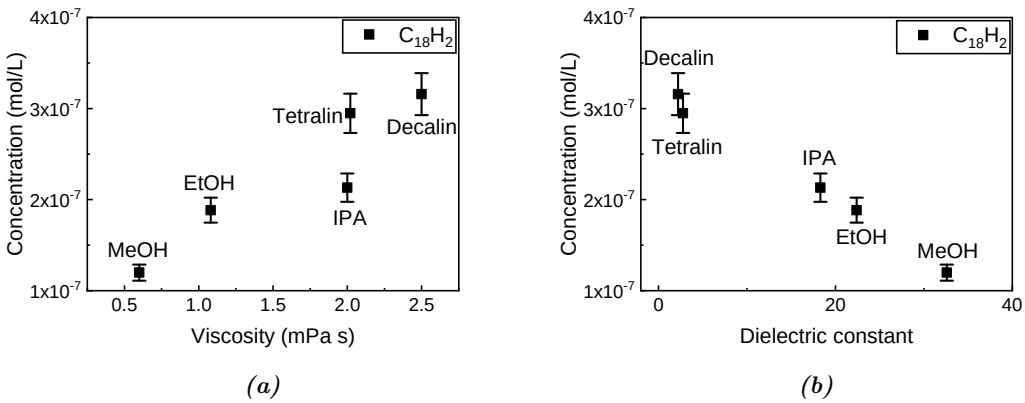

Figure 4.4: *Concentration of $HC_{18}H$ correlated to viscosity (a) and polarity (b)*

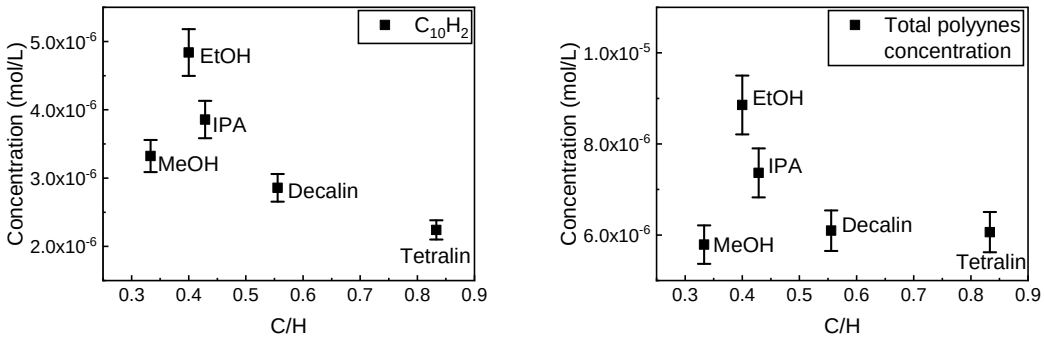

(a) *(b)*

Figure 4.5: *(a) Concentration of $HC_{10}H$ in the different pure solvents. (b) Overall concentration of H-capped polyynes from 10 to 18 carbon atoms. Results are presented as a function of the C/H ratio.*

in Fig. 4.4b. In this work, polarity is quantified by the dielectric constant and listed in Table 3.1.

The study of the concentration of $HC_{10}H$, taken as reference short polyyne in this analysis and shown in Fig. 4.5a, led to different considerations than before. Excluding methanol, a decreasing trend in the concentration of $HC_{10}H$ is observed when employing solvents with higher C/H ratio. It seems, thus, that low C/H solvents are more prone to form short polyynes. In other terms, termination seems favoured at the expense of polymerization in low C/H solvents. Fig. 4.5b shows the trend of the total amount of polyynes in terms of C/H ratio. Only polyynes of 10, 12, 14, 16 and 18 carbon atoms have been considered. The trend is closely related to the one of short polyynes, since these are the most concentrated ones. The main difference is that tetralin and decalin lead to almost the same amount of polyynes, even though both $HC_{10}H$ and $HC_{18}H$ are more concentrated in decalin. This is because tetralin shows a higher amount of $HC_{12}H$, $HC_{14}H$ and $HC_{16}H$. Methanol is the worst solvent in terms of long and total amount of polyynes. To explain this, I suppose that a major role is played by the absence of a C-C bond in its chemical structure. The other solvents, instead, all feature at least one C-C bond. Indeed, methanol cannot contribute with any C_2 radical fragment in the polymerization process, while the other solvents can. Thus, it appears that, besides the C/H ratio, the viscosity and the polarity of the solvent, the production of long polyynes is promoted when solvents feature a higher number of consecutive C-C bonds in their chemical structure.

The results of the analysis of pure solvents are summarized in Fig. 4.6. In this graph, the concentration of polyynes of different length is plotted in relative percentage with respect to $HC_{10}H$ obtained in each solvent. In this way, it can be

seen how solvents with increasing C/H ratio have a stronger tendency to produce longer polyynes. In Fig. 4.7 the same results are plotted without tetralin as a function of the C/H ratio, and compared to a set of experiments performed with the following parameters before their optimization: 5 and 15 minutes ablation time, 50 and 100 mJ/pulse, 0.75 and 1 mm spot radius, 1.5 and 2 mL of solvent, reported in Fig.4.7a and 4.7b, respectively. Not including tetralin allows to keep HC_8H as short polyyne reference. At 15 minutes, a decreasing trend in the relative concentration of $HC_{10}H$ can be seen when moving from EtOH to decalin. The

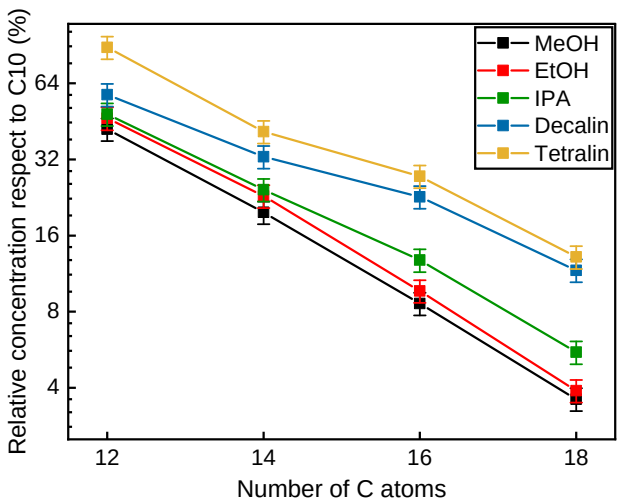

Figure 4.6: *Relative concentration of polyynes respect to that of $HC_{10}H$ in the set of solvents tested.*

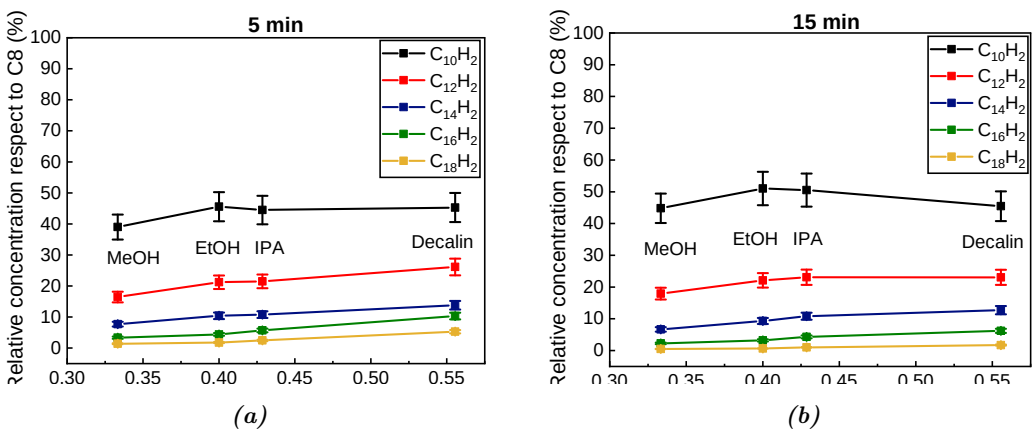

Figure 4.7: *Relative concentration of polyynes respect to that of HC_8H in the set of solvents tested at an ablation time of 5 minutes (a) and 15 minutes (b). Results are presented as a function of the C/H ratio.*

trend flattens for $HC_{12}H$, and becomes increasing for all longer polyynes. When the ablation time was set to 5 minutes, instead, the trend is almost flat for $HC_{10}H$ and increases for $HC_{12}H$ and all other longer polyynes. This is another way to see the positive effect of decreasing the ablation time in terms of the production of long polyynes.
In the next sections, I will discuss the attempt to study the effect of a more gradual C/H variation, by employing binary solutions as solvents for the ablations.

4.2 C/H effect of binary solutions on polyynes

Binary solutions of different kind have been used to vary the C/H ratio in a more step-wise manner. They will be divided in liquid mixtures of the solvents and naphthalene solutions, i.e. pure solvents with increasing amounts of dissolved naphthalene. All the ablations were performed with the laser parameters introduced in the last section. Due to the high concentrations of apolar compounds, in particular in the case of tetralin and naphthalene, it was often not possible to inject in the HPLC column volumes higher than 1 μL. This caused problems in the calculation of the chromatographic area of the peaks related to $HC_{18}H$ with the method used in the previous results, i.e. fitting the peaks with Gaussian curves. In all the following results, the peaks related to $HC_{18}H$ were manually integrated using the HPLC software, which lead to an overall light overestimation of the areas, and thus of the concentrations. The results, however, remain reliable in first approximation.

4.2.1 Liquid mixtures

Two kinds of liquid mixtures have been studied in this work: decalin and tetralin have been dissolved at increasing volume fractions in EtOH (10%, 20% and 50%). Homogeneous solutions were required to ensure that decalin and tetralin were equally distributed in the solution. EtOH was chosen because it is the lowest C/H solvent miscible with decalin and tetralin. Indeed, decalin and tetralin were found to be insoluble in MeOH and soluble in IPA. However EtOH was preferred to IPA because in this way we could obtain a sharper increase in the C/H ratio. Anyway, I imagined to observe a higher concentration of long polyynes at growing volume fractions of decalin and tetralin, similarly to the case of pure solvents. In the following part, I will first present the experimental results obtained in EtOH-decalin and then in EtOH-tetralin solutions. Then I will comment on the results by comparing the sets of experiments.

Ethanol-decalin mixtures

Ethanol-decalin solutions were the first binary mixture that have been investigated during this work. In fact, even if I found record in literature of injections of 5 μL of decalin in a C8 column like ours [43], decalin was never injected in our HPLC system. Therefore, I started with low amounts of decalin (10% in volume). Then I proceeded adding higher amounts and verified that no problems occurred even when injecting 5 μL of pure decalin.
The concentration of short ($HC_{10}H$) and long polyynes ($HC_{18}H$) in solutions of EtOH and decalin are reported in Fig. 4.8. A clear decreasing trend can be found in the concentration of $HC_{10}H$ as the content of decalin in solution is increased, with the value at 50% approaching the one obtained in pure decalin. This seems to confirm the results obtained in the analysis of pure solvents. However, the situation differs when looking at the results of $HC_{18}H$: the concentrations of the solutions lie always below the values observed in the pure solvents, with decalin yielding the maximum value. Thus, increasing the C/H ratio of the system in this way does not seem to be an effective way to promote the formation of long polyynes. I will make further considerations on this point after discussing the results regarding solutions of EtOH and tetralin. Fig. 4.9 shows the trend of the total concentration of polyynes at various concentrations of decalin. It is closely related to the trend of $HC_{10}H$, but with a relevant difference regarding the points at 50% and 100% decalin: they both presented similar amounts of $HC_{10}H$, but pure decalin shows a higher total amount of polyynes. This is due to the contribution of longer polyynes, which affects the overall concentration of all polyynes.

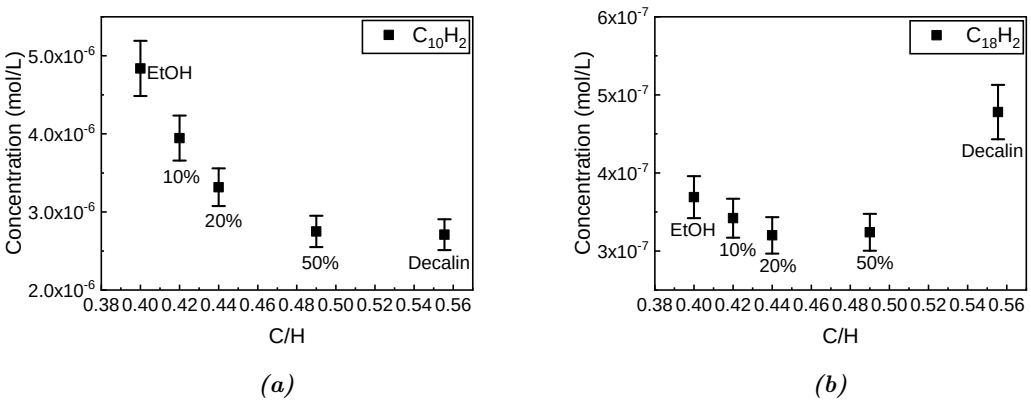

Figure 4.8: *$HC_{10}H$ (a) and $HC_{18}H$ (b) in solutions of EtOH with increasing volume fractions of decalin*

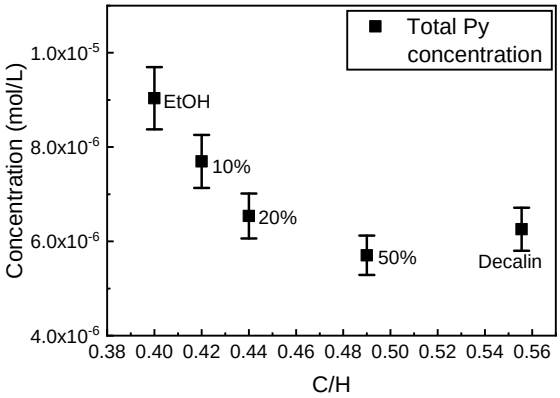

Figure 4.9: *Total concentration of polyynes in EtOH-decalin solutions at different compositions*

Ethanol-tetralin mixtures

The results obtained in EtOH and tetralin solutions are analogous to the previous ones, especially for the case of short polyynes. Concentrations of $HC_{10}H$ and $HC_{18}H$ are depicted in Fig. 4.10a and 4.10b, respectively. The amount of $HC_{10}H$

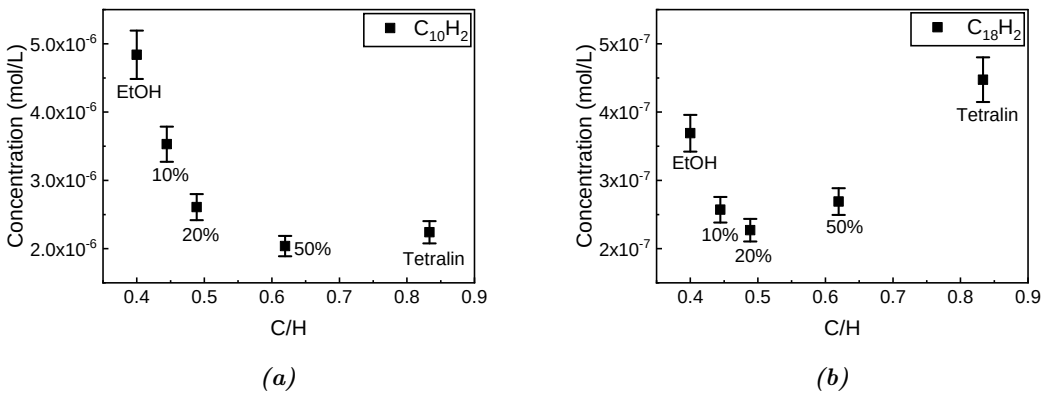

Figure 4.10: *$HC_{10}H$ (a) and $HC_{18}H$ (b) in solutions of EtOH with increasing volume fractions of tetralin*

in solution diminishes as the fraction of tetralin is increased. The value in pure tetralin, however, is slightly higher respect to the one at 50%. Regarding $HC_{18}H$, concentrations in the mixtures are lower than in the pure solvents, as in the case of EtOH and decalin. This time, however, the value at 50% is higher respect to 10% and 20%. About the total concentration of polyynes, reported in Fig. 4.11, considerations similar to the previous case can be drawn: the trend can be related to the one of short polyynes, but the concentration in pure tetralin is now higher

than the ones at 20%. Again, this is due to a larger concentration of long polyynes.

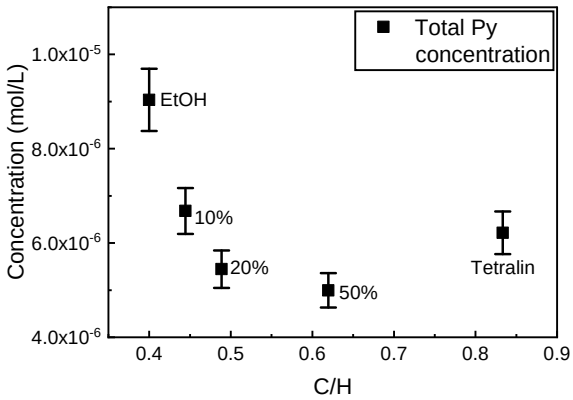

Figure 4.11: *Total concentration of polyynes in EtOH and tetralin solutions at different compositions*

Considerations on liquid mixtures

The results of EtOH-decalin and EtOH-tetralin solutions have shown that increasing the C/H ratio by mixing two different solvents does not promote the formation of long polyynes. Instead, it seems to be hindered, even though without a clear trend. The previously presented results of the two mixtures are compared in Fig. 4.12: it is immediate to see how the decalin solutions show a higher concentration of both short and long polyynes.

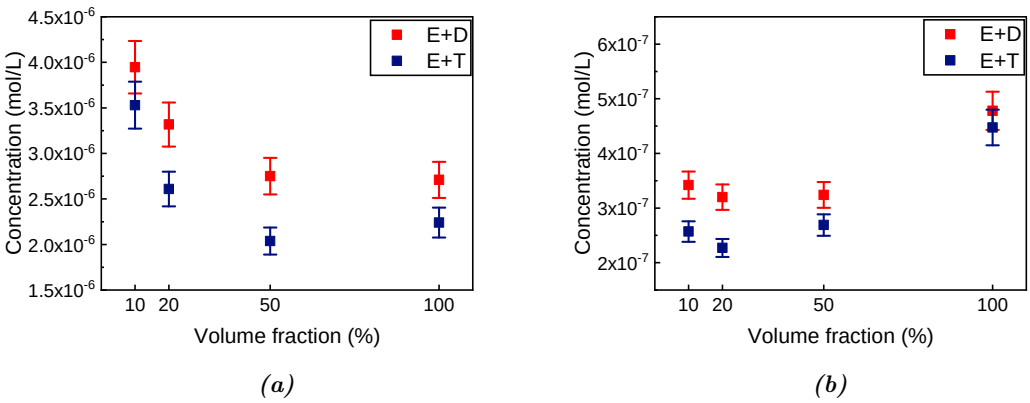

Figure 4.12: *Comparison of $HC_{10}H$ (a) and $HC_{18}H$ (b) between solutions of EtOH and decalin and EtOH and tetralin at the same volume fractions*

Let us consider some factors which might explain these results. The viscosities of the solutions have been calculated according to the model of Kendall and Monroe [111], who elaborated the following equation for mixtures of non-polar and non-associated liquids:

$$\eta_m = x_1\eta_1^{1/3} + x_2\eta_2^{1/3} \tag{4.2}$$

where η_m is the viscosity of the mixture, x_1 and x_2 are the molar fractions of the solvents, η_1 and η_2 the viscosities of the pure solvents. Table 4.1 shows the increase in viscosity at growing fractions of decalin or tetralin in solution according to this model. The increase is quite similar in the two cases, with decalin solutions being slightly more viscous at equal volume fractions. This is intuitive, considering that decalin features a higher viscosity respect to tetralin. Anyway, this could partly explain why polyynes are more concentrated in decalin solutions than tetralin ones. However, the main reason is believed to be the higher amount of impurities present in tetralin (97% pure, see Section 3.1.2. Moreover, in the pure solvents analysis in Fig. 4.4a, it was shown that higher concentrations of long polyynes are correlated to an increase in viscosity. For liquid mixtures, instead, this is not observed. Clearly, other properties need to be considered in order to explain the trend of long polyynes.
A major difference between EtOH and decalin lies in their dielectric constant, and thus in their polarity (22.4 for EtOH, 2.2 for decalin, as reported in Section 3.1.2). A similar difference holds also between EtOH and tetralin ($\epsilon_r = 2.77$). This difference in polarity probably prevents a complete interaction between the solvents, which would instead occur between substances with similar polarity. This implies that decalin and tetralin are not perfectly dissolved in EtOH at the microscale, as the homogeneity of the solution might suggest at first sight. In other terms decalin and tetralin might behave as solutes in solution. In Section 2.2.2 it was pointed out that, in the case of NPs produced by laser ablation, solutes can physically adsorb on their surface and limit their growth, acting like surfactants [62]. Even if it is difficult to associate a surface to polyynes, a similar effect can be supposed. Thus,

	EtOH + decalin	**EtOH + tetralin**
0%	1.074	1.074
10%	1.117	1.109
20%	1.167	1.149
50%	1.388	1.317
100%	2.5	2.02

Table 4.1: *Viscosities of liquid mixtures calculated according to the Kendall and Monroe model. Also the viscosities of pure EtOH, decalin and tetralin are reported.*

decalin and tetralin could act as barriers in the synthesis of polyynes when they are added to a solvent with a very different polarity. Indeed, tetralin employed in this work contains a higher amount of impurities than decalin, as explained in Section 3.1.2, and this may be another reason why polyynes are less concentrated in tetralin solutions.

4.2.2 Naphthalene solutions

The second class of binary solutions employed in the experiments consists in solutions in which naphthalene was dissolved at increasing concentrations. The selected solvents are ethanol, decalin and tetralin. This set of experiments was carried out with the main goal of obtaining polyynes with aromatic terminations. Unfortunately, these kind of polyynes have not been detected. However, since naphthalene features the highest C/H ratio (1.25) among all the investigated substances, these experiments allowed to continue to the analysis of synthesis yield of polyynes in terms of the C/H ratio of the solvent, although its variation was much less important compared to the case of the liquid mixtures. The results will be discussed following the scheme adopted in the previous section, first introducing the results in different solutions, and then drawing considerations based on the their comparison.

Ethanol-naphthalene solutions

Ethanol was the first solvent chosen to dissolve naphthalene. In this way, it was possible to compare the effect of naphthalene and its hydrogenated derivatives (i.e. decalin and tetralin) in the same solvent. However, being naphthalene far less soluble, it was difficult to reach the same fractions as in the other two cases. Fig. 4.13a and 4.13b shows the concentrations of $HC_{10}H$ and $HC_{18}H$, respectively, as increasing amounts of naphthalene are added to the solution. The trends are not monotonic and very similar for both short and long polyynes. The most important result is that, regardless of the quantity of naphthalene present in solution, the amount of polyynes is always lower respect to the case of pure ethanol. Indeed, it seems that the addition of naphthalene hinders the synthesis of polyynes similarly to the case of liquid mixtures. This further motivates the hypothesis that solutes adsorb to the sp chain and decrease the polymerization rate, as already observed in the liquid mixtures. Naphthalene, in fact, has a dielectric constant which is comparable to those of decalin and tetralin ($\epsilon_r = 2.87$ [112]). Moreover, their structures are closely related. We can so conclude that tetralin and decalin behave like naphthalene in EtOH, and thus like a solute obstructing the synthesis of polyynes. In order to compare the results obtained with naphthalene to those

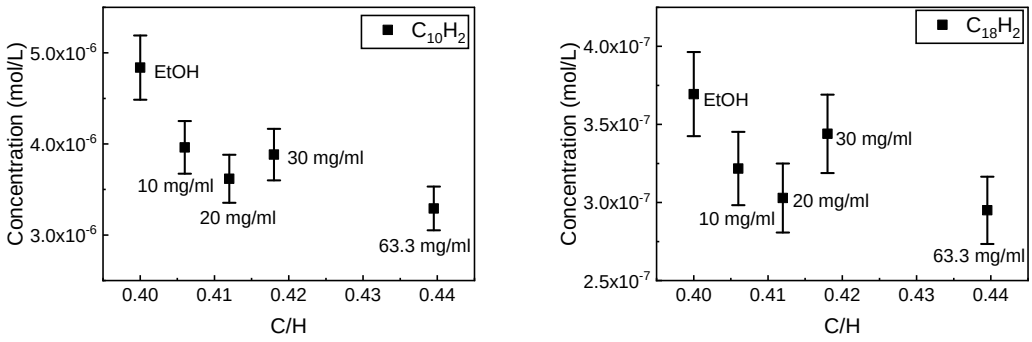

(a) *(b)*

Figure 4.13: *Concentrations of $HC_{10}H$ (a) and $HC_{18}H$ (b) in solutions of EtOH with increasing amounts of naphthalene*

obtained with decalin, we performed ablations at concentrations of naphthalene corresponding to he same C/H ratio of EtOH with 10 and 20% of decalin. The results, compared in Fig. 4.14, validate the hypothesis that decalin and naphthalene have a similar effect on the synthesis of polyynes when dissolved in ethanol. The amount of naphthalene required to reach the C/H ratio of 50% of decalin, i.e. 141.6 mg/ml, exceeds the solubility limit in EtOH (approximately 108 mg/ml, according to the IUPAC Solubility Data Series [113]), and thus it precipitates over the graphite target. Nevertheless, we performed the ablation at this concentration of naphthalene, but this result was not comparable to the corresponding ablation in 50% of decalin. So, we dissolved naphthalene in EtOH up to its solubility limit, and then we registered a precipitation of naphthalene powder on top of the target. The result of the ablation, reported in Fig. 4.15, were surprising: the concen-

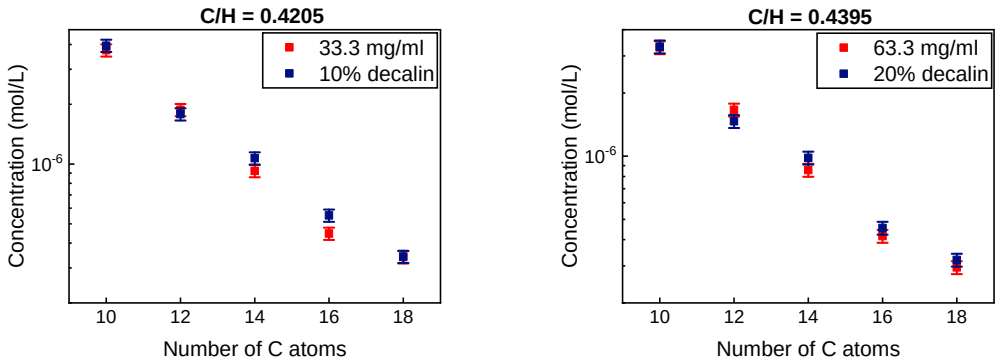

Figure 4.14: *Comparison between the concentrations of polyynes at the same C/H ratio with decalin and naphthalene. The results suggest a similar behaviour of decalin and naphthalene when the are dissolved in ethanol*

tration of $HC_{10}H$ seems to fit in the trend; $HC_{12}H$, instead, approaches the value observed in pure EtOH; longer polyynes are remarkably more concentrated. These results suggested that bulk naphthalene is a very appealing source of polyynes, in particular of longer ones, and motivated the idea of the ablation of a naphthalene target. This topic, however will be discussed in the last section of this chapter.

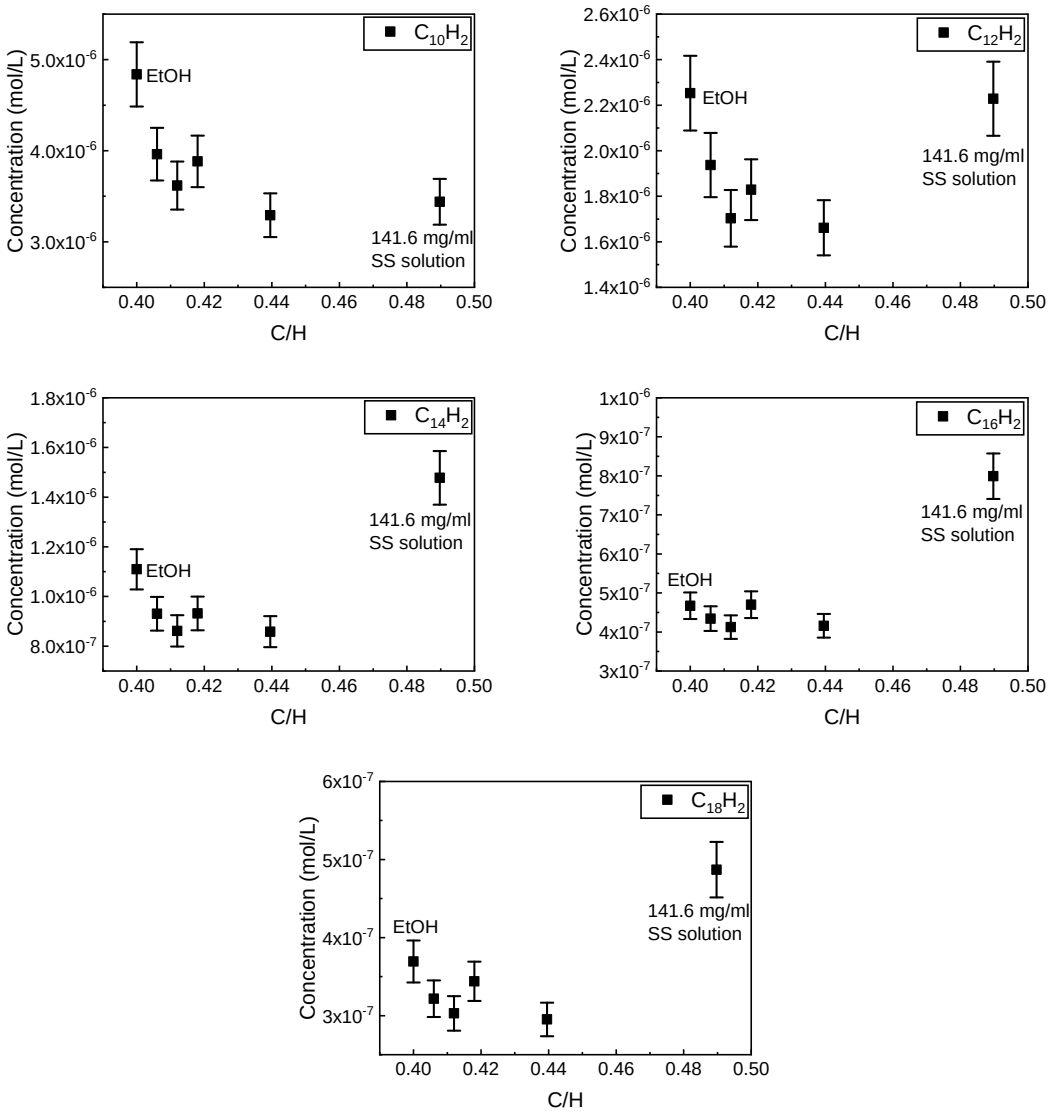

Figure 4.15: *Polyynes concentration as a function of spot radius. Ablations were performed for a time of 5 minutes in 1.5 mL of decalin, at 50 mJ/pulse. 0.75 mm appears to be the optimal spot radius for long polyynes.*

Decalin-naphthalene solutions

Decalin was the second solvent employed for the study of naphthalene in solution. Naphthalene is much more soluble in decalin (x_n = 0.22 at 300 K [113]) than in ethanol (x_n = 0.032 at 298 K [113]). Thus, in principle, a much higher amount of naphthalene could have been dissolved in solution, if it was not limited by the maximum loading capacitance of each analytes in the HPLC system.
The concentrations of $HC_{10}H$ and $HC_{18}H$ are reported in Fig. 4.16a and 4.16b, respectively. The results are very different from the EtOH-naphthalene solutions. Indeed, at any concentration of dissolved naphthalene, the amount of $HC_{10}H$ is higher than in pure decalin. The trend resembles a bell shape, with a maximum at 30 mg/ml. Regarding long polyynes, the values at 20, 40 and 50 mg/ml are within the error statistics. 30mg/ml is the maximum value also for $HC_{18}H$, even if less pronounced than in the short polyynes case. The concentrations of $HC_{18}H$ at 10 and 60 mg/ml are lower than in pure decalin. It seems that naphthalene dissolved in decalin contributes to the formation of shorter polyynes, regardless of its concentration in solution. I will further comment this point after presenting the results of the last set of naphthalene solutions.

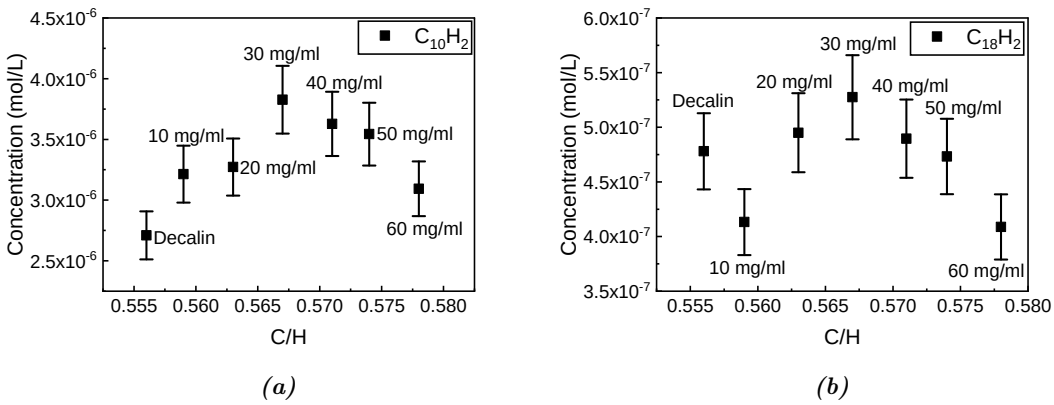

Figure 4.16: *Concentrations of $HC_{10}H$ (a) and $HC_{18}H$ (b) in solutions of decalin with increasing amounts of naphthalene*

Tetralin-naphthalene solutions

Tetralin and naphthalene solutions are the last set of binary mixtures used as solvents for the experiments. They represent the highest C/H ratios systems explored in this work. Naphthalene solubility in tetralin is slightly higher than in decalin (x_n = 0.36 at 306 K [113]). Moreover tetralin and decalin are closely related in terms of molecular geometry and properties, thus I expected similar results.
The concentrations of $HC_{10}H$ and $HC_{18}H$ are reported in Fig. 4.17a and 4.17b.

The trends are more similar to those obtained in decalin than in ethanol, as expected. However, some relevant differences can be highlighted. For example, the concentrations of $HC_{10}H$ are not always higher than in pure tetralin, as observed in decalin. At the same time there are also no values undoubtedly lower, assuming that the concentrations 10 mg/ml and 40 mg/ml are almost the same of pure tetralin. Regarding long polyynes, naphthalene seems to have a beneficial effect: in fact all solutions in which naphthalene was added showed a slightly higher concentration of $HC_{18}H$ respect to pure tetralin. Actually, it is incorrect to talk about pure tetralin, since its purity is $\geqslant 97\%$, as mentioned in Section 3.1.2. Since naphthalene traces were naturally present in tetralin, the reported concentrations of naphthalene refer only to the amount added in the laboratory.

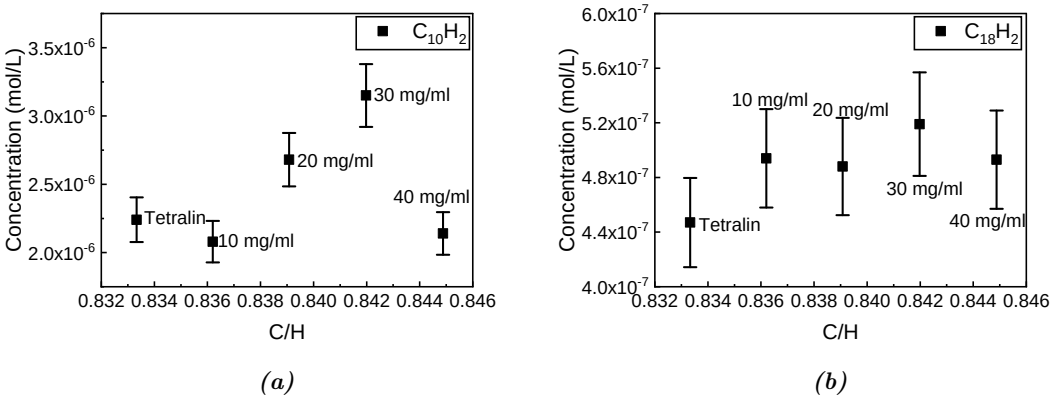

Figure 4.17: *Concentrations of $HC_{10}H$ (a) and $HC_{18}H$ (b) in solutions of tetralin with increasing amounts of naphthalene*

4.2.3 Final considerations on the solvents effect

The effect of the C/H variation of solvents, both in their pure form and as binary mixtures, has been discussed. In this section, I will summarize the results and try to give some new insights on the role of the solvent in the formation process of polyynes during laser ablation.

Regarding pure solvents, interesting correlations have been found between their properties and the production of polyynes. When moving from low to high C/H solvents, an overall decrease of short polyynes has been observed, except the case of MeOH, as well as an increase in the concentration of longer ones, with a big gap between MeOH an the other solvents. It has been hypothesized that this big difference is due to the absence of the C-C bond in its chemical structure, which indicates the impossibility to provide C_2 radicals to the synthesis process of polyynes. Decalin and tetralin could ideally contribute up to 10 consecutive C-C

bonds, assuming a complete opening of the hexagonal rings, which however does not seem to happen at my experimental conditions, given the limited difference respect to EtOH and IPA in terms of $HC_{18}H$ concentration and the reduction of $HC_{10}H$. The trend in long polyynes concentration has been further related to an increase in viscosity and a decrease in polarity of the solvent.
The study of liquid mixtures revealed that adding fractions of decalin or tetralin to EtOH did not favour the formation of long polyynes, but resulted in an overall decrease of polyynes concentration, despite the increase of the C/H ratio and viscosity. For naphthalene, similar results were found when it was dissolved in ethanol. Thus it has been concluded that the three closely related molecules hinder the formation of polyynes when they are dissolved in a solvent with a considerable different polarity. Basically, they all act as solutes limiting the synthesis of polyynes, in analogy to what observed in the synthesis of metal NPs by PLAL [62]. Instead, when naphthalene was added to a solvent with a more compatible solvent (i.e. decalin and tetralin), the overall concentration of polyynes increased, even if the behavior of the two solvents was quite different, as described in the last section In naphthalene-solutions, the effect of viscosity has been neglected because the amounts added in solutions were too low to give a relevant variation. This assumption is based on the results obtained in the work of Tamura *et al.*, in which the viscosities of benzene-naphthalene and toluene-naphthalene solutions have been studied [114]. Benzene and toluene are quite similar to decalin and tetralin in terms of molecular geometry (all based on hexagonal rings) and polarity. Thus, I will relate the variation in viscosity observed in benzene to that occurring in the solvents tested in this work, even in the case of EtOH, whose characteristics strongly differ from those of benzene, the approximation is less valid. Anyway, the authors proposed and validated with their experimental data the following equation to calculate the solution viscosity:

$$\eta = x_A w_A \frac{d}{d_A}\eta_A + x_B w_B \frac{d}{d_B}\eta_B + 2(x_A x_B w_A w_B \frac{d^2}{d_A d_B})^{1/2}\eta_{AB} \tag{4.3}$$

where x_A and x_B denote the molar fractions of the solvent and the solute, w_A and w_B their weight fractions, d, d_A and d_B the densities of the solution, the solvent and the solute respectively. η and η_A are the viscosities of the solution and of the solvents, while η_B and η_{AB}, the only two unknowns, are called "viscosity coefficient of the solute" and "mutual viscosity coefficient", respectively. They calculated these values by applying equation 4.3 to their experimental data, and by rearranging it in order to graphically extract the two unknowns (η_B = 1.98 mPa s and η_{AB} = 1.03 mPa s in the case of benzene [114]). η_B was found to be independent of the nature of the solvent, while η_{AB} was not. Since there was no way to calculate η_{AB} for the solvents tested in this work, I referred to the case

of benzene. The maximum molar fractions of naphthalene x_B employed in this work are 0.03 in ethanol, 0.07 in decalin and 0.04 in tetralin, approximately. The paper reports an increase in benzene viscosity of 0.071 mPa s (at 25 °C) when the content of naphthalene is $x_N = 0.069$, which is very close to the maximum concentration explored in this work. Assuming a similar variation also in ethanol, decalin and tetralin, I concluded that viscosity does not vary significantly for all the naphthalene fractions handled in my experiments, and that other factors, such as the difference in polarity, have a stronger impact on the synthesis of polyynes.
Now the effect of naphthalene dissolved in solution can be summarized as follows. In a polar solvent such as EtOH, naphthalene is not prone to contribute in the polyynes formation process, but appears to hinder it. The same holds for decalin and tetralin, when dissolved in EtOH. In solvents with comparable polarities, instead, it favours the synthesis of polyynes, with a stronger effect on shorter ones in decalin and a weaker effect on longer ones in tetralin. I thus suppose that naphthalene is a relevant source of short polyynes in a highly apolar solvent, but do not promote a larger generation of long polyynes.
The effect of bulk naphthalene seems to be very different from dissolved naphthalene. The ablation of the supersature solution in EtOH showed a remarkable increase in the concentration of longer polyynes and suggested the idea of the ablation of a bulk naphthalene target. This topic will be discussed in the final section of this chapter.
To conclude the analysis of the effect of the C/H ratio on the production of polyynes, I summarized the results of the ablations in pure solvents and liquid mixtures in Fig. 4.18. For naphthalene solutions, only one ablation in each solvent is reported, since the C/H variation was very small in those sets of experiments. At first sight, the plots appear unclear and very scattered. By taking a closer look, an overall decrease of the $HC_{10}H$ concentration can be observed when moving to higher C/H ratios. The trend seems to flatten for polyynes of 12 and 14 carbon atoms. For $HC_{16}H$ and $HC_{18}H$, a slight increasing tendency can be noticed as the C/H ratio is increased. The most noticeable effect, however, which holds true both in pure solvents and in liquid mixtures, is the decrease in the synthesis of short chains.

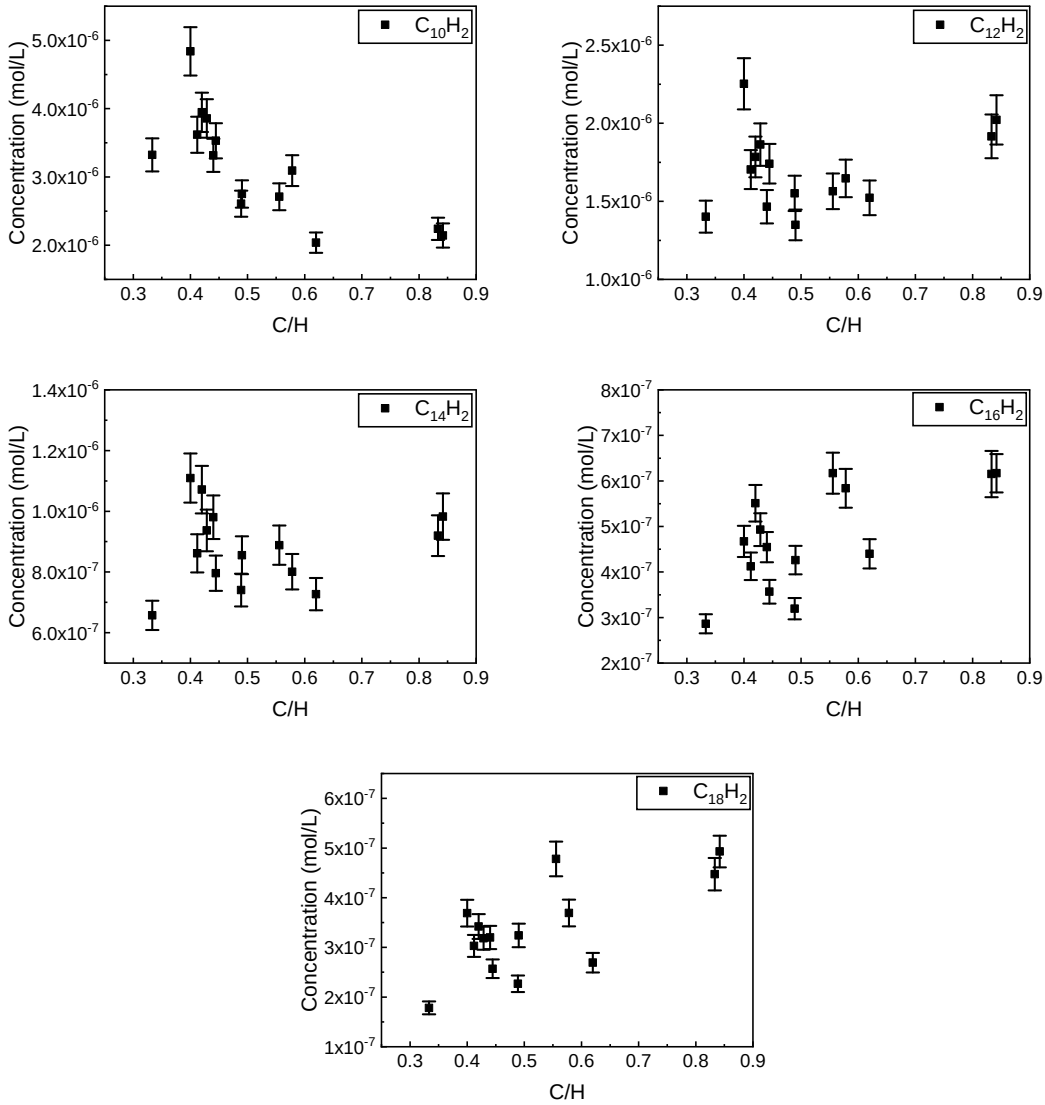

Figure 4.18: *Summarizing plots of concentration of polyynes obtained in pure solvents and in liquid mixtures. Only one value per solvent is reported in the case of naphthalene binary mixtures*

4.3 Naphthalene target analysis

In this last section, I report the results of the ablations of a naphthalene target. The solvents selected for these experiments are deionized water, MeOH, EtOH and IPA. Decalin and tetralin were discarded because naphthalene is too soluble in them. Indeed, injecting very high amounts of naphthalene-rich solution, as it is expected in decalin and tetralin after several minutes, could have seriously damaged the HPLC column. The amounts of naphthalene injected in the previous experiments already challenged the integrity of the column. Ablations with the same experimental parameters were performed also with the graphite target, in order to have a reference case to be compared with. The laser parameters were exactly the same as in the previous section, namely 5 minutes of ablation, pulse energy of 50 mJ, spot radius of 0.75 mm and 1.5 mL of solvent.

Water

Water was the first solvent chosen for the ablation of bulk naphthalene, mainly for two reasons. Water is the solvent in which naphthalene is less soluble among the available ones, and thus it allows larger injections, up to 10 μL, to prevent possible damages to the HPLC column. Secondly, and most importantly, since water does not contain carbon, I wanted to undoubtedly verify that naphthalene is a direct source of polyynes.

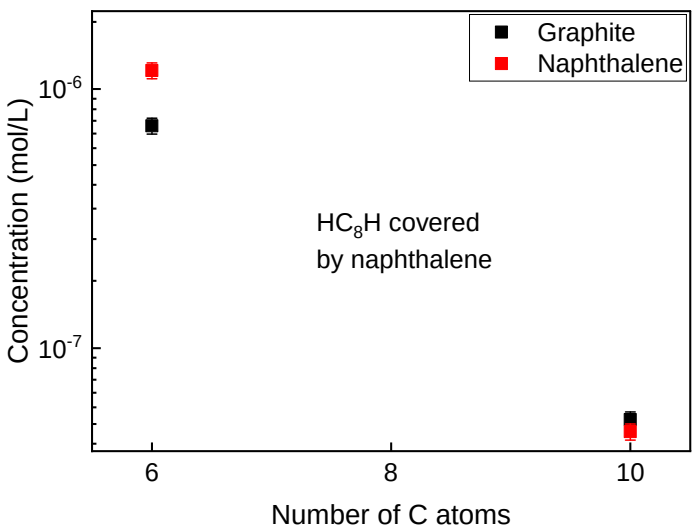

Figure 4.19: *Comparison between polyynes obtained in water from a naphthalene target and a graphite target*

The results obtained in water are shown in Fig. 4.19, compared to graphite ablation at the same conditions: with naphthalene, a considerably higher amount of HC_6H was measured, while the concentration of $HC_{10}H$ was approximately the same. Polyynes longer than 10 carbon atoms were not detected neither with naphthalene nor with graphite. As already said, naphthalene is eluted exactly at the same retention time of HC_8H, denying the possibility to collect data about this chain. Anyway, I confirmed that naphthalene is a direct source of polyynes, and, surprisingly, it leads to a higher total amount respect to a graphite target, in water. The higher amount of HC_6H suggests a ring-opening mechanism of naphthalene to form short polyynes. Indeed, C_6H^- was found to be one of the major fragmentation products detected in a plasma of pure naphthalene [53].

Alcohols

The ablations in alcohols returned very different results with respect to the case of water. It is necessary to mention that the naphthalene target resulted a lot more damaged in alcohols than in water, given the higher solubility in the former. Thus, the high amount of naphthalene present in the mixtures at the end of the ablation prevented injection volumes higher than 1 μL. A picture of the targets after the ablation in each solvent is shown in Fig. 4.20.

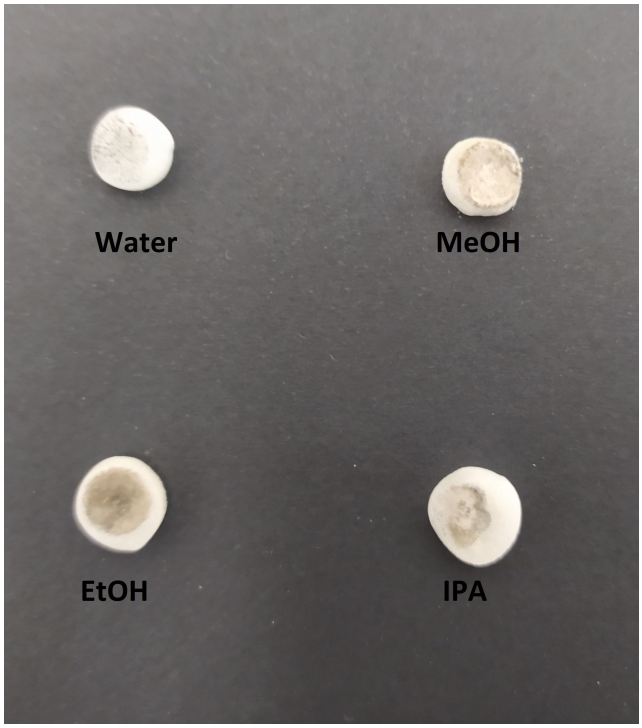

Figure 4.20: *Naphthalene targets after the ablation: it resulted less ruined in water than in alcohols*

Both with graphite and naphthalene, polyynes up to 18 carbon atoms have been detected. The results obtained in MeOH, EtOH and IPA, summarized in Fig. 4.21, 4.22 and 4.23, respectively, share some common features. Contrarily to what observed in water, in fact, the amount of HC_6H is now considerably lower when using naphthalene as a target, respect to graphite. Instead, H-polyynes composed by 10, 12, 14 and 16 carbon atoms are produced in a higher amount. Regarding $HC_{18}H$, the reported values are not totally reliable, since the measurements resulted very noisy. Nevertheless, naphthalene seems to favour the formation of longer polyynes in alcohols respect to graphite. Surprisingly though, the total amount of polyynes in each solvent results to be almost the same, as can be seen in Fig. 4.24. The difference in HC_6H concentration is compensated by a higher amount of longer polyynes. Thus, naphthalene and graphite lead approximately to the same amount of polyynes, but with a larger contribute of longer polyynes in the case of naphthalene respect to that of graphite. For what concerns EtOH, it is also possible to compare the results, shown in Fig. 4.22 to those obtained from the ablation of the supersature solution, discussed in Section 4.2.2. The results are quite in agreement with each other, considering that similar amounts of $HC_{10}H$ were produced in both cases and that the concentration of longer polyynes was considerably higher. This seems to confirm that bulk naphthalene is a source of long polyynes in organic solvents. We can now conclude the discussion about naphthalene and its tendency to participate in the formation process of polyynes in different ways. In analogy with the work of Tsuji *et al.*, who pointed out that graphite powder dispersed in solution yields a higher amount of short polyynes respect to a graphite pellet [82], the behaviour of naphthalene seems closely related: indeed, when it was dissolved in an apolar solvent it increased the concentration of short polyynes, while in its bulk form, both in the supersature solution and as a target, it largely favoured the synthesis of longer polyynes. Thus we can suppose that naphthalene dissolved in decalin and tetralin undergoes more easily termination because naphthalene molecules are more surrounded by solvent. Therefore the synthesis of short polyynes are favoured. Conversely, bulk naphthalene might open his rings under laser irradiation to yield polyynic fragments (in principle up to 10 carbon atoms), which can be combined to form longer polyynes.

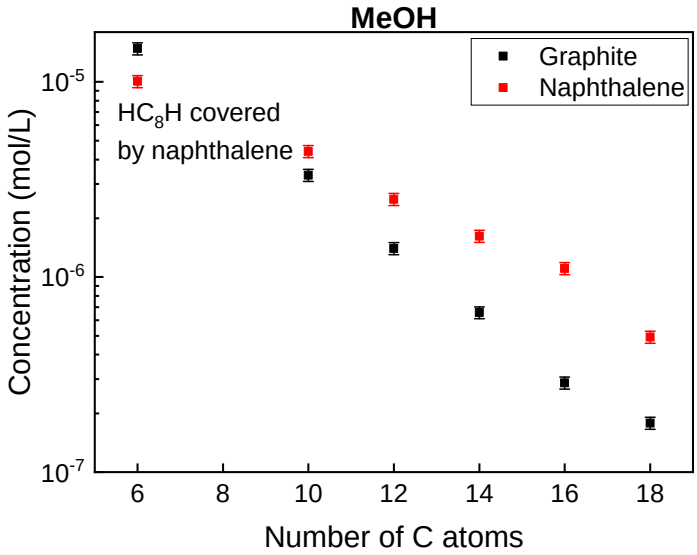

Figure 4.21: *Comparison between concentrations of polyynes obtained in MeOH from a naphthalene target and a graphite target*

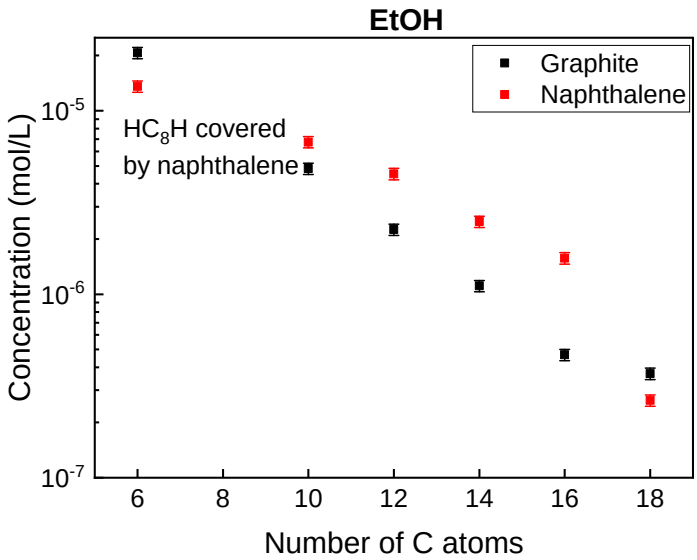

Figure 4.22: *Comparison between concentrations of polyynes obtained in EtOH from a naphthalene target and a graphite target*

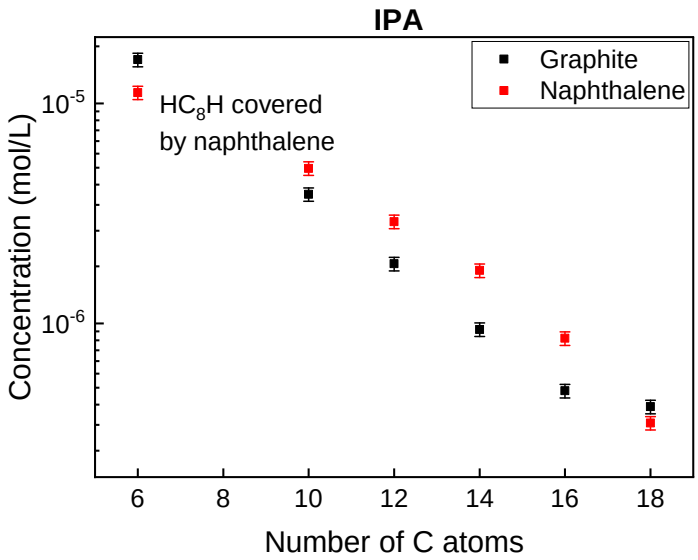

Figure 4.23: *Comparison between concentrations of polyynes obtained in IPA from a naphthalene target and a graphite target*

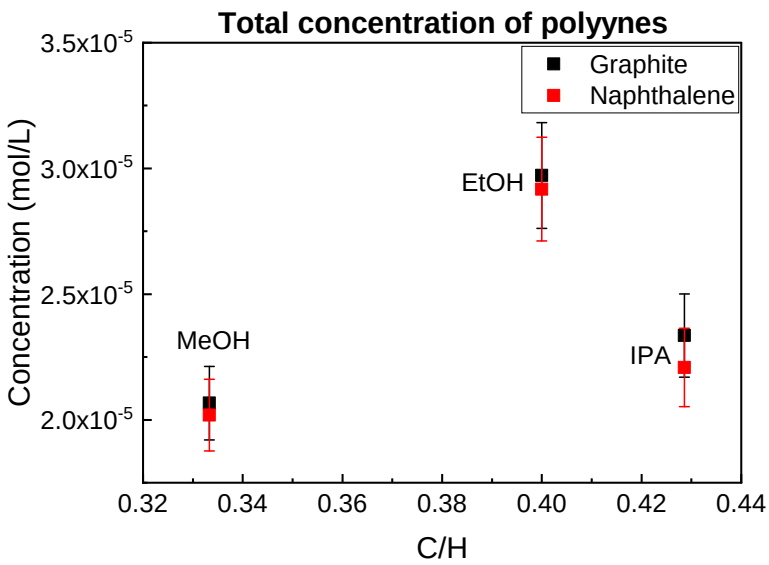

Figure 4.24: *Total concentration of polyynes obtained in alcohols by a naphthalene target and by a graphite target*

Chapter 5

Conclusion and perspectives

The main aim of this thesis work was the investigation of substances at increasing C/H ratios to promote the formation of longer H-polyynes by Pulsed Laser Ablation in Liquid (PLAL). Interesting considerations about the roles of the solvent in the formation process of polyynes have been drawn from experimental results. Indeed, the use of solvents in their pure form with high C/H ratio and viscosity, and with low polarity, was correlated to a higher concentration of $HC_{18}H$, the polyyne taken as a benchmark for long chains in this work. Moreover, it was suggested that the yield of long polyynes may be correlated also to the number of consecutive C-C bonds present in the solvent structure. These trends were not observed in the liquid mixtures analysis. In particular, the values of $HC_{18}H$ obtained in EtOH-decalin and EtOH-tetralin solutions were always lower than those of EtOH, decalin and tetralin in their pure form. A common result between the analysis of pure solvents and liquid mixtures was the decrease in short chains concentration as the C/H ratio of the solvent was increased. The results of the liquid mixtures were correlated to the ones obtained in the EtOH-naphthalene solutions. Indeed, the total amount of polyynes in solution decreased as higher amounts of naphthalene were added to the solution. Moreover, ablations in EtOH-decalin and EtOH-naphthalene solutions at the same C/H ratio returned surprisingly similar results. Exploring even more different solvents but with the same C/H ratio represents an interesting possible development of this thesis work. When naphthalene was dissolved in decalin and tetralin, instead, it visibly increased the concentration of shorter polyynes. It was supposed that solutions made by components with a relevant difference in polarity, such as the one existing between EtOH and naphthalene-like compounds, hinder the synthesis of polyynes, and that the solution might not be as homogeneous at the microscale as its appearance would suggest. Instead, when the difference in polarity was very little, as in the case of decalin and tetralin-naphthalene solutions, an increase in short polyynes concentration was observed. Thus, if naphthalene

is dissolved in a more compatible liquid, it contributes to the polyynes formation process.
The ablation of a naphthalene target in water undoubtedly proved that naphthalene is a source of polyynes. In fact, since water does not contain carbon atoms, polyynes could have formed only from naphthalene. The naphthalene target was ablated also in some alcohols, namely methanol, ethanol and isopropyl-alcohol. By comparing the results to the ablation of graphite at the same experimental conditions, it turned out that the total amount of polyynes is approximately the same, but with a larger contribute of longer polyynes in the case of naphthalene respect to that of graphite. The results involving naphthalene ablations seem to confirm that, under appropriate conditions, naphthalene undergoes a ring-opening mechanism to yield polyynes, which was already suggested by previous works [53]–[55]. To conclude the discussion about naphthalene, it can be stated that, when naphthalene is dissolved in an apolar compatible solvent, it contributes to the formation of short polyynes because the polyynic fragments generated from the opening of naphthalene rings are easily terminated by the H atoms of the solvents. When naphthalene is ablated in its bulk form, instead, the polyynic fragments are confined in a closer region and can combine to yield a large amount of long polyynes, delaying termination.
The use of Polycylic Aromatic Hydrocarbons with a high number of aromatic rings as target or suspension on top of a graphite target is surely an intriguing possibility to favour the formation of longer polyynes and, in the best case, polyynes with aromatic endgroups. However, the difficulties in handling high melting point compounds as anthracene and pentacene, suggest a revision of the crafting method of the PAH target. The best remedy would be to operate in a high temperature environment. As a last proposal, using an HPLC system in the normal phase configuration, rather than the reverse phase one, would allow higher injection volumes, and thus the possibility to detect less concentrated species such as the last mentioned ones. Anyway, a deeper screening of the ablation parameters, as well as of the chromatographic peaks, has to be done to check if we have already produced aromatic-capped polyynes.

Bibliography

[1] A. Hirsch, "The era of carbon allotropes," *Nature Mater*, vol. 9, pp. 868–871, 2010 (cit. on pp. 4, 6, 10).

[2] A. Milani, A. Li Bassi, V. Russo, M. Tommasini, and C. S. Casari, "Linear Carbon: From 1D to 2D hybrid sp-sp^2 nanostructures beyond graphene," *Handbook of Graphene: Volume 3*, pp. 297–340, 2019 (cit. on pp. 4, 5, 11, 12).

[3] H. O. Pierson, "Handbook of carbon, graphite, diamond and fullerenes - properties, processing and applications," *William Andrew Publishing/Noyes*, 2004 (cit. on p. 5).

[4] S. Nasir, M. Z. Hussein, Z. Zainal, and N. A. Yusof, "Carbon-based nanomaterials/allotropes: A glimpse of their synthesis, properties and some applications," *Materials*, vol. 11, no. 2, 2018, ISSN: 1996-1944 (cit. on pp. 5, 6, 8, 9).

[5] V. Vermeeren, S. Wenmackers, and P. Wagner, "Dna sensors with diamond as a promising alternative transducer material," *Sensors*, vol. 9, pp. 5600–5636, 2009 (cit. on p. 6).

[6] E. Zhmurikov, *Graphite in science and nuclear technology*, 2016 (cit. on p. 6).

[7] P. Atkins, T. Overton, J. Rourke, M. Weller, and F. Armstrong, "Inorganic chemistry," *Oxford university press*, 2010 (cit. on p. 6).

[8] H. Kroto, J. R. Heath, S. C. O'Brien, R. F. Curl, and R. E. Smalley, "C60: Buckminsterfullerene," *Nature*, vol. 318, pp. 162–163, 1985 (cit. on p. 6).

[9] S. Iijima, "Helical microtubules of graphitic carbon," *Nature*, vol. 354, p. 56, 1991 (cit. on p. 7).

[10] A. K. Geim and K. S. Novoselov, "Electric field effect in atomically thin carbon films," *Science*, vol. 306, pp. 666–669, 2004 (cit. on p. 7).

[11] ——, "The rise of graphene," *Nature Mater*, vol. 6, pp. 183–191, 2007 (cit. on pp. 7, 8).

[12] K. I. Bolotin, K. J. Sikes, Z. Jiang, M. Klima, G. Fudenberg, J. Hone, P. Kim, and H. L. Stormer, "Ultrahigh electron mobility in suspended graphene," *Solid State Communications*, vol. 146, no. 9, pp. 351–355, 2008, ISSN: 0038-1098 (cit. on p. 7).

[13] C. Soldano, A. Mahmood, and E. Dujardin, "Production, properties and potential of graphene," *Carbon*, vol. 48, no. 8, pp. 2127–2150, 2010 (cit. on pp. 7, 8).

[14] J. C. Charlier, P. C. Eklund, J. Zhu, and A. C. Ferrari, "Electron and phonon properties of graphene: Their relationship with carbon nanotubes," *Carbon Nanotubes*, pp. 673–709, 2008 (cit. on p. 8).

[15] K. S. Novoselov, S. V. Morozov, T. M. G. Mohinddin, L. A. Ponomarenko, D. C. Elias, R. Yang, I. I. Barbolina, and A. K. Gerim, "Electronic properties of graphene," *Physica Status Solidi (b)*, vol. 244, no. 11, pp. 4106–4111, 2007 (cit. on p. 8).

[16] Y. Hu, M. De Corato, A. Ruini, S. Zhao, and A. Narita, "Bandgap engineering of graphene nanoribbons by control over structural distortion," *Journal of the American Chemical Society*, vol. 140, no. 25, pp. 7803–7809, 2018 (cit. on p. 8).

[17] N. Jing, Q. Xue, C. Ling, M. Shan, T. Zhang, X. Zhou, and Z. Jiao, "Effect of defects on young's modulus of graphene sheets: A molecular dynamics simulation," *RSC Adv.*, vol. 2, pp. 9124–9129, 24 2012 (cit. on p. 8).

[18] X. Zang, Q. Zhou, J. Chang, Y. Liu, and L. Lin, "Graphene and carbon nanotube (cnt) in mems/nems applications," *Microelectronic Engineering*, vol. 132, pp. 192–206, 2015 (cit. on p. 8).

[19] A. Eatamadi, H. Daraee, H. Karimkhanloo, M. Kouhi, N. Zarghami, A. Akbarzadeh, M. Abasi, Y. Hanifehpour, and S. W. Joo, "Carbon nanotubes: Properties, synthesis, purification, and medical applications," *Nanoscale Research Letters*, vol. 9, 2014 (cit. on p. 9).

[20] A. Chuvilin, U. Kaiser, E. Bichoutskaia, N. A. Besley, and A. N. Khlobystov, "Direct transformation of graphene to fullerene," *Nature Chem*, vol. 2, pp. 450–453, 2010 (cit. on p. 10).

[21] O. Berne, J. Montillaud, G. Mulas, and C. Joblin, *30 years of cosmic fullerenes*, 2015 (cit. on p. 10).

[22] S. Collavini and J. L. Delgado, "Fullerenes: The stars of photovoltaics," *Sustainable Energy Fuels*, vol. 2, pp. 2480–2493, 2018 (cit. on p. 10).

[23] S. Bosi, T. Da Ros, G. Spalluto, and M. Prato, "Fullerene derivatives: An attractive tool for biological applications," *European Journal of Medicinal Chemistry*, vol. 38, no. 11, pp. 913–923, 2003 (cit. on p. 10).

[24] M. S. Dresselhaus, G. Dresselhaus, and P. C. Eklund, "Fullerenes," *Journal of Materials Research*, vol. 8, no. 8, pp. 2053–2097, 1993 (cit. on p. 10).

[25] N. Lang and P. Avouris, "Carbon-atom wires: Charge-transfer doping, voltage drop, and the effect of distortions," *Physical review letters*, vol. 84, no. 2, p. 358, 2000 (cit. on p. 11).

[26] S. Tongay, R. Senger, S. Dag, and S. Ciraci, "A b-i n i t i o electron transport calculations of carbon based string structures," *Physical review letters*, vol. 93, no. 13, p. 136 404, 2004 (cit. on p. 11).

[27] M. Liu, V. I. Artyukhov, H. Lee, F. Xu, and B. I. Yakobson, "Carbyne from first principles: Chain of c atoms, a nanorod or a nanorope," *ACS nano*, vol. 7, no. 11, pp. 10 075–10 082, 2013 (cit. on p. 11).

[28] Y. Zhu, H. Bai, and Y. Huang, "Electronic property modulation of one-dimensional extended graphdiyne nanowires from a first-principle crystal orbital view," *ChemistryOpen*, vol. 5, no. 1, pp. 78–87, 2016 (cit. on p. 11).

[29] S. C. Casari and A. Milani, "Carbyne: From the elusive allotrope to stable carbon atom wires," *MRS Communications*, vol. 8.2, pp. 207–219, 2018 (cit. on pp. 11, 31).

[30] C. S. Casari, M. Tommasini, R. R. Tykwinski, and A. Milani, "Carbon-atom wires: 1-d systems with tunable properties," *Nanoscale*, vol. 8, pp. 4414–4435, 8 2016 (cit. on pp. 11–14, 24, 25).

[31] A. Milani, M. Tommasini, V. Russo, A. Lucotti, F. Cataldo, and C. S. Casari, "Raman spectroscopy as a tool to investigate the structure and electronic properties of carbon-atom wires," *Beilstein J. Nanotechno*, vol. 6, pp. 480–491, 2015 (cit. on pp. 11, 14, 19–21).

[32] S. Peggiani, P. Marabotti, R. A. Lotti, A. Facibeni, P. Serafini, A. Milani, V. Russo, A. Li Bassi, and C. S. Casari, "Solvent-dependent termination, size and stability in polyynes synthesized via laser ablation in liquids," *Phys. Chem. Chem. Phys.*, vol. 22, pp. 26 312–26 321, 45 2020 (cit. on pp. 13–16, 18, 25, 34–38, 43).

[33] A. Ramadan, M. Welosowski, T. Wakabayashi, H. Shiromaru, T. Fujino, T. Kodama, W. Duley, and J. Sanderson, "Synthesis of hydrogen- and methyl-capped long-chain polyynes by intense ultrashort laser pulse irradiation of toluene," *Carbon*, vol. 118, pp. 680–685, 2017, ISSN: 0008-6223 (cit. on pp. 13, 18, 34, 36, 38).

[34] C. Franco, "Polyynes and cyanopolyynes: Their synthesis with the carbon arc gives the same abundances occurring in carbon-rich stars," *Orig Life Evol Biosph*, vol. 36, pp. 467–475, 2006 (cit. on p. 13).

[35] F. Coat, F. Paul, C. Lapinte, L. Toupet, K. Costuas, and J. Halet, "Chemistry of the 1,3,5,7-octatetraynediyl carbon rod end-capped by two electron-rich $(\eta^5 - c_5me_5)(\eta^2 - dppe)fegroups$," *Journal of Organometallic Chemistry*, vol. 683, pp. 368–378, 2003 (cit. on p. 13).

[36] F. Cataldo, O. Ursini, G. Angelini, M. Tommasini, and C. S. Casari, "Simple synthesis of α, $\omega - diarylpolyynespart1 : Diphenylpolyynes$," *Journal of Macromolecular Science, Part A: Pure and Applied Chemistry*, vol. 47.8, pp. 739–746, 2010 (cit. on pp. 13, 18, 24).

[37] J. A. Januszewski and R. R. Tykwinski, "Synthesis and properties of long [n]cumulenes (n 5)," *Chem. Soc. Rev.*, vol. 43, pp. 3184–3203, 9 2014 (cit. on pp. 14, 24).

[38] A. Milani, M. Tommasini, V. Barbieri, A. Lucotti, V. Russo, F. Cataldo, and C. S. Casari, "Semiconductor-to-metal transition in carbon-atom wires driven by sp2 conjugated end groups," *The Journal of Physical Chemistry C*, vol. 121, no. 19, pp. 10 562–10 570, 2017 (cit. on p. 14).

[39] F. Cataldo, "Polyynes production in a solvent-submerged electric arc between graphite electrodes. iii. chemical reactivity and stability toward air, ozone, and light," *Fullerenes, Nanotubes and Carbon Nanostructures*, vol. 12, no. 3, pp. 633–646, 2004 (cit. on p. 14).

[40] ——, "Storage stability of polyynes and cyanopolyynes in solution and the effect of ammonia or hydrochloric acid," *Fullerenes, Nanotubes, and Carbon Nanostructures*, vol. 15, no. 3, pp. 155–166, 2007 (cit. on p. 14).

[41] G. Yang, *Laser ablation in liquids: principles and applications in the preparation of nanomaterials*. CRC Press, 2012 (cit. on p. 14).

[42] L. Shi, P. Rohringer, K. Suenaga, Y. Niimi, J. Kotakoski, J. Meyer, H. Peterlik, and al., "Confined linear carbon chains as a route to bulk carbyne," *Nature materials*, vol. 15.6, p. 634, 2016 (cit. on p. 14).

[43] F. Cataldo, L. Ravagnan, E. Cinquanta, I. E. Castelli, N. Manini, G. Onida, and P. Milani, "Synthesis, characterization, and modeling of naphthyl-terminated sp carbon chains: Dinaphthylpolyynes," *The Journal of Physical Chemistry B*, vol. 114, pp. 14 834–14 841, 2010 (cit. on pp. 16–18, 24, 40, 58).

[44] A. Milani, M. Tommasini, and G. Zerbi, "Connection among raman wavenumbers, bond length alternation and energy gap in polyynes," *Journal of Raman Spectroscopy*, vol. 40, no. 12, pp. 1931–1934, 2009 (cit. on p. 17).

[45] "Introduction," in *Introduction to Modern Liquid Chromatography*. John Wiley Sons, Ltd, 2009, ch. 1, pp. 1–17, ISBN: 9780470508183 (cit. on p. 17).

[46] "Basic concepts and the control of separation," in *Introduction to Modern Liquid Chromatography*. John Wiley Sons, Ltd, 2009, ch. 2, pp. 19–86, ISBN: 9780470508183 (cit. on pp. 17, 18).

[47] S. Peggiani, A. Senis, A. Facibeni, A. Milani, P. Serafini, G. Cerrato, A. Lucotti, M. Tommasini, D. Fazzi, C. Castiglioni, *et al.*, "Size-selected polyynes synthesised by submerged arc discharge in water," *Chemical Physics Letters*, vol. 740, p. 137 054, 2020 (cit. on p. 18).

[48] R. Matsutani, K. Inoue, T. Sanada, N. Wada, and K. Kojima, "Preparation of long-chain polyynes of c28h2 and c30h2 by liquid-phase laser ablation," *Journal of Photochemistry and Photobiology A: Chemistry*, vol. 240, pp. 1–4, 2012, ISSN: 1010-6030 (cit. on pp. 18, 34, 35, 38, 43, 51, 54).

[49] R. Matsutani, F. Ozaki, R. Yamamoto, T. Sanada, Y. Okada, and K. Kojima, "Preparation of polyynes up to c22h2 by liquid-phase laser ablation and their immobilization into sio2 gel," *Carbon*, vol. 47, no. 7, pp. 1659–1663, 2009, ISSN: 0008-6223 (cit. on pp. 18, 34).

[50] F. Innocenti, A. Milani, and C. Castiglioni, "Can raman spectroscopy detect cumulenic structures of linear carbon chains?" *Journal of Raman Spectroscopy*, vol. 41, no. 2, pp. 226–236, 2010 (cit. on pp. 19, 20).

[51] A. K. Lemmens, D. B. Rap, J. Thunnissen, S. Gruet, A. L. Steber, S. Panchagnula, A. Tielens, M. Schnell, W. J. Buma, and A. M. Rijs, "Far-ir absorption of neutral polycyclic aromatic hydrocarbons (pahs): Light on the mechanism of ir-uv ion dip spectroscopy.," *The journal of physical chemistry letters*, vol. 11, no. 21, pp. 8997–9002, 2020 (cit. on pp. 21, 22).

[52] S. Kwok, "Organic matter in space: From star dust to the solar system," *Astrophysics and Space Science*, vol. 319.1, pp. 5–21, 2009 (cit. on p. 21).

[53] M. Alliati, D. Donaghy, X. Tu, and J. W. Bradley, "Ionic species in a naphthalene plasma: Understanding fragmentation patterns and growth of pahs," *The Journal of Physical Chemistry A*, vol. 123, no. 10, pp. 2107–2113, 2019 (cit. on pp. 21, 22, 71, 76).

[54] T. Chen and Y. Luo, "Formation of polyynes and ring-polyyne molecules following fragmentation of polycyclic aromatic hydrocarbons," *Monthly Notices of the Royal Astronomical Society*, vol. 486, no. 2, pp. 1875–1881, Apr. 2019, ISSN: 0035-8711 (cit. on pp. 21, 76).

[55] A. K. Lemmens, D. Rap, J. Thunnissen, B. Willemsen, and A. Rijs, "Polycyclic aromatic hydrocarbon formation chemistry in a plasma jet revealed by ir-uv action spectroscopy," *Nature Communications*, vol. 11, no. 269, 2020 (cit. on pp. 22, 23, 39, 40, 76).

[56] C. Glaser, "Beiträge zur kenntniss des acetenylbenzols," *Berichte der deutschen chemischen Gesellschaft*, vol. 2, no. 1, pp. 422–424, 1869 (cit. on p. 24).

[57] W. Chalifoux and R. Tykwinski, "Synthesis of polyynes to model the sp-carbon allotrope carbyne," *Nature Chem*, vol. 2, pp. 967–971, 2010 (cit. on p. 24).

[58] N. Gulia, K. Osowska, B. Pigulski, T. Lis, Z. Galewski, and S. Szafert, "Mori–hiyama versus hay coupling for higher polyynes," *European Journal of Organic Chemistry*, vol. 2012, no. 25, pp. 4819–4830, 2012 (cit. on p. 24).

[59] T. Wakabayashi, M. Saikawa, Y. Wada, and T. Minematsu, "Isotope scrambling in the formation of cyanopolyynes by laser ablation of carbon particles in liquid acetonitrile," *Carbon*, vol. 50, no. 1, pp. 47–56, 2012 (cit. on pp. 25, 38).

[60] Y.-E. Park, S.-K. Shin, and S.-M. Park, "The solvent effects on the formation of polyynes by laser ablation," *Bulletin of the Korean Chemical Society*, vol. 33, no. 7, pp. 2439–2442, 2012 (cit. on pp. 25, 32, 34–36, 38).

[61] H. Sadeghi, E. Solati, and D. Dorranian, "Producing graphene nanosheets by pulsed laser ablation: Effects of liquid environment," *Journal of Laser Applications*, vol. 31, no. 4, p. 042 003, 2019 (cit. on p. 25).

[62] A. Vincenzo and M. Moreno, "What controls the composition and the structure of nanomaterials generated by laser ablation in liquid solution?" *Physical Chemistry Chemical Physics*, vol. 15.9, pp. 3027–3046, 2013 (cit. on pp. 26–31, 61, 67).

[63] R. Fabbro, J. Fournier, P. Ballard, D. Devaux, and J. Virmont, "Physical study of laser-produced plasma in confined geometry," *Journal of Applied Physics*, vol. 68, no. 2, pp. 775–784, 1990 (cit. on pp. 26, 27).

[64] M. Hashida, H. Mishima, S. Tokita, and S. Sakabe, "Non-thermal ablation of expanded polytetrafluoroethylene with an intense femtosecond-pulse laser," *Opt. Express*, vol. 17, no. 15, pp. 13 116–13 121, Jul. 2009 (cit. on p. 27).

[65] C. Momma, B. N. Chichkov, S. Nolte, F. von Alvensleben, A. Tünnermann, H. Welling, and B. Wellegehausen, "Short-pulse laser ablation of solid targets," *Optics Communications*, vol. 129, no. 1, pp. 134–142, 1996, ISSN: 0030-4018 (cit. on pp. 27, 29).

[66] D. Perez, L. J. Lewis, P. Lorazo, and M. Meunier, "Ablation of molecular solids under nanosecond laser pulses: The role of inertial confinement," *Applied Physics Letters*, vol. 89, no. 14, p. 141 907, 2006 (cit. on p. 27).

[67] Y. Sano, N. Mukai, K. Okazaki, and M. Obata, "Residual stress improvement in metal surface by underwater laser irradiation," *Nuclear Instruments and Methods in Physics Research Section B: Beam Interactions with Materials and Atoms*, vol. 121, no. 1, pp. 432–436, 1997, Materials Synthesis and Modification by Ion and/or Laser Beams, ISSN: 0168-583X (cit. on p. 27).

[68] T. Tsuji, Y. Tsuboi, N. Kitamura, and M. Tsuji, "Microsecond-resolved imaging of laser ablation at solid–liquid interface: Investigation of formation process of nano-size metal colloids," *Applied Surface Science*, vol. 229, no. 1, pp. 365–371, 2004, ISSN: 0169-4332 (cit. on pp. 27, 28).

[69] D. G. Shchukin and M. Helmuth, "Sonochemical nanosynthesis at the engineered interface of a cavitation microbubble," *Phys. Chem. Chem. Phys.*, vol. 8, pp. 3496–3506, 2006 (cit. on p. 28).

[70] Z. Yan, R. Bao, Y. Huang, and D. B. Chrisey, "Hollow particles formed on laser-induced bubbles by excimer laser ablation of al in liquid," *The Journal of Physical Chemistry C*, vol. 114, no. 26, pp. 11 370–11 374, 2010 (cit. on p. 28).

[71] V. Amendola and M. Meneghetti, "Laser ablation synthesis in solution and size manipulation of noble metal nanoparticles," *Phys. Chem. Chem. Phys.*, vol. 11, pp. 3805–3821, 20 2009 (cit. on pp. 28, 29).

[72] W. T. Nichols, T. Sasaki, and N. Koshizaki, "Laser ablation of a platinum target in water. i. ablation mechanisms," *Journal of Applied Physics*, vol. 100, no. 11, p. 114 911, 2006 (cit. on p. 28).

[73] L. V. Zhigilei, Z. Lin, and D. S. Ivanov, "Atomistic modeling of short pulse laser ablation of metals: Connections between melting, spallation, and phase explosion," *The Journal of Physical Chemistry C*, vol. 113, no. 27, pp. 11 892–11 906, 2009 (cit. on pp. 28, 29).

[74] W. T. Nichols, T. Sasaki, and N. Koshizaki, "Laser ablation of a platinum target in water. ii. ablation rate and nanoparticle size distributions," *Journal of Applied Physics*, vol. 100, no. 11, p. 114 912, 2006 (cit. on p. 28).

[75] P. Wagener, A. Schwenke, B. N. Chichkov, and S. Barcikowski, "Pulsed laser ablation of zinc in tetrahydrofuran: Bypassing the cavitation bubble," *The Journal of Physical Chemistry C*, vol. 114, no. 17, pp. 7618–7625, 2010 (cit. on p. 29).

[76] Z. Yan, R. Bao, Y. Huang, A. N. Caruso, S. B. Qadri, C. Z. Dinu, and D. B. Chrisey, "Excimer laser production, assembly, sintering, and fragmentation of novel fullerene-like permalloy particles in liquid," *The Journal of Physical Chemistry C*, vol. 114, no. 9, pp. 3869–3873, 2010 (cit. on p. 29).

[77] G. Yang, in *Laser ablation in liquids: principles and applications in the preparation of nanomaterials*. CRC Press, 2012 (cit. on p. 29).

[78] G. C. Messina, P. Wagener, R. Streubel, A. De Giacomo, A. Santagata, G. Compagnini, and S. Barcikowski, "Pulsed laser ablation of a continuously-fed wire in liquid flow for high-yield production of silver nanoparticles," *Phys. Chem. Chem. Phys.*, vol. 15, pp. 3093–3098, 9 2013 (cit. on p. 30).

[79] G. Yang, "Laser ablation in liquids: Applications in the synthesis of nanocrystals," *Progress in Materials Science*, vol. 52, no. 4, pp. 648–698, 2007, ISSN: 0079-6425 (cit. on p. 31).

[80] A. Wakisaka, J. J. Gaumet, Y. Shimizu, Y. Tamori, H. Sato, and K. Tokumaru, "Growth of carbon clusters. the simplest process, 2c1→ c2, observed via spectrometry and chemical reaction," *J. Chem. Soc., Faraday Trans.*, vol. 89, pp. 1001–1005, 7 1993 (cit. on p. 31).

[81] J. J. Gaumet, A. El Ouachini, S. Peter, E. Millon, and J. F. Muller, "Formation of carbon clusters c(1 n 4) by laser vaporization of graphite and a study of their chemical reactivity by gas chromatography–mass spectrometry," *J. Chem. Soc., Faraday Trans.*, vol. 92, pp. 1831–1834, 11 1996 (cit. on p. 32).

[82] M. Tsuji, T. Tsuji, S. Kuboyama, S.-H. Yoon, Y. Korai, T. Tsujimoto, K. Kubo, A. Mori, and I. Mochida, "Formation of hydrogen-capped polyynes by laser ablation of graphite particles suspended in solution," *Chemical Physics Letters*, vol. 355, no. 1, pp. 101–108, 2002, ISSN: 0009-2614 (cit. on pp. 32–35, 72).

[83] G. Compagnini, V. Mita, R. S. Cataliotti, L. D'Urso, and O. Puglisi, "Short polyyne chains produced by pulsed laser ablation of graphite in water," *Carbon*, vol. 45, pp. 2445–58, 2007 (cit. on pp. 32, 35, 36).

[84] R. Matsutani, K. Inoue, N. Wada, and K. Kojima, "Wavelength dependence of polyyne preparation by liquid-phase laser ablation using pellet targets," *Chem. Commun.*, vol. 47, pp. 5840–5842, 20 2011 (cit. on p. 33).

[85] Y. E. Park, S. K. Shin, and S. M. Park, "The physical effects on the formation of polyynes by laser ablation," *Chemical Physics Letters*, vol. 568-569, pp. 112–116, 2013, ISSN: 0009-2614 (cit. on pp. 33, 34).

[86] ——, "Power dependence on formation of polyynes by laser ablation in water," *Bulletin of the Korean Chemical Society*, vol. 34, no. 4, pp. 1039–1042, 2013 (cit. on pp. 33, 34).

[87] R. Matsutani, T. Kakimoto, H. Tanaka, and K. Kojima, "Preparation of polyynes by liquid-phase laser ablation using different irradiation target materials and solvents," *Carbon*, vol. 49, no. 1, pp. 77–81, 2011 (cit. on pp. 33–35, 37, 38).

[88] A. Hu, J. Sanderson, A. Zaidi, C. Wang, T. Zhang, Y. Zhou, and W. Duley, "Direct synthesis of polyyne molecules in acetone by dissociation using femtosecond laser irradiation," *Carbon*, vol. 46, no. 13, pp. 1823–1825, 2008 (cit. on p. 34).

[89] A. A. Zaidi, A. Hu, D. D. Henneke, and W. W. Duley, "Femtosecond laser irradiation of liquid alkanes: Mechanism of polyyne formation," *Chemical Physics Letters*, vol. 723, pp. 151–154, 2019, ISSN: 0009-2614 (cit. on p. 34).

[90] K. Bagga, R. McCann, M. Wang, A. Stalcup, M. Vázquez, and D. Brabazon, "Laser assisted synthesis of carbon nanoparticles with controlled viscosities for printing applications," *Journal of colloid and interface science*, vol. 447, pp. 263–268, 2015 (cit. on p. 34).

[91] Y. Sato, T. Kodama, H. Shiromaru, J. Sanderson, T. Fujino, Y. Wada, T. Wakabayashi, and Y. Achiba, "Synthesis of polyyne molecules from hexane by irradiation of intense femtosecond laser pulses," *Carbon*, vol. 48, no. 5, pp. 1673–1676, 2010 (cit. on p. 34).

[92] A. Santagata, A. De Bonis, A. De Giacomo, M. Dell'Aglio, A. Laurita, G. S. Senesi, R. Gaudiuso, S. Orlando, R. Teghil, and G. P. Parisi, "Carbon-based nanostructures obtained in water by ultrashort laser pulses," *The Journal of Physical Chemistry C*, vol. 115, no. 12, pp. 5160–5164, 2011 (cit. on p. 34).

[93] H. Tabata, M. Fujii, and S. Hayashi, "Synthesis of polyynes by laser ablation of diamond nanoparticles suspended in solution," *Eur. Phys. J. D*, vol. 134, pp. 223–225, 2005 (cit. on pp. 34, 35).

[94] S. K. Shin, J. K. Song, and S. M. Park, "Preparation of polyynes by laser ablation of graphite in aqueous media," *Applied Surface Science*, vol. 257, no. 12, pp. 5156–5158, 2011, E-MRS 2010 Spring Meeting Symposium R. "Laser Processing and Diagnostics for Micro and Nano Applications", ISSN: 0169-4332 (cit. on p. 34).

[95] M. Tsuji, S. Kuboyama, T. Matsuzaki, and T. Tsuji, "Formation of hydrogen-capped polyynes by laser ablation of c60 particles suspended in solution," *Carbon*, vol. 41, no. 11, pp. 2141–2148, 2003 (cit. on p. 35).

[96] J. Zhao, Y. Zhang, Y. Fang, Z. Fan, G. Ma, Y. Liu, and X. Zhao, "Synthesis of polyynes by intense femtosecond laser irradiation of swcnts suspended in methanol," *Chemical Physics Letters*, vol. 682, pp. 96–100, 2017 (cit. on p. 35).

[97] M. J. Wesolowski, B. Moores, Z. Leonenko, R. Karimi, J. H. Sanderson, and W. W. Duley, "Synthesis of polymer-like hydrogenated amorphous carbon by fs-pulsed laser induced plasma processing of solid hexane," *Plasma Processes and Polymers*, vol. 9, no. 7, pp. 701–708, 2012 (cit. on p. 35).

[98] A. Zaidi, I. Alkhesho, R. Karimi, J. Sanderson, and W. Duley, "Femtosecond laser ablation of solid methane," *International Journal of Mass Spectrometry*, vol. 376, pp. 32–34, 2015 (cit. on p. 35).

[99] Y. Taguchi, H. Endo, T. Kodama, Y. Achiba, H. Shiromaru, T. Wakabayashi, B. Wales, and J. Sanderson, "Polyyne formation by ns and fs laser induced breakdown in hydrocarbon gas flow," *Carbon*, vol. 115, pp. 169–174, 2017 (cit. on p. 37).

[100] Y. Taguchi, H. Endo, Y. Abe, J. Matsumoto, T. Wakabayashi, T. Kodama, Y. Achiba, and H. Shiromaru, "Polyyne formation by graphite laser ablation in argon and propane mixed gases," *Carbon*, vol. 94, pp. 124–128, 2015 (cit. on p. 37).

[101] G. Forte, L. D'Urso, E. Fazio, S. Patanè, F. Neri, O. Puglisi, and G. Compagnini, "The effects of liquid environments on the optical properties of linear carbon chains prepared by laser ablation generated plasmas," *Applied surface science*, vol. 272, pp. 76–81, 2013 (cit. on p. 38).

[102] Y. Wada, K. Koma, Y. Ohnishi, Y. Sasaki, and T. Wakabayashi, "Photoinduced reaction of methylpolyynes h (c≡ c) nch3 (n= 5-7) and polyyne h (c≡ c) 5h with 12 molecules formation of molecular complex vs. degradation," *The European physical journal. D, Atomic, molecular and optical physics (Print)*, vol. 66, no. 12, 2012 (cit. on p. 38).

[103] K. Kim, J. Oh, T. W. Kim, J. H. Park, J. W. Han, and Y.-W. Suh, "Different catalytic behaviors of pd and pt metals in decalin dehydrogenation to naphthalene," *Catalysis Science & Technology*, vol. 7, no. 17, pp. 3728–3735, 2017 (cit. on p. 38).

[104] M. McHugh and M. E. Paulaitis, "Solid solubilities of naphthalene and biphenyl in supercritical carbon dioxide," *Journal of chemical and engineering data*, vol. 25, no. 4, pp. 326–329, 1980 (cit. on p. 40).

[105] I. Smallwood, *Handbook of organic solvent properties*. Butterworth-Heinemann, 2012 (cit. on p. 43).

[106] D. Davidson, P. Eggleton, and P. Foggie, "The diffusion of atmospheric gases through fats and oils," *Quarterly Journal of Experimental Physiology and Cognate Medical Sciences: Translation and Integration*, vol. 37, no. 2, pp. 91–105, 1952 (cit. on p. 43).

[107] P. Luehring and A. Schumpe, "Gas solubilities (hydrogen, helium, nitrogen, carbon monoxide, oxygen, argon, carbon dioxide) in organic liquids at 293.2 k," *Journal of Chemical and Engineering Data*, vol. 34, no. 2, pp. 250–252, 1989 (cit. on p. 43).

[108] R. Sander, "Compilation of henry's law constants (version 4.0) for water as solvent," *Atmospheric Chemistry and Physics*, vol. 15, no. 8, pp. 4399–4981, 2015 (cit. on p. 43).

[109] J. J. Kirkland and J. W. Dolan, "Properties of hplc solvents," *INTRODUCTION TO MODERN LIQUID CHROMATOGRAPHY*, p. 879, 2010 (cit. on p. 46).

[110] R. Eastmond, T. Johnson, and D. Walton, "Silylation as a protective method for terminal alkynes in oxidative couplings: A general synthesis of the parent polyynes h (c c) nh (n= 4–10, 12)," *Tetrahedron*, vol. 28, no. 17, pp. 4601–4616, 1972 (cit. on p. 50).

[111] D. S. Viswanath, T. K. Ghosh, D. H. Prasad, N. V. Dutt, and K. Y. Rani, "Viscosities of solutions and mixtures," in *Viscosity of Liquids*, Springer, 2007, pp. 407–442 (cit. on p. 61).

[112] K. Ishii, M. Kinoshita, and H. Kuroda, "Dielectric constant measurement on organic crystalline powder," *Bulletin of the Chemical Society of Japan*, vol. 46, no. 11, pp. 3385–3391, 1973 (cit. on p. 62).

[113] W. Aeree Jr, *Polycyclic aromatic hydrocarbons: Binary non-aqueous systems: Part 2 (solutes fx); iupac solubility data series*, 1995 (cit. on pp. 63, 65).

[114] M. Tamura, M. Kurata, and S. Sata, "On the viscosity of solutions of non-electrolytes," *Bulletin of the Chemical Society of Japan*, vol. 25, no. 2, pp. 124–126, 1952 (cit. on p. 67).